July 2020

SYNTHESIS AND CHARACTERIZATION OF GEOPOLYMERS CAST AND CURED IN SALINE WATER AND THE POTENTIAL APPLICATION IN CONSTRUCTION ENGINEERING

Xiaonan Ge
University of Massachusetts Amherst

SYNTHESIS AND CHARACTERIZATION OF GEOPOLYMERS CAST AND CURED IN SALINE WATER AND THE POTENTIAL APPLICATION IN CONSTRUCTION ENGINEERING

A Dissertation Presented

by

XIAONAN GE

Submitted to the Graduate School of the
University of Massachusetts Amherst in partial fulfillment
of the requirements for the degree of

DOCTOR OF PHILOSOPHY

May 2020

Civil and Environmental Engineering

SYNTHESIS AND CHARACTERIZATION OF GEOPOLYMERS CAST AND CURED IN SALINE WATER AND THE POTENTIAL APPLICATION IN CONSTRUCTION ENGINEERING

A Dissertation Presented

by

XIAONAN GE

Approved as to style and content by:

_____
Guoping Zhang, Chair

_____
Don J. DeGroot, Member

_____
Mingjiang Tao, Member

_____
Wen Chen, Member

_____
John E. Tobiason, Department Head
Civil and Environmental Engineering

DEDICATION

To my parents, wife, daughter, and son

ACKNOWLEDGMENTS

This research was funded primarily by the National Science Foundation (Award No: CMMI-1405745/1301070) and Jincheng Jinju Industrial Co., LTD.

Firstly, I would like to express my sincere gratitude to my advisor Prof. Guoping Zhang for the continuous support of my Ph.D. study and related research, for his patience, motivation, and immense knowledge. His guidance helped me in all the time of research and writing of this thesis.

Besides my advisor, I would like to thank the rest of my committee members: Prof. Don DeGroot, Prof. Mingjiang Tao, and Prof. Wen Chen, for their insightful comments and encouragement.

My sincere thanks also go to Prof. Sheila Seaman, Dr. Pete Dawson, who gave access to the laboratory and research facilities and provided me the help to complete experiments. Without their precious support it would not be possible to conduct this research.

I thank my lab mates for related academic discussion and technical support, especially Dr. Yongkang Wu, Dr. Shengming Luo, and Lindsay E. Duran.

Last but not the least, I would like to thank my family: my parents, my wife, my daughter, and my son for supporting me spiritually throughout writing this thesis and my life in general.

ABSTRACT

SYNTHESIS AND CHARACTERIZATION OF GEOPOLYMERS CAST AND CURED IN SALINE WATER AND THE POTENTIAL APPLICATION IN CONSTRUCTION ENGINEERING

MAY 2020

XIAONAN GE, B.S., XI'AN UNIVERSITY OF ARCHITECTURE AND TECHNOLOGY

M.S., TONGJI UNIVERSITY

Ph.D., UNIVERSITY OF MASSACHUSETTS AMHERST

Directed by: Professor Guoping Zhang

The characteristics of underwater cast and cured geopolymers were experimentally studied to understand the interactions between geopolymer slurry and curing saline water and pertinent effects on its strength development. Geopolymers were synthesized from a mixture of Class C fly ash and metakaolin, and the influences of two different Si/Al molar ratios (1.78 and 2.00) and four different Na/Al (0.67, 0.80, 0.84, and 1.00) molar ratios were investigated, respectively. The geopolymer slurry was prepared and then cast into porous molds, followed by immediately submerged into 0, 15, and 35 ppt saline solutions (prepared with commercial seasalts) for 28-days' curing in ambient laboratory environment. Parallel experiments were also performed on Class G oil well cement. The mineralogy, chemical composition, microstructure, and mechanical properties of the cured geopolymers were characterized by X-ray diffraction, X-ray fluorescence spectroscopy, scanning electron microscopy, and unconfined compression testing, respectively, together with measurements of the pH and salinity of all the curing solutions. The oil well cement exhibits a decreased compressive strength in high-salinity solutions, while geopolymers display the distinguishable performance. For the two geopolymers with different Si/Al

ratios, strength increases with increasing salinity, and a higher Si/Al ratio brings greater strength. For geopolymers with four Na/Al ratios, the results are relatively complicated. The strength of the geopolymers with Na/Al ratios of 0.67 and 0.80 increases with increasing salinity, while opposite to that with Na/Al ratios of 0.84 and 1.00. Under the same curing condition, a higher Na/Al ratio results in a decrease of strength. The results of X-ray fluorescence, pH, and salinity measurements show that the important alkali ions (e.g., Na^+, OH^-) not only leach out from the geopolymer slurry cured in relatively low-salinity solutions but also intrude into the slurry cured in high-salinity ones, thus leading to the change in the mechanical performance. Moreover, Na content of geopolymers as a direct indicator reflects the strength's variation trend. The underlying mechanism is the chemical exchanges, particularly the leaching or ingress of the alkali ions via dispersions, between the curing solution and being-cured geopolymer slurry, affecting the development of geopolymeric structure, which mainly contributes to the development of strength.

TABLE OF CONTENTS

Page

ACKNOWLEDGMENTS v

ABSTRACT vi

LIST OF TABLES xiii

LIST OF FIGURES xiv

LIST OF SYMBOLS xix

LIST OF ABBREVIATIONS xxi

CHAPTER

1 INTRODUCTION 1

1.1 Background 1

1.2 Dissertation Objectives and Motivation 3

1.3 Scope of Study 4

1.4 Research Significance 6

1.5 Dissertation Arrangement 6

2 LITERATURE REVIEW 9

2.1 Geopolymer Technology 9

2.1.1 Geopolymer 9

2.1.2 Brief History of Geopolymer 9

2.1.3 Mechanism of Geopolymerization 10

2.2 Research Methodology 12

2.2.1 Raw Materials Used to Synthesize Geopolymer 12

2.2.1.1 Fly Ash 12

2.2.1.2 Metakaolin 13

2.2.2 Synthesis of Geopolymer Mixtures 15

2.2.2.1 Mixture Design 15
2.2.2.1.1 Paste Mixture 16
2.2.2.1.2 Mortar Mixture.....16
2.2.2.1.3 Concrete Mixture 17
2.2.2.2 Synthesis of Paste 17
2.2.2.3 Synthesis of Mortar.....18
2.2.2.4 Synthesis of Concrete 18
2.2.2.5 Synthesis of Concrete 19
2.2.3 Geotechnical Experiments 20
2.2.3.1 Water Content 21
2.2.3.2 Specific Gravity 22
2.2.3.3 Sieve Analysis and Hydrometer Analysis.....22
2.2.3.4 Atterberg Limit (Plastic Limit and Liquid Limit Tests).....23
2.2.3.5 Unconfined Compression Testing.....24
2.2.3.6 pH Test.....25
2.2.3.7 Electrical Conductivity 26
2.2.4 Techniques of Analyzing Chemical and Mineral Composition and Micromorphology 26
2.2.4.1 Scanning Electron Microscope 27
2.2.4.2 X-ray Diffraction 28
2.2.4.3 X-ray Fluorescence 29
2.3 Resistance to Salts Corrosion.....31
2.4 Summary 41
3 SALINE WATER CURED GEOPOLYMER: EFFECT OF SI TO AL RATIO 55
3.1 Introduction.....55

3.2 Materials and Methods....59
3.2.1 Materials....59
3.2.2 Sample Preparation....61
3.2.3 Mechanical, Microstructural, and Chemical Characterization....63
3.3 Results and Discussion....65
3.3.1 Compositional Analysis by XRD....65
3.3.2 Mechanical Properties....66
3.3.3 Microstructure....69
3.3.4 X-ray Fluorescence Analysis....73
3.3.5 pH Measurements....76
3.4 Discussion....77
3.4.1 Difference from Prior Studies....77
3.4.2 Mechanisms for Strength Development....78
3.4.3 Practical Implications....79
3.5 Conclusions....80
4 SALINE WATER CURED GEOPOLYMER: EFFECT OF NA TO AL RATIO....98
4.1 Introduction....98
4.2 Materials and Methods....101
4.2.1 Materials....101
4.2.2 Geopolymer Syntheses....102
4.2.3 Mechanical, Microstructural, and Chemical Characterization....104
4.3 Analysis of Results....105
4.3.1 Compositional Analysis by XRD....105
4.3.2 Mechanical Properties....106
4.3.3 Microstructure....108

4.3.4 X-ray Fluorescence Analysis 110
4.3.5 pH Measurements 114
4.3.6 Salinity Measurements 115
4.4 Conclusions 116
5 THE POTENTIAL APPLICATION OF FLY ASH-BASED GEOPOLYMER CEMENT 137
5.1 Introduction 137
5.2 Materials and Methods 140
5.2.1 Materials 140
5.2.2 Sample Preparation 141
5.2.3 Characterization 142
5.3 Analysis of Results 143
5.3.1 Measurement of Feasible Range of Si/Al and Na/Si Molar Ratios 143
5.3.1.1 Effect of Si/Al Molar Ratio 144
5.3.1.2 Effect of Na/Si Molar Ratio 146
5.3.2 Effect of Water/Fly Ash Mass Ratio 146
5.3.3 Confirmation of Optimal Proportions 148
5.3.4 Effect of Fly Ash from Different Combustion Systems 149
5.3.5 Effect of Sand/Fly Ash Mass Ratio 150
5.4 Conclusions 152
6 THE POTENTIAL APPLICATION OF FLY ASH-BASED GEOPOLYMER CONCRETE 171
6.1 Introduction 171
6.2 Materials and Methods 173
6.2.1 Materials 173

6.2.2 Sample Preparation 174
6.2.2.1 Laboratory Test 174
6.2.2.2 Field Test 175
6.3 Results and Discussion 176
6.3.1 Effect of Proportion of Aggregates on Mechanical Performance 176
6.3.2 Durability of Geopolymer Concrete Road 177
6.4 Conclusions 178
7 CONCLUSIONS 198
7.1 Overview 198
7.2 Conclusions 199
8 REFERENCES 203

LIST OF TABLES

Table Page

2.1: Chemical requirements of fly ash. 51

2.2: Geopolymer mortar mix design example..... 52

2.3: Geopolymer concrete mixture design example (mass ratio). 53

2.4: Chemical composition of sea salts. 54

3.1: Size fraction (wt.%) and chemical composition[a] (wt.%) of fly ash and metakaolin. 96

3.2: The average Si/Al molar ratios of all geopolymer samples cured in different saline solutions. 97

4.1: Size fraction (wt.%) and chemical composition[a] (wt.%) of fly ash and metakaolin. 135

4.2: The actual average Na/Al and Si/Al molar ratios of all geopolymer samples cured in different saline solutions. 136

5.1: Size fraction (wt.%) and chemical composition (wt.%) of different fly ash. 169

5.2: Details of fly ash-based geopolymer mixture designs. 170

6.1: Details of fly ash-based geopolymer concrete mixture designs. 197

LIST OF FIGURES

Figure Page

1.1: Schematic diagram of application of geopolymer cement used in deep well.....8

2.1: Conceptual model for geopolymerization.....42

2.2: Structure of a kaolinite layer.....43

2.3: Paste mix procedure (from left to right: powder mix, alkaline mix, slurry).....44

2.4: Mortar mix procedure.....45

2.5: Concrete mixture and blender.....46

2.6: Split specimen molds made of porous HDPE cylinders: (a) a completely disassembled mold showing the two split half cylinders and two end caps; (b) a fully assembled mold fastened by a clamp; (c) partially assembled molds that are ready for geopolymer precursor casting. Note that a layer of plastic thin film is inserted between the end of the cylinder and the end cap to maintain better sealing.....47

2.7: The mold for concrete grout.....48

2.8: Schematic of an SEM.....49

2.9: Schematic illustration of Bragg's Law.....50

3.1: Particle size distribution of two raw materials, fly ash and metakaolin, used for geopolymer synthesis.....82

3.2: XRD patterns of raw materials and geopolymer samples cured in different saline solutions: (a) GC-1.78; (b) GC-2.00 (MK = metakaolin, CFA = Class C fly ash, Mu = Mullite, Ca = Calcite, He = Hematite, M = Magnetite, Q = Quartz).....83

3.3: Example stress-strain curves of Class G oil well cement and geopolymer samples.....84

3.4: Mechanical and physical property indexes of Class G oil well cement and geopolymer cement samples after 28 days curing: (a) unconfined compressive strength; (b) failure strains; (c) Young's modulus; (d) bulk densities (the error bars represent one standard deviation, which applies to other figures as well).....86

3.5: SEM micrographs of raw materials: (a) Class C fly ash; (b) metakaolin.....87

3.6: An SEM micrograph showing the overall microstructure and composition of the geopolymer samples 88

3.7: SEM micrographs of the GC-1.78 cured in saline water: (a) 0 ppt; (b) 15 ppt; (c) 35 ppt 89

3.8: Different appearance and microstructure of the exterior and interior layers of 15 ppt saline water-cured GC-2.00 samples: (a) and (b) optical images of the cross-sectional surface of two different cylindrical samples; (c) SEM micrograph of the exterior layer; (d) SEM micrograph of the interior layer 90

3.9: SEM micrographs of the GC-2.00 samples cured in different saline water: (a-b) 0 ppt; (c-d) 15 ppt; (e-f) 35 ppt; (a), (c), and (d) are from the exterior layer; (b), (d), and (f) are from the interior layer 91

3.10: SEM micrographs showing the different micromorphological features of fly ash particles: (a) unreacted hollow sphere; (b) unreacted cenosphere; (c) partially reacted solid sphere; (d) completely reacted solid sphere 92

3.11: Molar ratio of elemental composition of GC-2.00 (0 ppt) among Al, Na, Fe, Mg, Ca, K, and Si 93

3.12: Percentage of Na_2O of geopolymer samples under different curing conditions 94

3.13: Average pH value (a) and increment (b) of pH (ΔpH) of curing water (BC = before curing process; AC = after curing process) 95

4.1: Particle size distribution of raw materials used for geopolymer synthesis 117

4.2: XRD patterns of raw materials and geopolymer samples (GC-0.67, GC-0.80, GC-0.84 and GC-1.00) cured in different salinity solutions (MK = metakaolin, CFA = Class C fly ash; AC = air-curing, Mu = Mullite, Ca = Calcite, He = Hematite, M = Magnetite, Q = Quartz) 118

4.3: Example stress-strain curves of Class G oil well cement and geopolymer samples 119

4.4: Mechanical and physical property indexes of Class G oil well cement and geopolymer samples after 28 days curing: (a) unconfined compressive strength; (b) failure strains; (c) Young's modulus; (d) bulk densities (the error bars represent one standard deviation, which applies to other figures as well) 121

4.5: SEM micrographs of raw materials: (a) Class C fly ash; (b) metakaolin 122

4.6: An SEM micrograph showing the overall microstructure and composition of the geopolymer samples 123

4.7: optical images of the cross-sectional surface of two different cylindrical samples 124

4.8: SEM micrographs of the GC-0.67 samples cured in different saline water: (a-b) 0 ppt; (c-d) 15 ppt; (e-f) 35 ppt; (a), (c), and (d) are from the exterior layer; (b), (d), and (f) are from the interior layer 125

4.9: SEM micrographs of the GC-0.80 samples cured in different saline water: (a-b) 0 ppt; (c-d) 15 ppt; (e-f) 35 ppt; (a), (c), and (d) are from the exterior layer; (b), (d), and (f) are from the interior layer 126

4.10: SEM micrographs of the GC-0.84 samples cured in different saline water: (a-b) 0 ppt; (c-d) 15 ppt; (e-f) 35 ppt; (a), (c), and (d) are from the exterior layer; (b), (d), and (f) are from the interior layer 127

4.11: SEM micrographs of the GC-1.00 samples cured in different saline water: (a-b) 0 ppt; (c-d) 15 ppt; (e-f) 35 ppt; (a), (c), and (d) are from the exterior layer; (b), (d), and (f) are from the interior layer 128

4.12: The elemental composition of GC-0.67 sample cured in fresh water 129

4.13: Percentage of Na_2O in the final geopolymer samples cured under different conditions 130

4.14: Relationship between percentage of Na_2O of the interior layer and unconfined compressive strength: (a) GC-0.67, (b) GC-0.80, (c) GC-0.84, (d) GC-1.00 132

4.15: pH measurements of different curing solutions: (a) pH values before and after curing process; (b) the change in the pH (ΔpH) of the curing solutions (BC = before curing; AC = after curing) 133

4.16: The change in the salinity (Δsalinity) of curing solutions 134

5.1: Particle size distribution of fly ash (YC) and fly ash (JMNY) 154

5.2: The color of fly ash (JMNY and YC) 155

5.3: SEM images of fly ashes: (a) JMNY, (b) YC 156

5.4: The mold of geopolymer sample (1”-inside diameter, 2.5”-height) 157

5.5: Samples of geopolymer paste (Si/Al = 1.5, Na/Si = 1.25) 158

5.6: Samples of geopolymer paste (Si/Al = 1.5, Na/Si = 1.5) 159

5.7: Samples of geopolymer paste (Si/Al = 1.5, Na/Si = 2.0) 160

5.8: Average UCS of geopolymer samples with different Si/Al molar ratios: (a) Na/Si ratio of 1.25, (b) Na/Si ratio of 1.5, (c) Na/Si ratio of 2.0 161

5.9: Samples of geopolymer paste (Si/Al=2.0, Na/Si=1.0) 162

5.10: Summary of average UCS of geopolymer samples: Si/Al ratio of 1.65 to 2.0; Na/Si ratio of 1.25 to 2.0; water/fly ash ratio of 0.55 163

5.11: Mold of geopolymer sample (cube with 50 mm length) 164

5.12: Average UCS of geopolymer samples for different water/fly ash ratios..... 165

5.13: Summary of average UCS of geopolymer samples: Si/Al ratio of 1.5 to 1.8; Na/Si ratio of 1.5 to 2.0; water/fly ash ratio of 0.4 166

5.14: Average UCS of geopolymer samples synthesized from YC fly ash 167

5.15: Summary of average UCS of geopolymer mortar samples: 1.65-1.5; 1.80-1.5; 1.90-1.5 168

6.1: Concrete mixer, 0.5 m^3 180

6.2: Mold for concrete specimens: 150*150*150 (mm) 181

6.3: Shaking table 182

6.4: Thermotank for sample storage 182

6.5: Fly ash-based geopolymer concrete samples 184

6.6: Concrete mixer plant 185

6.7: Sodium silicate solution added from bucket to blender 186

6.8: NaOH solution added into blender 187

6.9: Mixing in blender 188

6.10: Concrete grout container 189

6.11: Schematic diagram of cast-in-situ site, 4*5 m^2 190

6.12: Construction site of area 1 ,2, 3 (cast-in-place) 191

6.13: Precast slabs produced at concrete mixer plant (left graph) and installed at construction site (right graph) 192

6.14: Summary of average UCS of geopolymer concrete samples in different proportion of aggregates 193

6.15: Summary of average UCS of geopolymer concrete samples using different batches of fly ash 194

6.16: Construction site 195

6.17: Summary of long-term average UCS of geopolymer concrete specimens 196

LIST OF SYMBOLS

Symbol	Description
Al	Aluminum
Al_2O_3	Aluminum oxide
$Al(OH)_3$	Aluminum hydroxide
CO_2	Carbon dioxide
Ca	Calcium
$CaCl_2$	Calcium chloride
$CaCO_3$	Calcium carbonate
$Ca(OH)_2$	Calcium hydroxide
CaO	Calcium oxide
Cl	Chlorine
Fe_2O_3	Iron oxide
H_2O	Water
H_2S	Hydrogen sulfide
K^+	Potassium cation
KeV	Kiloelectronvolt
KOH	Potassium hydroxide
KCl	Potassium chloride
K_2CO_3	Potassium carbonate
K_2O	Potassium oxide
M^+	Alkali cation
Mg	Magnesium
$MgCl_2$	Magnesium chloride
$MgCO_3$	Magnesium carbonate
$Mg(OH)_2$	Magnesium hydroxide
$MgSO_4$	Magnesium sulfate
MgO	Magnesium oxide
Na^+	Sodium cation
Na	Sodium
Na_2O	Sodium oxide
NaOH	Sodium hydroxide
Na_2SO_4	Sodium sulfate
Na_2SiO_3	Sodium silicate
O	Oxygen
Si	Silicon
Sr	Strontium
SiO_2	Silicon dioxide
SO_3	Sulfur trioxide
SO_4^{2-}	Sulfate ion
g	Gram
Kg	Kilogram
kV	Kilovolt
Lb	Pound
M	Molar per liter
ml	Milliliter

mmol	Millimolar
meq	Milliequivalents
MPa	Megapascal
ppt	Part per thousand
min	Minute
d	Day
h	Hour
s	Second
wk	Week
y	Year
cm	Centimeter
m	Meter
nm	Nanometer
mm	Millimeter
µm	Micronmeter
°C	Degree Celsius

LIST OF ABBREVIATIONS

AAFA	Alkali-activated fly ash
API	American Petroleum Institute
ASTM	American Society of Testing and Materials
BSE	Back-scattered electrons
BW	Brine water
CFA	Class C fly ash
CL	Cathodoluminescence
C-S-H	Calcium silicate hydrate
FG	Fly ash geopolymer
Fig	Figure
FSG	Fly ash-slag geopolymer
GC	Geopolymer cement
HP	High-pressure
HT	High-temperature
JMNY	Jinmeinengyuan
LOI	Loss on ignition
MK	Metakaolin
No.	Number
OPC	Ordinary Portland cement
OWC	Class G oil well cement
pH	Potential of hydrogen
PN	Percentage of Na_2O
RH	Relative humidity
RHA	Rice husk ash
RO	Reverse osmosis water
SE	Secondary electrons
SEM	Scanning electron microscopy
SD	Standard deviation
TB	Total Bicarbonate
TCO_2	Total CO_2 gas
UCS	Unconfined compressive strength
UCT	Unconfined compression testing
USA	The United States of America
W	Water
wt	Weight
XRD	X-ray diffraction
XRF	X-ray fluorescence
YC	Yangcheng

CHAPTER 1

INTRODUCTION

1.1 Background

Ordinary Portland cement (OPC), a typical cementitious binder, is the most common type of cement used in general around the World as an elementary constituent of mortar, concrete, stucco, and grout. OPC shows excellent strength and is considered as an adaptable and affordable material widely used in construction.

However, the universal application of OPC also brings many issues including safety issue and environmental effects. One of the widely recognized problems is the carbon dioxide (CO_2) emission, one of the key greenhouse gases causing global warming, whose threats may include the inundation of low-lying coastal zones due to the melting of polar ice caps, regional decreases in food production, the deterioration of eco-systems, and the spread of diseases [1]. The quantity of CO_2 released in the manufacturing of cement is around one ton for one ton of cement clinker. CO_2 is responsible for 64% of the effects among all greenhouse gases [2]. There are two main methods to reduce the amount of CO_2 emissions: (1) directly capture and store the CO_2 such as geo-sequestration, which may be considered to be one of the largest-scale mitigation methods to combat the greenhouse gases [3–5]. The sequestration wells play a major role in the success of sequestration project, and the well integrity should be maintained for efficient sequestration; (2) reduce the CO_2 emissions caused by industrial production. For example, new cementitious materials with low or no CO_2 emissions can replace the OPC in most of the constructions. Another problem is the limitations or drawbacks of the OPC used in well-cementing. In the USA, Class G or H cement is generally recommended as well cementing for geo-

sequestration or deep wellbores that usually exist in brine formations. However, it has been demonstrated by several studies that there are many problems associated with the applications of the well cements, such as cement degradation, lack of enough chemical (e.g., acid) resistance, lack of long-term durability, leakage, and strength reduction in high-salinity environments [6–12]. Therefore, it is necessary to resolve the issues pertinent to the applications of OPC to deep well projects, such as low-resistance to acid and salt corrosion, particularly at high-temperature (HT) and high-pressure (HP) environments in the deep subsurface by investigating or developing new cementitious materials.

Geopolymer, as a new class of cementitious material, has attracted considerable attention all over the World, because of its superior compressive strength, low permeability, excellent chemical resistance, and exceptional fire resistance, among others [13–21]. This developing class of cementitious material has many advantages over the traditional OPC, such as low energy consumption and hence more sustainable, and low carbon footprint. These advantageous properties of geopolymer can meet the above demands. It is a potential alternative to OPC and other cementitious binders that may find plenty viable applications in civil infrastructure [22,23].

The Part I of thesis research will be conducted to assess the performance of geopolymer cement as a viable potential oil well cement using traditional OPC-based Class G oil well cement as a reference for comparison. The considered potential application focuses on the oil wells at depths of ~10,000 ft (3,048 m), as shown in Fig 1.1. In order to replace potentially the Class G oil well cement, several requirements[24] should be satisfied: (1) long-term integrity; (2) resistance to water; (3) little or no shrinkage; (4) supporting mechanical loads and impacts; (5) resistance to different chemicals and other

substances (H_2S, CO_2, hydrocarbons, and saline water), especially at HT and HP; (6) ensured bonding to steel; (7) non-harmful damage to the steel rebars integrity. The main focus of this part is on analyzing the effects of saline water on the microstructure, physical, chemical, and mechanical properties of geopolymers.

The Part II of the research is to test the performance of different design mixes of paste, mortar and concrete based on the fly ash-based geopolymer in order to obtain the optimal recipes. And then the recipe of geopolymer concrete will be applied in the small-scale field experiments, which should at least satisfy the demand of traditional OPC concrete on the engineering application. But in this thesis, study will mainly focus on the strength and durability.

In this study, strength of geopolymer samples was gained by unconfined compression testing (UCT). Then Chemical and mineralogical compositions analyses, including the pH and salinity of the curing water, scanning electron microscopy (SEM), X-ray diffraction (XRD), and X-ray fluorescence spectroscopy (XRF), were conducted to investigate the mechanisms for the different performance of geopolymer samples.

1.2 Dissertation Objectives and Motivation

This planned research aims to reach two major objectives. The first one is to investigate the effects of the Si/Al and Na/Al molar ratios on the performance of geopolymers cast and cured in saline water on the mechanical properties, microstructure, and the changes in the chemical and mineralogical compositions at ambient environments. The second one is to study the possible transfer of the geopolymer technology into practical applications.

1.3 Scope of Study

To achieve the three objectives described above, the scope of this research is confined as follows:

The first objective: Effects of the Si/Al and Na/Al molar ratios on the geopolymers cast and cured in the saline water at ambient environments.

1) Investigation and determination of raw aluminosilicate materials for synthesizing geopolymer samples in the laboratory, including the type and fraction of different raw materials in the design mix; Some basic physical and chemical properties of the raw materials will also be determined, including the specific gravity [25], Atterberg limits [26], water content [27], particle size distribution [28], microstructure by SEM, chemical or elemental composition by XRF, mineralogical composition and estimation of reactivity via XRD.

2) Manufacturing of sample molds that can best simulate the actual subsurface conditions of deep oil wells or CO_2 geo-sequestration wells. In this part of research focusing on the ambient environments, more attention is paid on only the molds that can permit the possible ion exchange with salts in water but do not react with the chemicals in water or geopolymer slurry. Therefore, porous high-density polyethylene mold is a more appropriate choice.

3) Since the ion exchange through the porous mold between geopolymer slurry and saline water is permitted during the curing process, the changes in the pH and salinity of curing solutions should be monitored during curing and upon the completion of curing process. This is achieved by measuring the pH [29] and electrical conductivity [30] of the

curing saline solutions. The volume of curing solutions for each sample is kept constant to ensure accuracy and comparability.

4) Conducting the UCT to obtain strength data. It is important to develop the correlations between the unconfined compressive strength (UCS) and mixture design as well as the salinity of curing solutions.

5) Sections of the cured geopolymer samples in the interior and exterior cylinders will be analyzed the microstructure and chemical compositions via SEM, XRD, and XRF, and hence to find the relationships between UCS and chemical compositions and further help explain the variations of UCS.

6) Evaluation of all experimental results and comparison with previous literature.

The second objective: Transfer of the laboratory research to the practical engineering constructions.

1) Studying the basic characteristics of fly ash from different power plants including specific gravity, water content, particle size distribution, microstructure by SEM, chemical or elemental composition by XRF, mineralogical composition and estimation of reactivity via XRD.

2) Obtaining the range of UCS through testing different mixture designs by altering the molar ratios of Si/Al and Na/Al and the mass ratio of water/fly ash.

3) Considering other important factors such as cost together with different UCS to find some optimal mixture designs.

4) Converting the findings of the laboratory-research to field trials and demonstration experiments.

1.4 Research Significance

1) This study will obtain the deeper understanding of effect of saline water on the performance of geopolymer.

2) As a potential general engineering material, the research can promote the widely application of geopolymer paste, mortar and concrete in different fields of engineering construction. And at the same time, it possibly brings the new method to solve the environmental pollution problems caused by solid waste.

1.5 Dissertation Arrangement

The thesis is organized in seven chapters as outlined below:

Chapter 1 introduces the background, motivation and scope of study, and research significance.

Chapter 2 presents the concept of geopolymer as well as its brief historical development and the generally accepted mechanism. Then the type of raw materials and their physical and chemical properties are described. And then it establishes the mixture design and experimental methods. Finally, the recent development in the geopolymer's resistance to salt corrosion is stated.

Chapter 3 presents the effect of Si/Al molar ratio on the properties of fly ash and metakaolin-based geopolymer cured in saline water such as mechanical, microscope, and chemical properties.

Chapter 4 presents the influence of Na/Al molar ratio of fly ash and metakaolin-based geopolymer cured in saline water.

Chapter 5 presents the investigation of the potential application of fly ash-based geopolymer cement, including the factors as Si/Al molar ratio, Na/Si molar ratio, water/fly ash mass ratio, which are used to confirm the optimal proportions. Besides, fly ash from different combustion system is studied to verify the distance of quality. Finally, it studies the effect of sand/fly ash mass ratio on the mechanical property of fly ash-based geopolymer mortar.

Chapter 6 presents the results of compression testing of fly ash-based geopolymer concrete in laboratory which investigates the effect of proportion of aggregates and obtain the optimal mixture for field testing. Then it shows the process of field-testing including blending of raw materials, casting, and pre-casting and the final product: road pavement.

Chapter 7 presents the final conclusions.

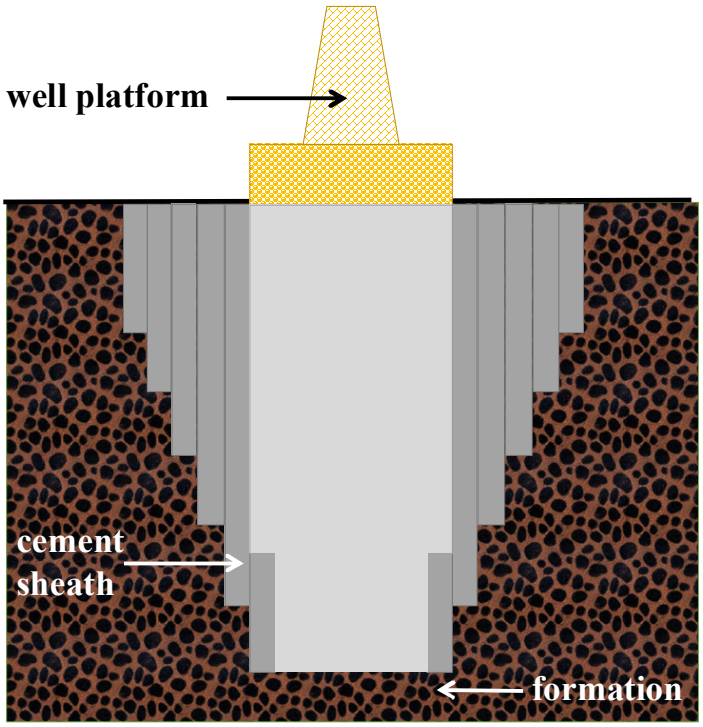

Figure 1.1: Schematic diagram of application of geopolymer cement used in deep well.

CHAPTER 2

LITERATURE REVIEW

2.1 Geopolymer Technology

2.1.1 Geopolymer

The term “geopolymer” was formed and applied in 1979, by a French scientist, Joseph Davidovits. This mentioned geopolymer is a kind of inorganic polymer, possessing three-dimensional aluminosilicate structures comprising of linked SiO_4 and AlO_4 tetrahedral by sharing all the oxygen atoms [32–34]. The geopolymer material’s chemical structure is parallel to usual zeolitic materials, but the microstructure is amorphous instead of crystalline [35,36].

2.1.2 Brief History of Geopolymer

Geopolymer and alkali-activation technology have been known in the field of cement and concrete industry for approximately eight decades. Purdon [37] synthesized the first alkali-activated binder using furnace slag and sodium hydroxide. In the 1950s, Glukhovsky [38] proposed a general mechanism for the alkali activation of materials primarily comprising silica and reactive alumina. His model divides the process into three stages: (a) destruction-coagulation; (b) coagulation-condensation; (c) condensation-crystallization, which is the initial model of recently theories developed by different authors. In late 1970s, Davidovits developed a mineral polymer with three dimensional polysialate chains, which resulted from the hydroxylation and poly-condensation reaction of natural minerals such as clay, slag, fly ash and pozzolan on alkaline activation [39].

During the period from 1979 to 1999, there are only around 91 journal papers and patents as well as one conference proceedings (Geopolymer 99) that were published in the field of geopolymer and geopolymerization [40]. However, high-quality research on geopolymeric materials was accelerated [41] in late 1990s and there was an obvious growth tendency in geopolymer research in the most recent 20 y. The team of Fernandez-Jimenez and Palomo in Spain and a team of van Jaarsveld and van Deventer in Australia published immense amounts of research on geopolymer technology especially focusing on the microstructure and morphology of different kinds of alkali activated materials. Bakharev and Nasvi also reported numerous studies on the chemical resistance of geopolymer materials such as acid and salts. Then variety of potential applications of geopolymers were discovered and studied, including fire resistant materials, decorative stone artifacts, thermal insulation, low-tech building materials, low energy ceramic tiles, refractory items, thermal shock refractories, bio-technologies (materials for medicinal applications), foundry industry, cements and concretes, composites for infrastructures repair and strengthening, high-tech resin systems, radioactive and toxic waste containment, arts and decoration, cultural heritage, archaeology and history of sciences [22].

2.1.3 Mechanism of Geopolymerization

Geopolymer is production of activating different aluminosilicate materials with strong alkaline solution such as sodium hydroxide, potassium hydroxide, sodium silicate solution. Geopolymerization is the process of combining many small molecules known as oligomers (dimer, trimer, tetramer, pentamer) into a covalently bonded network. The specific process can be shown with an example of fly ash in alkaline medium: (1) The

aluminosilicates from the fly ash particle dissolve in the alkaline medium, releasing aluminates and silicates, probably as monomers; (2)These monomers inter-react to form dimers, which in turn react with other monomers to form trimers, tetramers and so on; (3) When the solution reaches saturation, an aluminum-rich gel (denominated Gel 1) precipitates; (4) As the reaction progresses, more Si-O groups from the initial solid source dissolve, increasing the silicon concentration in the medium and gradually raising the proportion of silicon in the zeolite precursor gel (Gel 2); (5) Polycondensation into zeolite-like 3D-frameworks. Duxson et al. [14] presented these in a conceptual model as shown in Fig 2.1.

A common formula for the chemical structure of geopolymers is as follows: $M^{+}_{n}\{-(SiO_2)_z\text{-}AlO_2\text{-}\}_n$, where M^+ is an alkali cation (K^+ or Na^+) for balancing the negative charge for Al, n is the degree of polymerization, and z is the Si/Al molar ratio, fluctuating from 1 to 15, and up to 300 [42–44]. Some typical structures of geopolymer are:

Si/Al = 1, poly-sialate, { − Si − O − Al − O − }

Si/Al = 2, poly-sialate siloxo { − Si − O − Al − O − Si − O − }

Si/Al = 3, poly-sialate disiloxo { − Si − O − Al − O − Si − O − Si − O − }

Si/Al > 3, sialate link

Geopolymers present different properties with the different Si/Al ratios: Low Si/Al ratios (< 3) lead to three-dimensional and cross-linked networks with stiff and brittle properties (such as cement and ceramics); high ratios (> 3) result in two-dimensional networks or linearly linked networks with adhesive and rubbery properties [45].

According to popular mechanisms [14,33,46–48], geopolymerization can be divided into three major steps that interact with each other along the reaction:

(1) the amorphous aluminosilicate materials dissolved by alkali hydroxide solution to form reactive silica and alumina.

(2) reorientation, which is the transportation, orientation, or condensation of dissolved precursor ions into monomers.

(3) the dissolved species polycondense into amorphous or semi-crystalline aluminosilicate polymers.

The formation of geopolymers contains two following reactions [49,50]:

$$n(Si_2O_5, Al_2O_2) + 2nSiO_2 + 4nH_2O + NaOH/KOH \rightarrow Na^+, K^+ + n(OH)_3\text{-}Si\text{-}O\text{-}Al^-(OH)_2\text{-}O\text{-}Si\text{-}(OH)_3$$

(Si-Al material) (Geopolymer precursor)

$$n(OH)_3\text{-}Si\text{-}O\text{-}Al^-(OH)_2\text{-}O\text{-}Si\text{-}(OH)_3 + NaOH/KOH \rightarrow (Na^+, K^+)\text{-}(\text{-}Si\text{-}O\text{-}Al^-(O)\text{-}O\text{-}Si\text{-}(O)\text{-}) + 4nH_2O$$

(Geopolymer precursor) (Geopolymer backbone)

2.2 Research Methodology

2.2.1 Raw Materials Used to Synthesize Geopolymer

2.2.1.1 Fly Ash

Fly ash is a coal combustion product that is composed of the particulates (fine particles of burned fuel) that are driven out of coal-fired boilers together with the flue gases, processed by the dust collection system, either mechanically or by using electrostatic precipitators before they are discharged to the atmosphere. Fly ash particles are typically sphere, finer than Portland cement and lime, ranging in diameter from 0.5 μm to 100 μm. The major influence on the fly ash chemical composition comes from the type of coal. The combustion of sub-bituminous coal contains more calcium and less iron than fly ash from

bituminous coal. The physical and chemical properties are determined by the combustion methods, coal source, and particle shape. The chemical compositions of various fly ashes show a wide range, indicating that there is a wide variation in the coal used in power plants all over the world [51].

According to ASTM C618 [52], the fly ash is divided into three classes: Class N, Class F and Class C. The main difference among these classes is the content of calcium in ash, as well as silica, alumina, and iron. Fly ash shall conform to the requirements as to chemical composition prescribed in Table 2.1.

Class N—Raw or calcined natural pozzolans that comply with the applicable requirements for the class as given herein, such as some diatomaceous earths; opaline cherts and shales; tuffs and volcanic ashes or pumicites, calcined or un-calcined; and various materials requiring calcination to induce satisfactory properties, such as some clays and shales.

Class F—Fly ash that meets the applicable requirements for this class as given herein. This class of fly ash has pozzolanic properties.

Class C—Fly ash that meets the applicable requirements for this class as given herein. This class of fly ash, in addition to having pozzolanic properties, also has some cementitious properties.

2.2.1.2 Metakaolin

Kaolinite is a clay mineral (Fig 2.2 [53]) with the chemical composition $Al_2Si_2O_5(OH)_4$. It is a layered silicate mineral, with one tetrahedral sheet of silica (SiO_4) lined through oxygen atoms to one octahedral sheet of alumina (AlO_6) octahedra [54].

Rocks that are rich in kaolinite are known as kaolin or China clay [55]. Individual particles of kaolinite form stacks with hydrogen bonds and van der Waals forces holding together successive particles [56]. The strength of these bonds prevents water from entering the interlayer spaces and causing swelling [56]. Cation exchange capacity (CEC) values for kaolinite typically range between 3 to 15 meq / 100 g [56].

The name “kaolin” is derived from “Gaolin”, a Chinese village near Jingdezhen in southeastern China’s Jiangxi Province. Kaolinite has a low shrink-swell capacity, traditionally used in the manufacture of porcelain. It is a soft, earthy, usually white mineral, produced by the chemical weathering of aluminum silicate minerals like feldspar.

Metakaolin is the anhydrous calcined form of the clay mineral kaolinite associated with the reaction of $Al_2Si_2O_5(OH)_4 \rightarrow Al_2Si_2O_7 + 2H_2O$ [57]. The dehydroxylation of kaolin to metakaolin is an endothermic process due to the large amount of energy required to remove the chemically bonded hydroxyl ions. Reported optimum activation temperatures vary between 550 and 850 ℃ for varying duration, however, the range 650 - 750 ℃ is most commonly quoted [58]. Metakaolin is a highly pozzolanic and reactive material. However, in order to produce a pozzolan (supplementary cementitious material) nearly complete dehydroxylation must be reached without overheating, i.e., thoroughly roasted but not burnt. This produce an amorphous, highly pozzolanic state, whereas overheating can cause sintering, to form a dead burnt, nonreactive refractory, containing mullite and a defect Al-Si spinel (ACT 2010).

2.2.2 Synthesis of Geopolymer Mixtures

2.2.2.1 Mixture Design

Based on the previous reports, the chemical composition and reactivity of the raw materials and activators are the two important factors that mainly controls the properties of alkali activated cement.

Palomo et al. [35] studied the Class F fly ash-based geopolymer activated by the different activators with the solution-to-fly ash ratio of 0.25 and 0.30 by mass. The range of Si/Al and Na/Al molar ratios for the products of reaction was 1.5 to 2.8 and 0.46 to 0.48, respectively. The results showed that a combination of sodium hydroxide and sodium silicate solution lead to the highest compressive strength after curing the specimens for 24 h at 65 °C. Barbosa et al. [59] designed seven mixtures of metakaolin-based geopolymer paste with the following range of molar ratios: $0.4<Na/Si<0.96$ (activator), $1.65<Si/Al<2.25$, and $10<H_2O/Na_2O<25$. The tests performed on the paste samples presented that the optimum composition occurred when the ratios of Na/Si (activator), Si/Al, and H_2O/Na_2O were 0.5, 2.25, and 10, respectively. He et al. [60] explored the effect of Si/Al molar ratio on the compressive strength of metakaolin-based geopolymer. Such geopolymer was designed at three different Si/Al ratios of 1.25, 1.75, and 2.25 with constant molar ratio H_2O/Na_2O of 17.5. As a result, the compressive strength increased almost linearly with the Si/Al ratio. Zhang et al. [61] studied the feasibility of metakaolin-based geopolymer in stabilizing soils with Si/Al molar ratio of 1.5 to 2.0 and a constant Na/Al molar ratio of 1, as shown in the literature that these Si/Al molar ratios bring

geopolymer with high mechanical strength. The final testing results presented that UCS was maximized at Si/Al molar ratio of 1.7.

2.2.2.1.1 Paste Mixture

The part of this study was to prepare paste samples, in which the mixture of fly ash and metakaolin or the pure fly ash was the one and only aluminosilicate resource. Alkaline activator was the mix of sodium hydroxide and sodium silicate solution. The variables existed in the mixture design contained:

- The molar ratio of Si/Al: (1) research Part I, 1.78 and 2.0; (2) research Part II, 1.5 to 2.0.
- The molar ratio of Na/Al: 0.67, 0.80, 0.84, and 1.00.
- The molar ratio of Na/Si (activator): 1.0 to 2.0.
- The mass ratio of water/aluminosilicate raw material: 55%, 50%, 45%, 40%, 35%, 25%, 20%.

2.2.2.1.2 Mortar Mixture

In research Part II, three different mix designs were chosen to study the effect of amount of sand on the compressive strength of geopolymer. Fly ash was the only aluminosilicate raw material. The activator solution was same to that in paste mixture design. The mass ratio of sand/fly ash was from 1 to 3. Such mortar mixtures were proposed based on the GB/T14685-2011 [62]. Table 2.2 shows the recipes for mortar mix design.

2.2.2.1.3 Concrete Mixture

This study was based on the geopolymer concrete in which fly ash was the only aluminosilicate raw material. Mixture of sodium hydroxide and sodium silicate solution was still the alkaline activator. The primary concrete mixtures were proportioned based on the previous works on the fly ash-based geopolymer concrete in this study. While the strength and durability of the final product is significant, economy and sustainability are other factors that should be considered. Unlike OPC concrete, geopolymer concrete has no explicit mix design guideline. Thus, the selection of aggregates was based on some published papers [63–66]. In addition, the workability of wet concrete based on its placement and compaction will affect the mechanical and durability of hardened concrete. Poor workability would lead to stiff concrete that is hard to process in the construction. Thus, it is necessary to take into consideration the workability of the mix design to ensure the easily usability of concrete. The wet geopolymer concrete is viscous to some extent so that addition of extra water can improve its workability. However, water is found to be detrimental to the mechanical properties of geopolymer. Therefore, it is essential to obtain the balance between workability and mechanical properties of final product. In the mixture design of geopolymer concrete, the Si/Al and Na/Al molar ratios came from the optimal results of paste mixture in section 2.2.2.1.1, and options of fine and coarse aggregates is shown in Table 2.3.

2.2.2.2 Synthesis of Paste

The geopolymers were synthesized from pure fly ash or a mixture of fly ash and metakaolin, which should be dried in the oven overnight (at least 8 h). The alkaline solution

was prepared at least ahead of one day. Firstly, the NaOH and RO water were mixed by a glass stirring rod and left to cool down to the room temperature. Then sodium silicate solution was added to the NaOH solution, followed by mixing for at least 5 min and allow them to rest overnight with covering in order to fully blend. The blended solution was combined with the dry powder mixture, followed by mixing for a minimum of 15 min to ensure thorough mixing among the powder and solution, resulting in the formation of geopolymer precursor in the form of a slurry. The synthesis procedure is as follows (Fig 2.3).

2.2.2.3 Synthesis of Mortar

The mixing of geopolymer mortars followed the same steps as paste mixtures. The sand was dried before mixing. The alkaline solution was prepared one day before mixing with powder. Due to the addition of sand, the geopolymer mortar was mixed automatically in a mix blend to obtain a uniform mortar mixture. The powder and solution were mixed together for 5 min to gain paste. Then the sand was added, and mixing was continued for another 5 min until a consistent mixture was obtained. Fig 2.4 shows the process of mixing.

2.2.2.4 Synthesis of Concrete

The mixing of geopolymer concrete mixture followed some steps as mortar mixtures. All materials were prepared well ahead of mixing. The alkaline solution was prepared one day before mixing and stored in beaker sealed with plastic film after cooling. In order to control the designed water content, a little moist fly ash was dried ahead in oven overnight as well as the fine aggregate. The coarse aggregate was dried in the air. Before

final mixing, the blender was cleaned to remove any other materials left from last testing. Its inner surface was moistened slightly to avoid water adsorption from the mixture. Firstly, the fly ash was mixed with alkaline solution for 5 min. Then the fine and coarse aggregates were added into the blender and mixed for another 5 min. If required, additional water was added to the mixture to improve the fluidity. Fig 2.5 presents the blender and concrete mixture.

2.2.2.5 Synthesis of Concrete

In research I, to create commonly shaped specimens for mechanical testing, one part of prepared geopolymer precursors were transferred into preassembled cylindrical porous molds (Fig 2.6) with an inner diameter of 1 inch and height of 2.5 inch (i.e., an aspect ratio of 2.5 to minimize the end effects), vibrated by hand to remove the trapped air, followed by totally immersing and curing in saline water with different salinity (0, 15, 35 ppt) in a laboratory ambient environment for 28 d. Saline water was made of Sea Salts from Instant Ocean Company [67], which was compositionally the closest to ocean water. Table 2.4 shows the chemical composition of such sea salts.

The other slurry was poured into a plastic split mold (air-curing) with an inner diameter of 2 cm and height of 5 cm, followed by fixing with steel clamp, where no transfer of chemicals was allowed in the samples. Prior to assembling, the interior of mold was coated with a thin layer of vacuum grease for easy removal of specimens after 28 d curing duration. To ensure repeatability, normally 3-4 samples were prepared for each type of geopolymer. For OWC, the same method of sample preparation for geopolymer was

adopted with liquid to solid ratio of 0.5. After 28 d of curing, each specimen was de-molded and then allowed to air dry for a minimum of one week.

In research II, prior to casting, all molds (Fig 2.7) were cleaned to eliminate the residue and impurities. The inner surface was cleaned and greased with a release agent. The concrete mixture was cast immediately after mixing. The molds were filled in two layers. After pouring each layer, the mixture was compacted by rodding and then vibrated on vibration table [68]. The molds were then stored in thermotank of 20 - 23 ℃ and 90% relative humidity. The surface of the mold was sealed with plastic film. After 3 - 7 d, the samples were de-molded and left in the thermotank until 28 d.

2.2.3 Geotechnical Experiments

For experiments in the lab, every kind of powder raw material should be dried before testing. Thus, water content can be measured during such process, although it was not important index. However, before conducting the field testing, it is necessary to obtain the data of water content of fly ash and sand, since this part of water existed in the raw materials will directly affect the calculation of designed water content in the geopolymer mixture, which should be considered ahead. In order to obtain the particle size distribution of fly ash and metakaolin, the specific gravity should be done firstly, after which the result will be used together with the data of sieve analysis and hydrometer analysis for calculation. The Atterberg limit testing were conducted to acknowledge the plastic limit and liquid limit of powder. According to the purpose of this research, the mechanical properties of samples will be offered by the UCT. Because of some samples dipped in the curing solution, in

which the ion exchange will happen in the whole process of curing, the value of pH and salinity (electrical conductivity) should be monitored for the chemical analysis.

2.2.3.1 Water Content

According to ASTM D2216 [27], water content, ω, is the ratio of the mass of water contained in the pore spaces of soil or rock material, to the solid mass of particles in that material, expressed as a percentage. The standard method for measuring the water content is that a test specimen is dried in an oven at a temperature of 110 ± 5°C to a constant mass. For many materials, the water content is one of the most significant index properties used in establishing a correlation between soil behavior and its index properties. The water content of a material is used in expressing the phase relationships of air, water, and solids in a given volume of material. In fine-grained (cohesive) soils, the consistency of a given soil type depends on its water content. The water content of a soil, along with its liquid and plastic limit as determined by Test Method ASTM D4318 [26], is used to express its relative consistency or liquidity index. The water content is calculated as follows:

$$\omega = [(M_{cms} - M_{cds})/(M_{cds} - M_c)] \times 100 = (M_\omega / M_s) \times 100$$

where:

ω = water content, %

M_{cms} = mass of container and moist specimen, g,

M_{cds} = mass of container and over dry specimen, g,

M_c = mass of container, g,

M_w = mass of water, g,

M_s = mass of oven dry specimen, g.

2.2.3.2 Specific Gravity

According to ASTM D854 [25], specific gravity of soil solid, Gs, is the ratio of the mass of a unit volume of a soil solids to the mass of the same volume of gas-free distilled water at 20℃. The specific gravity of soil solids is used in calculating the phase relationships of soils, such as void ratio and degree of saturation. The term "soil solids" is typically assumed to mean naturally occurring mineral particles or soil like particles that are not readily soluble in water. The specific gravity, Gs, is calculated as follows:

$$G_s = \rho_s / \rho_{w,t} = M_s / [M_{\rho w,t} - (M_{\rho ws,t} - M_s)]$$

where:

ρ_s = the density of the soil solids Mg/m^3 or g/cm^3,

$\rho_{w,t}$ = the density of water at the test temperature (Tt), g/ml or g/cm^3,

M_s = the mass of the oven dry soils, g,

$M_{\rho w,t}$ = the mass of pycnometer and water at the test temperature (Tt), g,

$M_{\rho ws,t}$ = the mass of pycnometer, water, and soil solids at the rest temperature (Tt), g.

2.2.3.3 Sieve Analysis and Hydrometer Analysis

Sieve analysis is a practice or procedure used to access the particle size distribution of a granular material by allowing the material to pass through a series of progressively smaller mesh size and weighing the amount of material that is stopped by each sieve as a fraction of the whole mass. Hydrometer measures the specific gravity of the soil suspension

at the center of its bulb. The specific gravity depends upon the mass of solids present, which in turn depends upon the particle size.

According to ASTM 422 [28], the distribution of particle sizes larger than 75 μm (retained on the No. 200 sieve) is determined by sieving. Conducting the sieving operation by means of a lateral and vertical motion of the sieve, accompanied by a jarring action in order to keep the sample moving continuously over the surface of the sieve. Determine the mass of each fraction on a balance. At the end of weighing, the sum of the masses retained on all the sieves used should equal closely the original mass of the quantity sieved. The distribution of particle sizes smaller than 75 μm is determined by a sedimentation process, using a hydrometer to secure the necessary date. Immediately after dispersion, transfer the soil-water slurry to the glass sedimentation cylinder, using the palm of the hand over the open end of the cylinder (or a rubber stopper in the open end), turn the cylinder upside down and back for a period of 1 min to complete the agitation of the slurry. or as many as may be needed, depending on the sample or the specification for the material under test: 2, 5, 15, 30, 60, 250, and 1440 min.

2.2.3.4 Atterberg Limit (Plastic Limit and Liquid Limit Tests)

According to ASTM D4318 [26], Originally, six “limits of consistency” of fine-grained soils were defined by Albert Atterberg: the upper limit of viscous flow, the liquid limit, the sticky limit, the cohesion limit, the plastic limit, and the shrinkage limit. In current engineering usage, the term usually refers only to the liquid limit, plastic limit, and in some references, the shrinkage limit.

Liquid limit (LL, w_L) is the water content, in percent, of a soil at the arbitrarily defined boundary between the semi-liquid and plastic states. Plastic limit (PL, w_P) is the water content, in percent, of a soil at the boundary between the plastic and semi-solid states. Plasticity index (PI) is the range of water content over which a soil behaves plastically. Numerically, it is the difference between the liquid limit and the plastic limit (PI = LL - PL). Liquidity index is the ratio, expressed as a percentage of the water content of a soil minus its plastic limit, to its plasticity index.

2.2.3.5 Unconfined Compression Testing

According to ASTM D2166 [69], UCT is the compressive stress at which an unconfined cylindrical specimen of soil will fail in a simple compression test. In this test method, UCS is taken as the maximum load attained per unit area or the load per unit area at 15% axial strain, whichever is secured first during the performance of a test. But in this study, the samples are similar to the hydraulic cement mortars or cylindrical concrete specimens. Therefore, the concept of UCS was borrowed, and the process of compression test is based on ASTM C39 [31] and ASTM C109 [70].

In the lab of UMass Amherst, cured samples were tested for their UCT using Geotest instruction strain-controlled loading frame with 10,000 lb load cell at a persistent strain rate of 0.5%/min for OWC and geopolymer samples. The two ends of each specimen were capped with Plaster of Paris, followed by correcting with sandpaper and level gauges to allow perpendicularity requirement. Before compression testing, a very thin coating of lubricant was applied to the two ends of each sample in order to decrease the resistance and hence shear stress development among the samples end surfaces and stainless-steel

end platens of the loading frame. In Jincheng, China, compression test was conducted [66,71].

2.2.3.6 pH Test

In chemistry, pH is a scale used to specify how acidic or basic a water-based solution is. The pH scale is logarithmic and approximates the negative of the base 10 logarithm of the molar concentration of hydrogen ions in a solution. At 25 ℃, solutions with a pH less than 7 are acidic and solutions with a pH greater than 7 are basic. According to ASTM D1293 [29], the Test Method A-Precise Laboratory Measurement was used, which covering the precise measurement of pH in water utilizing at least two of seven standard reference buffer solutions for instrument standardization.

For this research, in order to monitor leaching of chemical components, the pH of curing water was obtained prior to the beginning of curing and after the completion of curing (28 d). After dropping the fixed molds into containers, the curing water of 150 ml was poured into containers, before which the pH value of curing water has been measured. During the whole process of wet curing, containers were closed in order to avoid evaporation of water and influence from outside of containers. And the curing water would not be renewed until to the end of curing time. After taking out of molds, the remaining curing water was measured again to collect all data of pH value [29]. The pH was tested using Mettler Toledo SevenCompact S220 pH meter calibrated by the buffer solutions of pH of 4.00, 7.00 and 10.00.

2.2.3.7 Electrical Conductivity

According to ASTM D5391 [30], electrical conductivity is a fundamental property of a material that qualifies how strongly it conducts the flow of electric current. The SI unit of electrical conductivity is siemens per meter. Salinity is a measure of the mass of dissolved salts (ionic constituents) in a given mass of solution and usually expressed as parts per thousand (ppt). Ions commonly found in water include calcium, magnesium, potassium, and sodium cations and bicarbonate, carbonate, chloride, nitrate, and sulfate anions, all of which can be the carrier of electric current. Thus, conductivity is a good measure of salinity in water.

In order to monitor leaching of chemical components, the salinity of the curing water was obtained prior to start curing and then after its completion. The operation method was same to that of measuring the pH values. However, in this research, electrical conductivity was monitored by YSI model 30 electrical conductivity meter, which should be transformed to the value of salinity. Therefore, calibration of sea salts water with 0, 5, 10, 15, 20, 25, 30 and 35 ppt measured by YSI model 30 electrical conductivity meter to build a connection between salinity and electrical conductivity was done at same testing environment before the beginning of preparing geopolymer samples.

2.2.4 Techniques of Analyzing Chemical and Mineral Composition and Micromorphology

SEM, XRD, and XRF are the important tools for investigating the mineral composition, micromorphology, and chemical elements of geopolymers samples and raw materials used in this study.

2.2.4.1 Scanning Electron Microscope

SEM is a type of electron microscope that generates images of a sample by scanning the surface with a focused beam of electrons. The electrons interact with atoms in the sample to produce diverse signals which contain information about the sample's surface topography and its composition. The electron beam is scanned in a raster scan pattern, and the position of the beam is combined with the intensity of the detected signal to produce an image. SEM can achieve resolution better than 1 nm. Specimens are observed in high vacuum in conventional SEM, or in low vacuum or wet conditions in variable pressure or environmental SEM, and at a wide range of cryogenic or elevated temperatures with specialized instruments [72].

The signals used by SEM to form an image result from interactions of the electron beam with atoms at various depths within the sample. Several types of signals are produced including secondary electrons (SE), reflected or back-scattered electrons (BSE), characteristic X-rays and light (cathodoluminescence) (CL), absorbed current (specimen current) and transmitted electrons. Secondary electron detectors are standard equipment in all SEMs, but it is rare for a single machine to have detectors for all other possible signals.

Schematic of a typical SEM is shown in Fig 2.8. An electron beam is thermionically emitted from an electron gun fitted with a tungsten filament cathode. The electron beam, which typically has an energy ranging from 0.2 keV to 40 keV, is focused by one or two condenser lenses to a spot about 0.4 nm to 5 nm in diameter. The beam passes through pairs of scanning coilsor pairs of deflector plates in the electron column, typically in the final lens, which deflect the beam in the x and y axes so that it scans in a raster fashion over a rectangular area of the sample surface. When the primary electron

beam interacts with the sample, the electrons lose energy by repeated random scattering and absorption within a teardrop-shaped volume of the specimen known as the interaction volume, which extends from less than 100 nm to approximately 5 μm into the surface. The energy exchange between the electron beam and the sample results in the reflection of high-energy electrons by elastic scattering, emission of secondary electrons by inelastic scattering and the emission of electromagnetic radiation, each of which can be detected by specialized detectors. Electronic amplifiers of various types are used to amplify the signals, which are displayed as variations in brightness on a computer monitor.

In this study, the microstructure of raw materials and geopolymer samples was tested using JEOL Neoscope JCM-5000 SEM at an accelerating voltage of 10 kV.

2.2.4.2 X-ray Diffraction

XRD relies on the dual wave or particle nature of X-rays to obtain information about the structure of crystalline materials. A primary use of the technique is the identification and characterization of compounds based on their diffraction pattern. The dominant effect that occurs when an incident beam of monochromatic X-rays interacts with a target material is scattering of those X-rays from atoms within the target material. In materials with regular structure (i.e. crystalline), the scattered X-rays undergo constructive and destructive interference. This is the process of diffraction.

The diffraction of X-rays by crystals is described by Bragg's Law:

$$n\lambda = 2d\sin\theta$$

where λ is the wavelength of X-ray, d is the distance between parallel atomic layers, θ is the angle between incident rays and parallel atomic planes, and n is an integer (Fig 2.9).

Although Bragg's law was used to explain the interference pattern of X-rays scattered by crystals, diffraction has been developed to study the structure of all states of matter with any beam, e.g., ions, electrons, neutrons, and protons, with a wavelength similar to the distance between the atomic or molecular structures of interest.

The directions of possible diffractions depend on the size and shape of the unit cell of the material. The intensities of the diffracted waves depend on the kind and arrangement of atoms in the crystal structure. However, most materials are not single crystals, but are composed of many tiny crystallites in all possible orientations called a polycrystalline aggregate or powder. When a powder with randomly oriented crystallites is placed in an X-ray beam, the beam will see all possible interatomic planes. If the experimental angle is systematically changed, all possible diffraction peaks from the powder will be detected.

For the XRD sample preparation in this study, the coarse powdery samples were conducted by wet crushing with Isopropyl alcohol in McCrone Micronising Mill for 2 min, which makes a fine powder with particle sizes $\leqslant$45 μm. The mineral composition of fly ash, metakaolin and different types of geopolymer samples was characterized by using Philips X'Pert-MPD diffractometer. All XRD scans used Cu Kα radiation, a step size of 0.02°, a scan speed of 0.02° per 1 s, and a scan range of 5-70° 2θ (diffraction angle).

2.2.4.3 X-ray Fluorescence

XRF is the emission of characteristic "secondary" (or fluorescent) X-rays from a material that has been excited by being bombarded with high-energy X-rays or gamma rays. The phenomenon is widely used for elemental analysis and chemical analysis, particularly in the investigation of metals, glass, ceramics and building materials (i.e., cement).

When materials are exposed to short-wavelength X-rays or to gamma rays, ionization of their component atoms may take place. Ionization consists of the ejection of one or more electrons from the atom, and may occur if the atom is exposed to radiation with an energy greater than its ionization energy. X-rays and gamma rays can be energetic enough to expel tightly held electrons from the inner orbitals of the atom. The removal of an electron in this way makes the electronic structure of the atom unstable, and electrons in higher orbitals "fall" into the lower orbital to fill the hole left behind. In falling, energy is released in the form of a photon, the energy of which is equal to the energy difference of the two orbitals involved. Thus, the material emits radiation, which has energy characteristic of the atoms present. The term fluorescence is applied to phenomena in which the absorption of radiation of a specific energy results in the re-emission of radiation of a different energy (generally lower).

Each element has electronic orbitals of characteristic energy. Following removal of an inner electron by an energetic photon provided by a primary radiation source, an electron from an outer shell drops into its place. Each of these transitions yields a fluorescent photon with a characteristic energy equal to the difference in energy of the initial and final orbital. The wavelength of this fluorescent radiation can be calculated from Planck's Law:

$$E=nh\nu$$

where E is the energy of oscillator, n is an integer, h is Planck's constant, and ν is the frequency of the oscillator. The fluorescent radiation can be analyzed either by sorting the energies of the photons (energy-dispersive analysis) or by separating the wavelengths of the radiation (wavelength-dispersive analysis). Once sorted, the intensity of each characteristic radiation is directly related to the amount of each element in the material.

In order to prepare appropriate samples for XRF test in this research, the coarse powdery samples were conducted by wet grinding with Isopropyl alcohol in McCrone Micronising Mill for 2 min, which generates a fine powder with particle sizes ⩽45 μm. The elemental chemical analysis was performed using a Siemens MRS400 MP and a Philips PW2400 XRF.

2.3 Resistance to Salts Corrosion

Lee and Deventer [73] specially studied the effects of inorganic salt on the strength and durability of geopolymers, which was made from fly ash and kaolin. The activator is composed of sodium silicate solution and KOH solution. But there is one difference that the concentration of KOH solution in system I is less than that in system II. Inorganic salts were dissolved or suspended in the mixing water and added to the early pastes before setting to simulate process contamination involving the activating solutions. These salts included KCl, K_2CO_3, KOH, $CaCl_2$, $CaCO_3$, $Ca(OH)_2$, $MgCl_2$ / $6H_2O$, $MgCO_3$ and $Mg(OH)_2$. The salts of 0.08 moles were dissolved (KCl, K_2CO_3, $CaCl_2$, $MgCl_2$ / $6H_2O$) or suspended ($CaCO_3$, $Ca(OH)_2$, $MgCO_3$ and $Mg(OH)_2$) in 20 g of distilled water, 5 min before their addition. For system I, it was found that chloride salts such as KCl, $CaCl_2$ and $MgCl_2$ were detrimental to System I geopolymer. They decreased the product durability by gradually causing precipitation and crystallization in the aluminosilicate gel---the binding phase of geopolymer. But K_2CO_3, $Ca(OH)_2$ and $CaCO_3$ could improve the strength and durability. These were beneficial by lowering the dissolved water contents and preventing hydrolytic attacks on the gels. For system II, the whole trend of mechanical properties of all geopolymers with every salts contamination showed an increase. It indicated that higher

concentration of KOH as one part of activator solution could promote the resistance to many kinds of salts. Bakharev [74] studied the durability of geopolymer materials, manufactured using Class F fly ash and alkaline activators, in sodium and magnesium sulfate solutions. Fly ash was activated by sodium hydroxide (8FA), a mixture of sodium hydroxide and magnesium hydroxide (8FAK) and sodium silicate solutions (8FASS), providing 8-9% Na in mixtures and water /binder ratio of 0.3. Before durability tests, the mixtures were cured for 24 h at room temperature; after that, the mixtures were ramped to 95 ◦C and cured at this temperature for 24 h, and then the materials cooled down with the oven and were cured at room temperature for 2 d. The resistance of materials to sulfate attack was studied by immersion of specimens in 5% solutions of sodium and magnesium sulfate, and solution of 5% sodium sulfate (Na_2SO_4) +5% magnesium sulfate ($MgSO_4$). In the sodium sulfate solution, significant fluctuations of strength occurred with strength reduction 18% in the 8FASS and 65% in the 8FAK, while 4% strength increase was measured in the 8FA. In the magnesium sulfate solution, 12% and 35% strength increase were measured in the 8FA and 8FAK specimens, respectively; and 24% strength decline was measured in the 8FASS samples. The most significant deterioration was observed in the sodium sulfate solution and it appeared to be connected to migration of alkalis into solution. In the magnesium sulfate solution, migration of alkalis into the solution and diffusion of magnesium and calcium to the subsurface areas was observed in the 8FASS and 8FAK specimens. Fernandez-Jimenez et al. [14] studied the durability of Class F fly ash based geopolymer mortars exposed to different environments: air, deionized water, seawater, sodium sulphate (Na_2SO_4). Two alkali activating solutions were used: N = 8 M NaOH and W = mixture 85% 12.5 M NaOH + 15% sodium silicate (SiO_2/Na_2O = 0.16).

The solution/ash ratios were 0.35 for solution N and 0.4 for solution W. The mortars had a sand/ash ratio of 2/1. Mortar specimens were cured in an oven for 20 h at 85 °C and a relative humidity of 99%, followed by demolding and immersing in the respective aggressive media. In general, alkali-activated fly ash mortars, regardless of the type of activator used, are generally more durable than OPC mortars at the experimental conditions analyzed in this study. AAFA pastes and mortars perform satisfactorily when exposed to sulphates and seawater. In the presence of sulphates, small amounts of sodium sulphate are formed as a degradation product. In seawater Na ions are replaced by Mg ions, making the gel microstructure slightly more porous. Sindhunata et al. [75] did some research in the effects of immersion in alkaline solutions on the gel structure and pore network of fly ash based geopolymers. Immersion in carbonate or hydroxide solutions (NaOH, KOH, Na_2CO_3, K_2CO_3) of up to pH 14 results in very little leaching of framework components (Si or Al) from the geopolymer gel, and a largely unchanged mesoporous gel structure. Higher concentrations, up to 8 M NaOH, cause more damage to the gel framework as species are leached into solution and the pore network collapses. The zeolitic products formed are in general the same products that are observed in geopolymers cured at elevated temperatures for extended periods of time, suggesting that the reactions taking place during alkaline immersion are to some extent a continuation of the initial geopolymerization process. Rattanasak et al. [76] studied the performance of rice husk ash (RHA)-based geopolymer mortars after immersion in the 5% $MgSO_4$ solution by weight. In this study, RHA and $Al(OH)_3$ were mixed to obtain a homogeneous powder, activated by mixture of 10M NaOH and Na_2SiO_3 solutions. The specimens were subsequently cured in an oven at 115 °C for 48 h. Then they were immersed in the 5% by weight sulphate solution for 90 d. The results

showed that the resistance to the 5wt% $MgSO_4$ solution is not good, as indicated by a slightly larger strength reduction with the same immersion time. Thokchom et al. [77] aimed to study the performance of Class F fly ash based geopolymer mortar specimens in magnesium sulphate solution. Specimens were cured along with the molds in an oven for a period of 48 h at 85 °C and allowed to cool inside the oven before being removed to room temperature. In addition, specimens were exposed in 10 % solution of Magnesium Sulphate ($MgSO_4$) after 28 d from manufacture. The duration of exposure was 24 wk and specimens were kept fully immersed in the sulphate solution having total volume as four times the volume of specimens immersed. The results showed that specimens received white deposits on the surfaces during exposure to magnesium sulphate solution which should be gypsum and ettringite; no visible cracks were noticed on the specimen though fine micro cracks were seen on a few specimens through optical microscope; residual compressive strength showed some fluctuations during the period of exposure. After 24 wk of exposure, specimen with highest Na_2O content retained maximum strength of 89.7%, and 44.13% for specimens with lowest Na_2O content. El-Sayed et al. [78] studied the resistance of alkalized activated water-cooled slag (WCS) geopolymer to magnesium sulphate attack. Alkaline activators included sodium hydroxide and/or sodium silicate in different ratios. For sulfate attack measurements, specimens were cast, cured in a fog room for 28 d, and then immersed in a solution containing about 5 % $MgSO_4$ solution. The solution in the container was replaced every 2 wk up to 6 mth. Compressive strength was measured periodically (monthly) over 6 months. The increased NaOH concentration caused positive effects on the mechanical properties of the geopolymeric materials. The reduced concentrations have negative impact. Sodium silicate has lower efficiency in dissolving aluminosilicate

network resulting in low mechanical properties. The results showed that mixing of both sodium hydroxide and sodium silicate in ratio of 3:3 wt.,% of dry mixes is the optimum one giving better mechanical as well as microstructural characteristics as compared with cement mortar that has various cement content (cement : sand were 1:3 and 1:2). Durability of the water-cooled slag in 5 % $MgSO_4$ as revealed by better microstructure and high resistivity-clarifying that activation by 3:3 sodium hydroxide and sodium silicate, respectively is better than using 2 and 6 % of sodium hydroxide. Kupwade-Patil and Allouche [79] investigated the performance of reinforced geopolymer concrete (GPC) in examination of chloride-induced corrosion. Specimens were made from Class F and Class C fly ash, mixed activator (1∶1 blend of sodium silicate and 14 M sodium hydroxide), fine aggregates and coarse aggregates. The specimens were subjected to intermittent wetting and drying cycles of saltwater, with the solution being placed in the Plexiglas dams during the wet cycles. Wet-dry saltwater cycles consisted of 14 d of 7.5% NaCl solution exposure (wet cycle), followed by air exposure for 14 d (dry cycle). Generally speaking, GPC specimens were found to exhibit lower average diffusion coefficients, chloride contents, and porosity compared with their OPC counterparts. GPC specimens made from Class F fly ash exhibited a significantly higher resistance to chloride-induced corrosion compared with OPC specimens, as well as GPC specimens made from Class C fly ash. It also appears that the amorphous geopolymer mass is highly resistant to chloride-induced corrosion, as micro-level corrosion sites were found to coincide with the presence of impurities in the geopolymer matrix. Giasuddin et al. [80] explored the effect of curing of fly ash based geopolymer in saline water compared to normal water at ambient conditions. Saline water exposed curing is relevant to wellbore cement used for geo-sequestration of

CO_2 in saline aquifer. The conventional OPC-based oil well cement have unfavorable results when cured in saline water. Class F fly ash was used as aluminosilicate source material for synthesization of geopolymeric cement, activated by mixture of sodium silicate solution and sodium hydroxide. Small percentage of ground granulated slag was blended with fly ash as an additive. The molds filled with slurry were kept in room temperature for 10 – 12 h to allow sufficient hardening and easy remolding. After remolding, specimens were immersed in two different curing waters for subsequent curing (saline water and normal water). Saline water was prepared by adding sodium chloride (NaCl) with water in different concentrations (0%, 8%, 15%). The results showed that curing of geopolymer in saline water leads to higher compressive strength than curing in normal water at ambient temperature (20 – 22 °C) and pressure conditions, but lower than curing in sealed condition. Therefore, the development of strength was still influenced by wet curing. Samples cured in saline water are associated to lower sorptivity thereby indicating lower porosity or micro-crack density than water cured samples. For curing in saline water, intrusion of salt inside the material is not prominent. So, chloride salt precipitation and crystallization are unlikely mechanisms cause damage. Both saline water and normal water curing causes leaching of alkali solution and metal cation from the sample. The leaching is significantly less in saline water. Nasvi et al. [81] had the same purpose of study to that of Giasuddin et al. [80]. To date, OPC-based oil well cement has been questioned at CO_2 sequestration conditions in wellbore, which is possible to be solved by geopolymer materials. However, in this study, different materials were used in tests: Class F fly ash-based geopolymer, sandstone, geopolymer-sandstone composite. The samples were oven-cured at 50 °C for a period of 24 h and allowed to cool for another 6 h.

The samples then immersed in the saturation containers with either water (W), 5% NaCl brine water (5% BW) or 15% NaCl brine water (15% BW), and saturated for periods of 14, 30, 60 or 90 d. Based on the results, it was found that G, S and G-S samples experience strength reduction in W and BW. However, the reduction rate of G is almost half of that of OPC-based oil well cement. In addition, the strength reduction rates of G and G-S were less in 15% BW compared to Wand 5% BW, due to the lower alkali leaching rates from G in BW compared to W. And among all data cured in saline water, high concentration of NaCl solution would lead to higher strength. Therefore, saline aquifers with high NaCl content are always favorable for G well cement. The S samples showed constant strength reduction regardless of the saturation medium, and hence NaCl does not show any significant effect on the mechanical behavior of quartz-rich sandstone. Kim et al. [82] also made an investigation of durability of rice husk ash-based geopolymer mortars immersed in 5% Na_2SO_4 and 5% $MaSO_4$ solutions over a period of 28 d. It is found that geopolymer concrete showed very less weight loss when compared to steam-cured mortar specimens. Bondar et al. [83] studied the sulfate resistance of alkali activated pozzolans based geopolymer concrete. In this study, two natural pozzolans were used. Potassium hydroxide (KOH) and sodium silicate solution were mixed as alkaline activator. Specimens were left at room temperature, covered by a plastic sheet and demolded after 24 h. Taftan specimens were exposed in two curing regimes and three different temperatures: sealed curing (20 ± 2, 40 ± 2 and 60 ± 2 ◦C and less than 70 % RH); fog curing ((20 ± 2, 40 ± 2 and 60 ± 2 ◦C and 98 % RH). Raw and calcined Shahindej specimens both were all cured at sealed curing conditions. It was found that raw Shahindej pozzolan needed at least 60 ◦C curing to provide moderate to high strength at early stages while the optimum temperature for curing

calcined Shahindej was found to be 20 ˚C. Therefore the ARSH concrete mixtures were cured at 60 ˚C and ACSH mixtures were cured at 20 ˚C and less than 70 % RH [84]. After de-molding, the samples were cured as described above using the different curing conditions and temperatures for 28 d. The specimens were then immersed in a solution containing 2.5 % Na_2SO_4 and 2.5 % $MgSO_4$ by weight of water. The samples were placed in containers and left in a temperature-controlled room at 20 ˚C for 6 months with some samples being retained for measuring changes in the compressive strength over 2 y. The container solutions were replaced every 2 wk for the first 3 months and then retained. The results showed that the strength of all sulfate cured concretes at 180 d was less than that for the samples cured outside of the solution initially with the exception of the ATAF1 samples cured at 20 ˚C in sealed and 40 ˚C fog conditions and the ATAF2 samples cured at 40 ˚C in sealed conditions. The trend of compressive strength development is to increase, except for Taftan samples cured at 40 ˚C at fog conditions and ARSH concrete mixes at this age. At the end of present investigation which was to evaluate the performance of natural alumina silica based geopolymer concrete in sodium and magnesium sulfate solution, the loss of compressive strength and percentage of expansion of AANP concrete was recorded up to 19.4 % and 0.074, respectively. Duan et al. [85] investigated the influence of sulfate attack on the mechanical properties and microstructure of fly ash and metakaolin based geopolymer paste. Fresh geopolymer pastes were cast in triplet steel cubes molds. After 24 h, all the specimens were released from the molds and were subjected to further curing in a standard condition of 20 ± 2 ˚C and 90 ± 5% relative humidity up to 28 d. Thereafter, some of the specimens were moved to a 5% sodium sulfate solutions (Na_2SO_4) made by dissolving reagent-grade chemicals in tap water and placed

inside an environmental chamber with standard temperature and relative humidity as mentioned above and all the specimens were continuously immersed in the solutions up to testing date of 28 d, 90 d, and 180 d, respectively. The sulfate solutions were renewed every 2 wk. Sample characterization was conducted on geopolymer paste specimens to evaluate the effects of the sodium sulfate solutions exposure and metakaolin addition on properties of them. The experimental results uncover that geopolymer suffers strength loss after sulfate attack exposure but gains strength with increasing replacement level of fly ash by metakaolin from 5% to 20% and obvious increasing in compressive strength could be observed when the replacement percentage exceeds 15%. The sulfate attack exposure shifts the peak value of pore size to a higher value and leads to the development of a macropore system with high porosity and deduction of surface Vickers-hardness. Compressive strength loss in geopolymer after sulfate attack exposure relates to the microcrack development and high porosity. Longer exposure leads to higher deduction in compressive strength and acceleration in deterioration degree which lead to expansion stress and cracks. Partial replacement of fly ash by metakaolin improves the mechanical properties, optimizes the microstructure, and reduces the level of damage from sulfate attack. Zainal et al. [86] presented the results of corrosion studies between fly ash geopolymer paste and fly ash-slag geopolymer paste. Geopolymer was made from aluminosilicate inorganic polymers mixed with the alkaline activator in order to reduce the CO_2 to the ecosystem. Samples then were cured at 60 °C for 24 h in the oven. Reinforcement bar is placed at the center of the paste. The samples were examined after 7, 14, and 28 d in terms of Open Circuit Potential (OCP) test, phase analysis and morphology analysis. The results showed that fly ash-slag geopolymer (FSG) paste had good corrosion resistance and low corrosion rate

compared to fly ash geopolymer (FG) paste. The paper from Wallah et al. [87] presents the study of the resistance of Class F fly ash-based geopolymer concrete to sulfate attack. Test specimens were soaked in sodium sulfate solution for certain periods of time, and the resistance of geopolymer concrete was studied by evaluating the amount of expansion, the change in the mass, and the residual compressive strength of test specimens after exposure. Test variables included exposure period and the concentration of the acid solution. The alkaline activator was a combination of sodium hydroxide solution and sodium silicate solution. About 30 minutes after casting, the specimens were placed in the oven for curing at 60 °C for 24 h. The specimens were soaked in 5% sodium sulfate solution (Na_2SO_4) to simulate the sulfate exposure. There was no significant change in the external appearance of the surface of specimens soaked in sodium sulfate. There was very little change in this value for specimens soaked in sodium sulfate solution. It can be seen from these data that exposure to sodium sulfate solution or water up to one y has very little effect on the compressive strength.

Generally speaking, there are some common ground among these research on different kinds of geopolymer resistance to salts solution: (1) most of geopolymer at the statement of slurry would be treated by HT which would to some extent improve the their mechanical properties as well as others; (2) in most cases, the components of salts solution is made up of one or two materials, in which such simulation cannot be compared to the really environment of nature seawater; (3) almost all of samples would be immersed in saline solutions after being de-molded, which means saline solutions can only influence the outside of samples. In addition, this design happen to miss the most important part of chemical reaction of geopolymerization which would happen in the first one or two days

from mixing of aluminosilicate source materials and alkaline activators; (4) the range of concentration of saline solution is not large enough to cover the most severe condition in natural environment.

2.4 Summary

Basic background information about geopolymer is presented in this chapter. More reviews on the specific properties are shown in the corresponding chapters later in this thesis. The recent research situation on resistance of geopolymer to salt corrosion has been shown in section 2.3. It is indicated that there still are several significant points of research in such area able to be improved. Therefore, the first goal of this research is confirmed to build an environment approached to the real seawater to study the mechanical properties of geopolymer and pursuit the mechanism of influence factors. The second purpose is to explore the potential application of fly ash-based geopolymer cement and concrete in Jincheng, China.

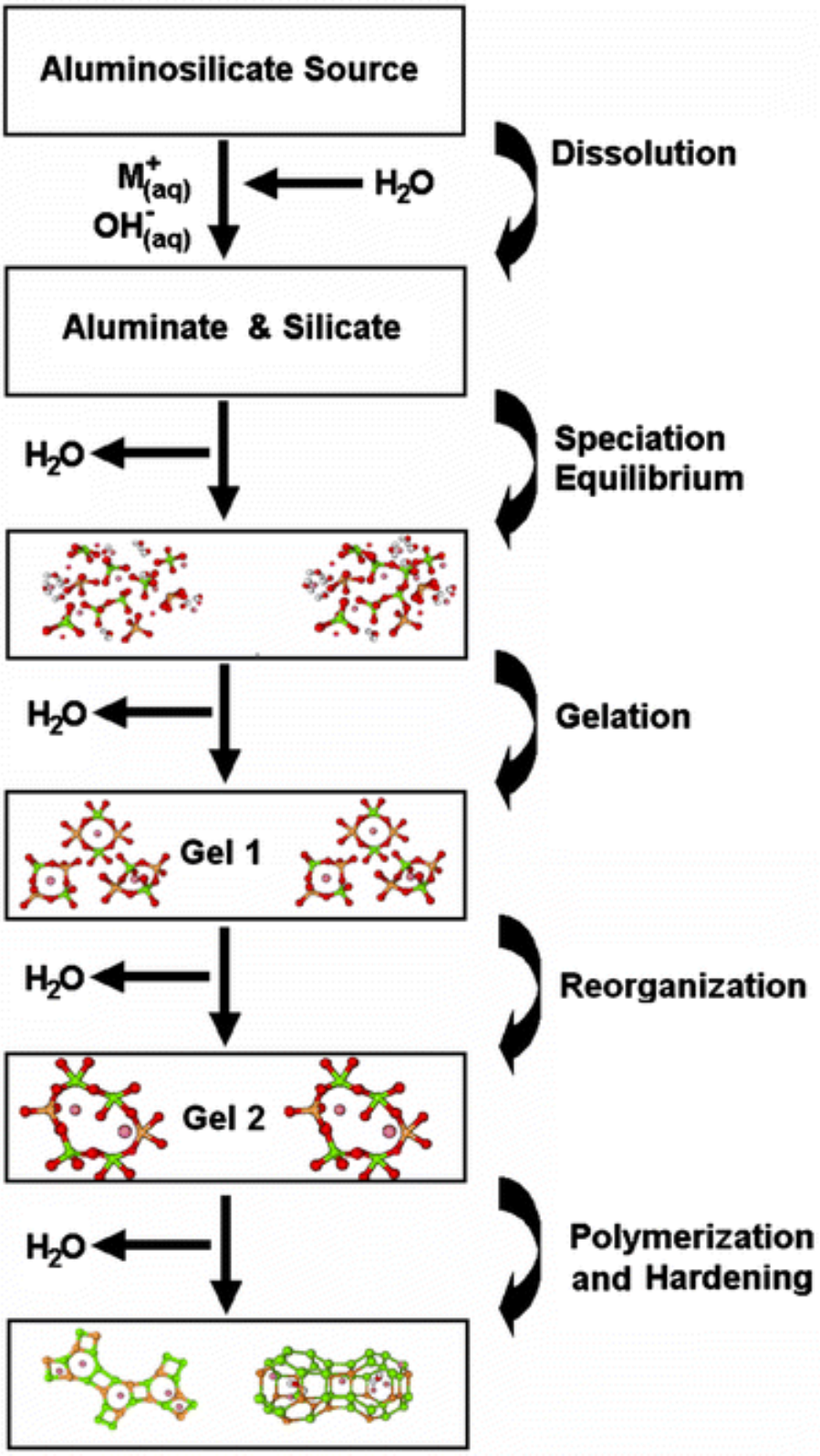

Figure 2.1: Conceptual model for geopolymerization.

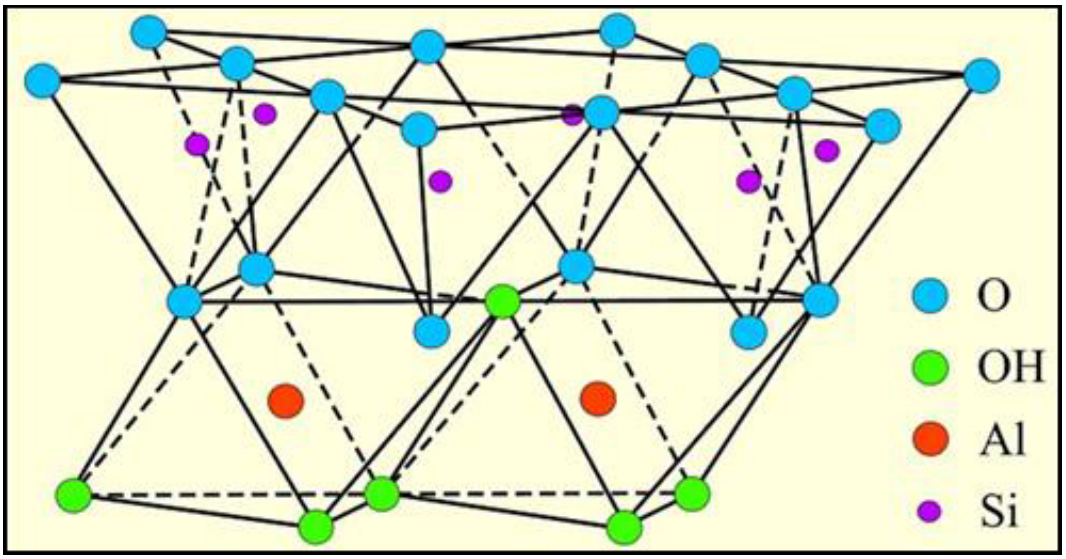

Figure 2.2: Structure of a kaolinite layer.

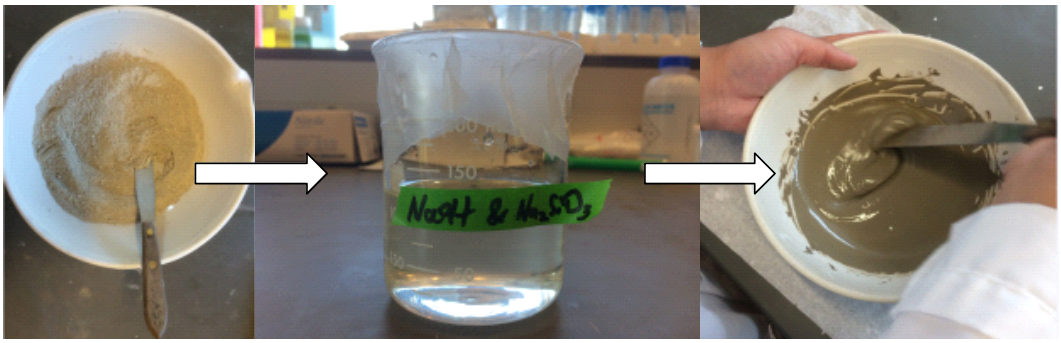

Figure 2.3: Paste mix procedure (from left to right: powder mix, alkaline mix, slurry).

Figure 2.4: Mortar mix procedure.

Figure 2.5: Concrete mixture and blender.

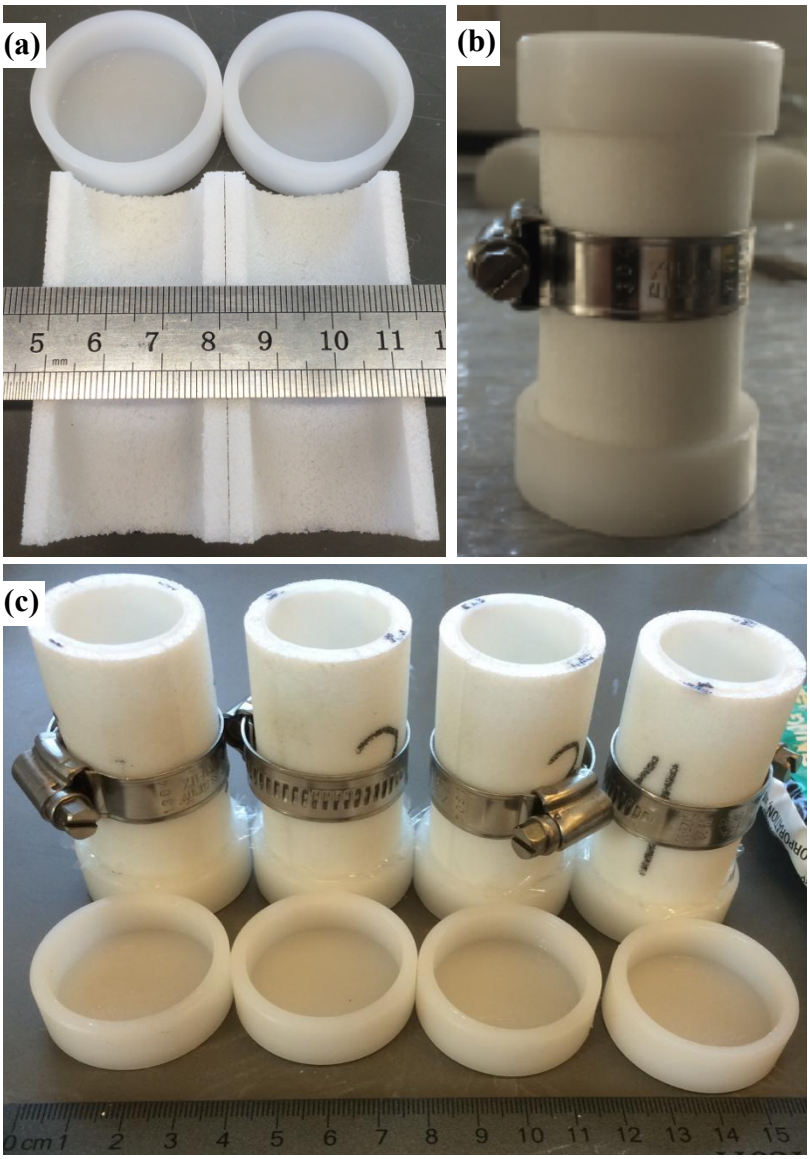

Figure 2.6: Split specimen molds made of porous HDPE cylinders: (a) a completely disassembled mold showing the two split half cylinders and two end caps; (b) a fully assembled mold fastened by a clamp; (c) partially assembled molds that are ready for geopolymer precursor casting. Note that a layer of plastic thin film is inserted between the end of the cylinder and the end cap to maintain better sealing.

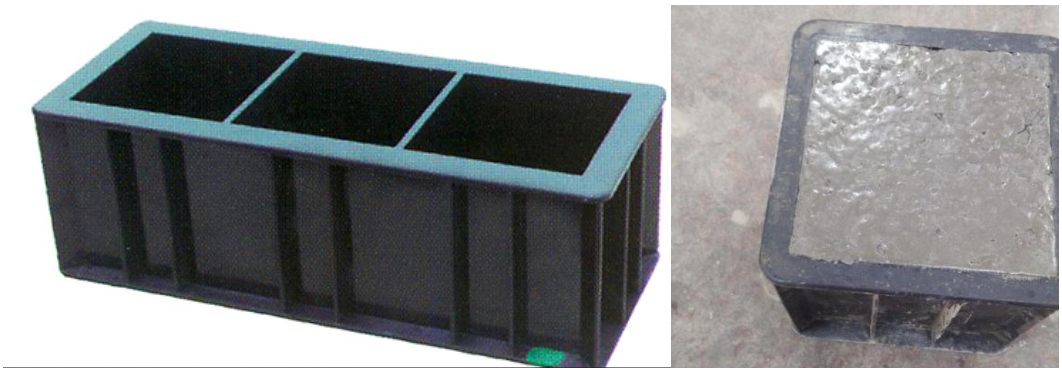

Figure 2.7: The mold for concrete grout.

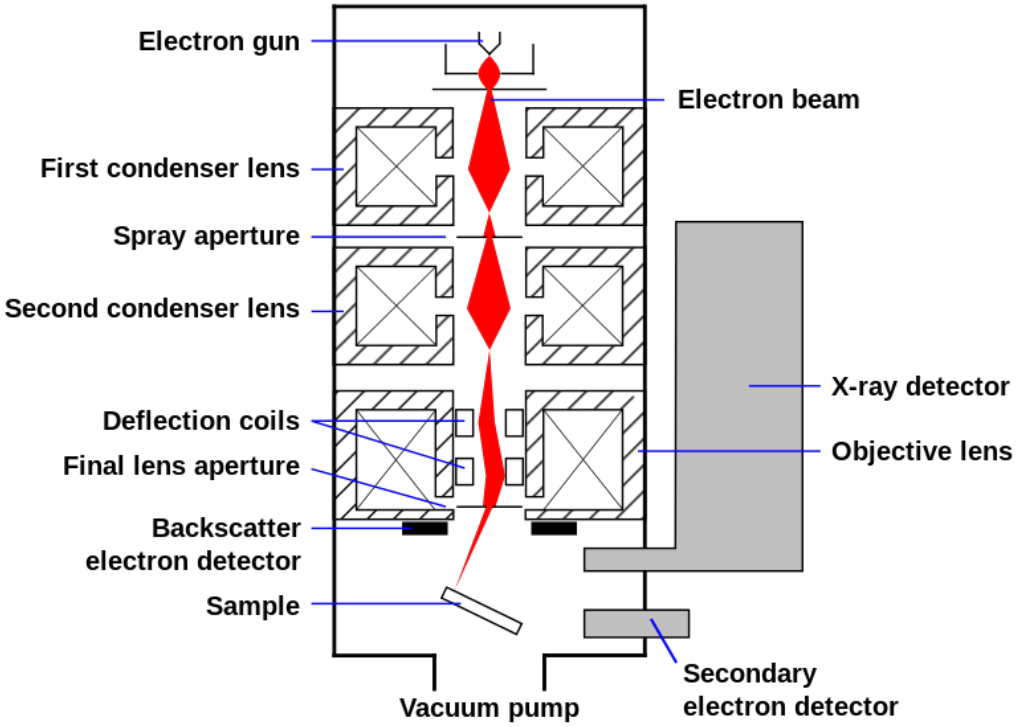

Figure 2.8: Schematic of an SEM.

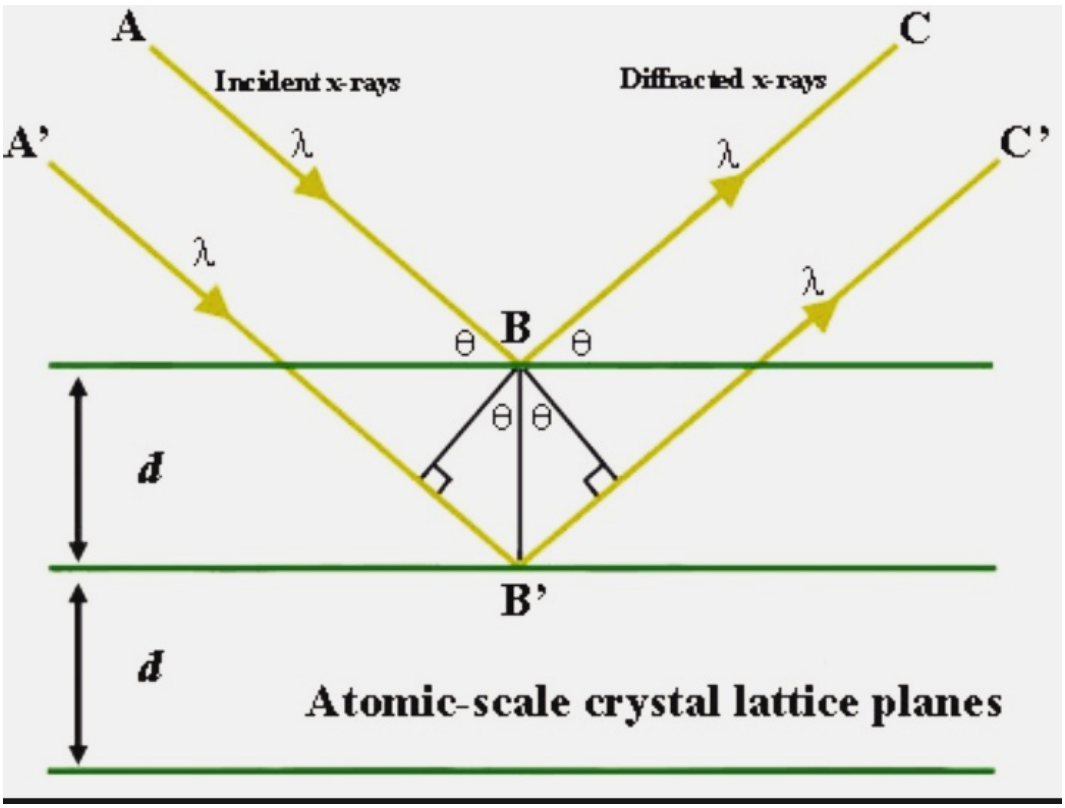

Fig 2.9: Schematic illustration of Bragg's Law.

Table 2.1: Chemical requirements of fly ash.

	Class N	Class F	Class C
Silicon dioxide (SiO_2) + aluminum oxide (Al_2O_3) + iron oxide (Fe_2O_3), min, %	70.0	70.0	50.0
Sulfur trioxide (SO_3), max, %	4.0	5.0	5.0
Moisture content, max, %	3.0	3.0	3.0
Loss on ignition, max, %	10.0	6.0	6.0

Table 2.2: Geopolymer mortar mix design example.

Si/Al molar ratio	Na/Si molar ratio (activator)	Water/fly ash mass ratio	Sand/fly ash mass ratio
1.65	1.5	55%	1:1, 2:1, 3:1
1.8	1.5	55%	1:1, 2:1, 3:1
1.9	1.5	55%	1:1, 2:1, 3:1

Table 2.3: Geopolymer concrete mixture design example (mass ratio).

No.	Fly ash	Sodium silicate solution	Sodium hydroxide	Fine aggregate	Coarse aggregate	Water
1	1	0.33	0.05	0.91	2.38	0.25
2	1	0.33	0.05	0.5	1.2	0.25
3	1	0.33	0.05	0.75	1.8	0.25
4	1	0.33	0.05	0.5	1.8	0.25
5	1	0.33	0.05	0.91	0.91	0.25
6	1	0.33	0.05	0.5	2.38	0.25
7	1	0.33	0.05	1.3	1.3	0.25

Table 2.4: Chemical composition of sea salts.

	Seawater	Instant ocean
ppt	35	29.65
Major cations (mmol kg^{-1})		
Na^{+}	470	462
K^{+}	10.2	9.4
Mg^{+2}	53	52
Ca^{+2}	10.3	9.4
Sr^{+2}	0.09	0.19
Sum	607	594
Major anions (mmol kg^{-1})		
Cl^{-}	550	521
SO_4^{-2}	28	23
TCO_2	1.90	1.90
TB	0.42	0.44
Sum	608	569

CHAPTER 3

SALINE WATER CURED GEOPOLYMER: EFFECT OF SI TO AL RATIO

3.1 Introduction

OPC is a typical, most widely used cementitious binder in the World's construction industry, owing to its excellent mechanical performance, adaptability, and affordability. On the other hand, the universal application of OPC also results in certain concerns, mainly including carbon dioxide (CO_2) emission, overconsumption of natural resources (e.g., limestone and clay), and high energy consumption in the manufacturing process. For example, producing one ton of OPC causes the emission of approximately one ton of CO_2 [33,50]. In fact, the Portland cement industry alone is responsible for approximately 5-7% of global carbon emissions [88,89]. Therefore, more environmentally friendly cementitious materials with low or no CO_2 emissions are desired as a potential alternative to or at least partial replacement for OPC.

Another concern is the limitations or drawbacks of OPC's use in saline or chemically harsh environments. In the USA, Class G or H OPC is generally recommended by the American Petroleum Institute (API) as a cementing binder in deep wellbores and geo-sequestration sites, which both usually exist in brine formations. However, it has been demonstrated by prior studies that there are potential concerns with the use of OPC in well cementing, such as degradation, lack of enough chemical (e.g., acid, saline, and sulfate) resistance, inadequate long-term durability, leakage, and strength reduction in high-salinity environments [9,12]. In fact, much work has been conducted to study the behavior of OPC in saline water. Suzuki et al. [90] studied the influence of NaCl on the calcium silicate hydrates (C-S-H) in OPC, and observed that Na^+ is adsorbed on the surface of C-S-H, thus

decreasing the Ca/Si molar ratio of C-S-H, and Cl- accelerates the leaching of Ca in C-S-H. Lécolier et al. [10] found that the API Class G OWC samples first air-cured at a temperature of 80 ℃ and a pressure of 7 MPa for one month and then aged in fresh water and crude oil at the same temperature and pressure for one year don't show any obvious degradation in strength, while the counterparts aged in low-salinity water with a concentration of 0.4 mol/L and Na^{+}, K^{+}, Ca^{2+}, Mg^{2+}, Cl^{-}, HCO^{3-}, SO^{4-} as the major ions exhibit a 50% decrease in strength, because of the leaching of portlandite from the cement matrix. Zhou et al. [8] investigated the effects of 0-36 wt.% NaCl solutions on the hydration of Class G OWC cured at 93 and 160 ℃ and 20.7 MPa, and their results showed that a low salt concentration accelerates hydration, while a high salt concentration impedes hydration. Besides, when the salt content is greater than 5 wt.%, the cement's strength decreases with increasing salinity, due to the effect of NaCl on the leaching of Ca from C-S-H. In addition, sulfate corrosion is another important, well-studied issue. It is generally recognized that the reaction between cement hydration products and sulfate solution results in the formation of ettringite and gypsum, directly or indirectly leading to such destruction as expansion and cracking, and the destruction definitely causes softening, disintegration, and strength reduction [91,92]. Because of these serious concerns, investigating and developing new cementitious materials that are stronger, more durable, and more stable than the OPC is necessary and a focus of much existing research.

Because of its several key advantages over traditional OPC, such as low energy consumption for production and hence better sustainability, low carbon emission, and high durability, geopolymer, composed of SiO_4 and AlO_4 tetrahedra linked by sharing all the oxygen atoms to form a three-dimensional aluminosilicate structure [32–34], has been

studied or recommended as a potential alternative to OPC and other cementitious binders, and may find plenty of viable applications in civil infrastructure and construction [14,15,23,93]. Geopolymerization is regarded as a complex process that generally consists of a series of reactions [42–44,94]: dissolution, reorientation, polycondensation, and solidification [14,33,46–48], which can overlap with each other and even take place almost simultaneously in the curing process. Although different source materials containing amorphous aluminosilicates can be used to synthesize geopolymer binders, fly ash and furnace slag have been widely used due to their comprehensive sources [95–97]. Metakaolin is another widely used raw material, which can improve the mechanical properties due to its high pozzolanic reactivity and finer particles [14,15,33].

To date, the durability of geopolymers cured in saline water has been studied to some extent. Lee and van Deventer [73] discovered that the durability of fly ash and metakaolin-based geopolymers is mainly adversely influenced by different chlorides, possibly related to the hydrolytic attack on the primary aluminosilicate gel by Cl^-. Bakharev [98] examined the durability of fly ash-based geopolymers exposed to a 5 wt.% sulfate solution, and found that the stability of the samples depends upon the types of used activators as well as the concentration and type of cations in the sulfate solution. Giasuddin et al. [80] studied the Class F fly ash-based geopolymers cured in fresh water, 8 and 15 wt.% NaCl solutions at ambient temperature, and found that geopolymers cured in saline waters exhibit a higher strength than that cured in freshwater, but still lower than the air-cured counterparts. Their findings indicated that the degradation of strength is unlikely caused by the intrusion of salt into the sample, but the leaching of alkali and metal cations from the sample. Duan et al. [85] found that every type of studied geopolymer samples

suffers the strength loss upon exposure to a 5 wt.% sodium sulfate solution, and longer exposure causes worse performance in mechanical strength, and they further noted that such deterioration mainly results from notable cracks, high porosity, and large pores.

As discussed above, curing geopolymers in saline solutions indeed causes certain negative influences on the mechanical properties. However, in these prior studies, the geopolymers subjected to curing or chemical attack in saline solutions have polycondensed and hardened or partially cured in air for certain durations. That is, none of these studies has started with underwater casting or immediate curing in saline water, i.e., by submerging immediately the geopolymer slurry into saline water, which may allow the exchange of chemicals between the saline water and geopolymer slurry. In fact, if geopolymer were to be used in well cementing, then the precursor would need to be injected as a slurry into the well where chemical exchanges (e.g., ion transport, dispersion) between the geopolymer slurry and permeable rock formations take place before and during the polycondensation and subsequent curing processes. Inundating the partially pre-hardened or pre-cured geopolymer samples in saline water actually fails to take into account the potential initial chemical reactions or exchanges between the slurry and surrounding environment (e.g., brine pore fluids from the rock formations), which may occur more rapidly in the slurry than the hardened cement. In summary, very little research has been conducted to study the effects of underwater casting and curing of geopolymer in saline solutions on its mechanical performance. The work presented in this paper is among the first to fill the gap, and its objective is two-fold: (1) to study the effects of casting and immediate curing in saline solutions on the characteristics of geopolymers in terms of mechanical properties, microstructure, and chemical and mineralogical compositions; (2) to investigate the effects

of two different Si/Al molar ratios on the geopolymers' performance. In terms of novelty, this work used a commercial sea salt, but not pure chlorides or sulfates (e.g., NaCl or Na_2SO_4), to simulate the chemistry of the brine fluids, and customer-built, porous, permeable molds for underwater casting and curing of geopolymer slurry, which distinguishes this study from others that usually submerge pre-hardened geopolymer samples into saline solutions of varying concentrations.

3.2 Materials and Methods

3.2.1 Materials

The raw materials selected for the synthesis of geopolymers consisted of Class C fly ash [52] (Headwater Resources, Inc., USA) and metakaolin (Advanced Cement Technologies, LLC, USA). Preliminary work found that the fly ash alone reacts too fast with the alkali activator solution, leaving little or no time for handling and casting the geopolymer slurry into the curing molds. Therefore, to reduce the rate of geopolymerization reactions, metakaolin was also added to the Class C fly ash at a mass ratio of 1:1 to form the raw material mixture. Table 3.1 summarizes the chemical compositions and size fractions of the dry fly ash and metakaolin, while Fig 3.1 shows their particle size distributions determined by the standard test method [28], with a median particle size (D_{50}) of 8.7 and 5.0 μm, respectively. In addition, for the purpose of comparison, Class G oil well cement (OWC) (LafargeHolcim, USA) was also studied in nearly all parallel testing. The activators included solid sodium hydroxide with a >95% purity quotient (Fisher Scientific, Inc., USA) and sodium silicate solution (Fisher Scientific,

Inc., USA) with a specific gravity of 1.4, consisting of 9.1 wt.% Na_2O, 29.2 wt.% SiO_2, and 61.7 wt.% H_2O.

In addition, a synthetic Instant Ocean sea salt (Spectrum Brands, Inc., USA) was used to prepare artificial saline water to simulate the natural seawater or brine solutions, because prior studies concluded that this commercial salt provides necessary cations and anions at concentrations closest to those of the natural ocean water [67]. In the descending order, this salt contains Na^+, Mg^{2+}, K^+, Ca^{2+}, Sr^{2+} as the major cations, and Cl^-, SO_4^{2-}, TCO_2 (total CO_2) and HCO^{3-} as the major anions. Since the highest salinity of natural ocean water is 35 ppt, three different salinities, 0, 15, 35 ppt, were used for the curing of geopolymer slurry.

Three kinds of split cylindrical molds were manufactured for the curing of geopolymer slurry under different conditions (Fig 2.6):

Type I: non-porous acrylic (or plexiglass) split molds of 2.0 × 5.0 cm in inner diameter and height were used to cure geopolymer slurry in air (i.e., air curing);

Type II: split high-density polyethylene (HDPE) molds of 3.81 cm (or 1.5 inch) in inner diameter and 8.89 cm (or 3.5 inch) in height with porous side walls of 10 μm in pore size were used to cure geopolymer slurry with a Si/Al ratio of 1.78 in saline water;

Type III: split HDPE molds of 2.54 cm (or 1.0 inch) in inner diameter and 6.35 cm (or 2.5 inch) in height with porous side walls of 10 μm in pore size were used to cure geopolymer slurry with a Si/Al ratio of 2.00 in saline water.

The Type I non-porous molds were used to air-cure geopolymers with an aim to avoid rapid water loss from the geopolymer slurry during curing. To simulate the field conditions of underground oil wells where the cement slurry is injected between the steel

casing and well wall (i.e., usually permeable rocks), porous molds (i.e., Types II and III) are preferred, since they permit possible chemical exchanges and even fluid flow between the curing chemical solutions and geopolymer slurry. The HDPE was chosen because it is highly stable and does not react with the chemicals in the curing solutions or geopolymer slurry. With respect to the dimensions, Type II molds resulted in relatively larger geopolymer samples that require a high-capacity loading frame for UCT. Therefore, relatively smaller Type III molds were also manufactured so that UCT could be performed in a low-capacity loading frame. Nevertheless, all three types of molds maintained an aspect ratio (i.e., height to diameter ratio) of 2.3 to 2.5 to minimize the end effects encountered in UCT. For each mold, the two end caps were non-porous or impermeable and are made of polyvinylidene fluoride (PVDF) that is also highly resistant to chemicals such as acid, alkali, and salt (Fig 2.6).

3.2.2 Sample Preparation

All of the studied geopolymers were pre-designed to have two different Si/Al molar ratios of 1.78 and 2.00, hereafter designated as "GC-1.78" and "GC-2.00" respectively, because prior work [61] showed that these two Si/Al ratios can result in geopolymers with relatively high strength. The activator solutions all had the same SiO_2/Na_2O molar ratio of 2.0, resulting in two final geopolymers: (1) GC-1.78: Si/Al ratio = 1.78, Na/Al ratio = 0.45; (2) GC-2.00: Si/Al ratio = 2.00, Na/Al = 0.67.

Geopolymer slurry was prepared by mixing the dry powder mixture of raw materials, consisting of fly ash and metakaolin at a mass ratio of 1:1, with the activator solution at a mass ratio of 1:2. The latter was prepared by dissolving solid NaOH in

deionized water, followed by adding the sodium silicate solution at the pre-designed SiO_2/Na_2O molar ratio of 2.0. After thorough mixing for at least 5 min, the activator solution was allowed to cure overnight in a sealed container. On the next day, the fly ash and metakaolin mixture was added to the activator solution, followed by mixing for a minimum of 15 min to ensure complete mixing and to facilitate the raw material-activator reactions, resulting in the formation of geopolymer slurry.

The aforementioned three types of split molds were then used to form cylindrical samples for mechanical testing. For the non-porous Type I molds, a thin layer of vacuum grease was applied to the inner surfaces of the mold and two end caps to facilitate the subsequent removal of the cured geopolymer samples. For the two types of porous molds, a layer of pre-wetted Whatman filter paper with a nominal pore size of 20 μm was inserted inside the molds and seamlessly and conformedly attached to its inner wall to facilitate subsequent removal of completely cured samples and to prevent clogging of the mold's porous walls. In addition, the filter paper still permitted chemical exchanges between the geopolymer slurry and curing solution. To achieve better sealing of the two end caps, a thin layer of plastic film was also used between the cap and the two split half cylinders (Fig 2.6).

The GC-2.00 geopolymer slurry was casted into the pre-assembled Type III molds, followed by hand-vibrating to remove trapped air, and then the top cap was fastened to seal the top of the cylindrical mold. Then the assembled molds filled with geopolymer slurry were immediately immersed in different saline solutions for curing in the ambient laboratory environment. The GC-1.78 slurry was casted in Type II molds. In addition to saline water curing, part of the slurry from each of the two geopolymers was also casted in

Type I molds and then cured in air. Three different salinities, 0, 15, and 35 ppt, were used to cure the geopolymer slurry. For each salinity, a group of 4 identical samples were cured for 28 days, resulting in a total of 2 x 3 x 4 = 24 samples cured in saline solutions and a total of 2 x 4 = 8 samples cured in air. In parallel, the OWC slurry mixed at a water to cement mass ratio of 0.5 were also prepared in the same curing conditions, resulting in 12 samples curried in solutions and 4 samples cured in air.

To facilitate subsequent estimation of the chemical exchanges between the curing solutions and the OWC and geopolymer samples, a constant volume (i.e., 150 ml) of saline solutions was used for curing all samples in a 500 ml beaker, which was completely sealed by Parafilm to prevent evaporation or water loss during the entire curing process, so that the concentrations of different chemicals could be accurately determined. After 28 days of curing, all samples were retrieved from the curing solutions and de-molded, followed by air-drying for a minimum of 7 days before mechanical testing, chemical analysis, and microstructure characterization.

3.2.3 Mechanical, Microstructural, and Chemical Characterization

For mechanical characterization, UCT were performed on the cured and air-dried GC-1.78 samples using an MTS loading frame (with a load capacity of 100,000 lb) in the Piece Laboratory at Massachusetts Institute of Technology at a recommended loading rate of 0.25 ± 0.05 MPa/s, while a Geotest loading frame with a load capacity of 10,000 lb was used to measure the UCS of GC-2.0 and OWC at a constant strain rate of 0.5%/min. The two ends of each sample were re-capped with the Plaster of Paris, followed by correcting and polishing with sandpaper and level gauges to ensure perpendicularity between the

sample's end surfaces and cylindrical axis. In addition, a very thin layer of lubricant coating was applied to the two ends of each sample in order to minimize the friction and hence shear stress development between the specimen's end surfaces and stainless-steel end platens of the loading frame.

The micromorphology and microstructure of the raw materials (including both fly ash and metakaolin) and the cured GC-2.00 samples were characterized in a Neoscope JCM-5000 SEM (JEOL, Ltd., Japan) using an accelerating voltage of 10 kV, while the cured GC-1.78 samples were examined in a high-resolution FEI Magellan 400 XHR SEM (FEI Company). Different pieces retrieved from both the interior core and exterior layer of the GC-2.00 cylindrical samples were examined separately, while only the interior of the GC-1.78 samples was studied. For SEM characterization, all examined samples were sputter-coated by a thin layer of gold.

Further chemical and mineralogical analyses were conducted by XRF and XRD, respectively. Both X-ray-based techniques require finely-ground powder samples. Therefore, the cured geopolymer samples were wet ground with isopropyl alcohol in a McCrone micronizing mill for 2 mins, which usually produces a fine powder with particle sizes of ≤ 45 μm. Elemental analysis was performed on the fine powders in a Siemens MRS 400 MP and a Philips PW2400 XRF spectrometer. The mineralogical composition of fly ash, metakaolin, and cured geopolymer samples was characterized using a Philips X'Pert-MPD diffractometer, and the random powder sample mount was prepared by the razor-tamped surface (RTS) method [61], which can minimize preferred orientation of platy particles such as clays in the sample mount. All XRD scans used Cu Kα radiation, a step size of 0.02°, a scan speed of 0.02° per second, and a scan range of 15-55° 2θ (diffraction

angle). The exchange of ions, particularly OH^-, between the geopolymer slurry and curing saline solutions, was also monitored by measuring the change in the pH of curing solutions before the placement of geopolymer samples and at the end of 28-day's curing (i.e., the completion of curing), using a SevenCompact S220 pH meter (Mettler-Toledo, LLC., Columbus, OH, USA), which was pre-calibrated by the standard buffer solutions of pH 4.00, 7.00, and 10.00.

3.3 Results and Discussion

3.3.1 Compositional Analysis by XRD

Fig 3.2a presents the XRD patterns of the GC-1.78 samples cured in three different saline solutions, while Fig 3.2b shows those for the two raw materials, Class C fly ash and metakaolin, and the GC-2.00 samples cured at different conditions (i.e., including curing in air and three saline solutions). In general, fly ash and metakaolin are mainly composed of amorphous aluminosilicates, which are manifested by their XRD patterns. In fact, there is a broad hump between 20-36° 2θ in the XRD pattern of fly ash, and metakaolin shows a pronounced broad hump between 15-35° 2θ. In addition, some crystalline phases indicated by the sharp reflections, some of which superimpose on the broad hump, are present as impurities in the raw materials: the fly ash contains quartz, mullite, calcite, hematite, and magnetite, while quartz, mullite, and magnetite are present in the metakaolin. As discussed later, these crystalline phases are non-reactive, and hence are present as impurities or solid fillers in the cured geopolymer.

For all GC-1.78 and GC-2.00 samples cured in different saline solutions, a pronounced broad hump between 15-40° 2θ, which is the characteristic reflection of amorphous geopolymers [34,60,80], is present in all XRD patterns. Overall, there is not too much obvious difference in the XRD patterns of the two types of geopolymers cured in the same salinity as well as the same kind of geopolymers cured in different salinities. In addition, some sharp peaks are also present, which clearly inherit from the crystalline phases in the two raw materials, validating that the crystalline phases are not involved in geopolymerization reactions and hence are present as inert fillers in the geopolymer binder. This is consistent with the popular standpoint that only amorphous phases in the raw materials are reactive and contribute to geopolymerization [44,60,100]. These results also prove that the cured end products are not purely amorphous but include crystalline phases as impurities and inclusions.

3.3.2 Mechanical Properties

Fig 3.3 shows some typical unconfined compression stress-strain curves selected from the two geopolymers cured in different saline solutions. For the purpose of comparison, some OWC stress-strain curves are also included. All curves show a well-defined linear elastic regime, but the yielding is poorly defined. Moreover, these curves show the obvious characteristics of brittle failure typically observed in cementitious materials such as geopolymers and OPC. A few curves show a non-linear elastic regime, which is most likely caused by the misalignment due to the samples' imperfect end surfaces. Nevertheless, the fundamental mechanical properties, such as peak strength, Young's

modulus, and failure strain, of these samples can be obtained from their respective stress-strain curves.

Fig 3.4a compares the UCS of all three different types of samples (i.e., OWC, GC-1.78, and GC-2.00) cured in different conditions. The OWC has the highest UCS of 63.16 ± 1.28 MPa under pure (i.e., 0 ppt salinity) water curing, validating that this cement can work well under freshwater casting and curing, while much lower UCSs of 54.95 ± 8.26 and 45.40 ± 1.82 MPa are obtained when the OWC is cured at 15 and 35 ppt saline solutions. The lowest OWC UCS of 37.75 MPa is obtained from air-curing, most likely due to the fact that the original cement-to-water ratio (which was provided by the OWC vendor) used to prepare the cement slurry is designed for direct in-water curing (e.g., casting and curing in underground oil wells). Another possible reason is that the OWC slurry cured in fresh and saline waters absorbs more water to achieve better hydration reactions for strength development. Overall, the UCS of OWC obviously decreases with increasing the curing solutions' salinity, with the maximum reduction of 28.1% at 35 ppt salinity. These results point to the definitive, negative effects of saline water curing on the strength development of OWC, and uncovering the underlying mechanisms requires further analysis of some possible complicate chemical reactions or exchanges between the cement slurry and curing solutions.

However, the opposite is observed for the GC-1.78 and GC-2.00 geopolymer samples cured in the same conditions. For the GC-1.78, an increase in the salinity of curing solutions causes a continuous increase in the UCS: from 31.50 ± 1.61 to 39.93 ± 1.18 and then to 49.87 ± 5.15 MPa for 0, 15, and 35 ppt respectively. A similar trend is also observed for the GC-2.00, although in general the GC-2.00 is stronger than GC-1.78. Compared to

the UCS obtained from the 0 ppt curing solution, the maximum increase in the UCS for GC-1.78 and GC-2.00 are 58.3% and 27.8%, respectively, and the former has an even higher percentage of increment. A noteworthy difference between the two geopolymers is that the UCS (i.e., 29.25 MPa) of air-cured GC-1.78 is lower than those cured in water or saline solutions, while that of GC-2.00 (i.e., 56.67 MPa) is higher than that cured in 0 ppt solution but less than those cured in saline solutions. This indicates that, compared to samples cured in freshwater, air-curing or dry-curing (i.e., without allowing chemical reactions or exchanges between the geopolymer slurry and curing solutions) in a non-porous mold has little influence on the GC-1.78 UCS, but results in a higher UCS for GC-2.00.

Fig 3.4b-3.4d compares the failure strain, Young's modulus, and bulk density of all samples, respectively. For the GC-1.78, the greatest failure strain (1.48%) and Young's modulus (5.43 GPa) occur at 35 and 15 ppt, respectively, while for the GC-2.00 the failure strain increases with the salinity. In general, at the same curing salinity, the GC-2.00 samples exhibit larger failure strains than the GC-1.78, indicating that the GC-2.00 can sustain larger strain or deformation before failure. Moreover, the failure strains of two geopolymers are all greater than those of OWC, indicating that the two geopolymers may perform better in terms of resistance to tensile cracking. This can be further demonstrated by the fact that the Young's moduli of two geopolymers are all smaller than those of OWC. In fact, the Young's modulus of GC-2.00 decreases with increasing salinity. Overall, saline-water curing appears to make the OWC weaker and more brittle, while the opposite occurs for the two geopolymers. Even more, the GC-2.00 can become stronger and more ductile than the GC-1.78 in the 35 ppt curing solution. Finally, the bulk density of OWC

decreases slightly with increasing the curing solution's salinity, but is much greater than those of the two geopolymers (Fig 5d). However, saline water curing causes little influence on the bulk density of the two geopolymers, and the GC-2.00 has a slightly higher bulk density than the GC-1.78. In general, a structural material with a lower bulk density but higher UCS can bring multiple benefits to the design and construction, such as smaller dead loads but higher resistance.

3.3.3 Microstructure

Knowledge of the micromorphological characteristics (e.g., particle size and shape) of the raw materials helps the recognition and identification of the microstructure and composition of the final, completely cured geopolymeric products, such as the presence of unreacted or partially reacted phases by observing their size and geometry. Fig 3.5 compares the micromorphological features of the two raw materials. The fly ash particles generally occur as microspheres of ~1 to 20 μm in diameter (Fig 3.5a). In fact, fly ash generally consists of three kinds of spheres: solid sphere, hollow sphere, and cenosphere [101]. As discussed later, all these three kinds of spheres can be observed in the studied geopolymer samples. In contrary, the majority of metakaolin particles (Fig 3.5b) are platy in shape, which is inherited from its parent material, platy kaolinite crystals, while some aggregates of 10-30 μm in size can also be observed. It appears that, although calcination of kaolinite at higher temperatures (e.g., >450-850 ^{o}C) causes dehydroxylation and hence partial or complete collapse of its crystal structure, metakaolin particles may still maintain their platy shape.

Fig 3.6 is a selected, example SEM micrograph showing the overall microstructure and major constituents of the cured geopolymer. It illustrates the multiphase nature of the final geopolymer products. According to a previous study [60], the final geopolymer products are actually a multiphase composite mainly consisting of unreacted fly ash and metakaolin particles, partially reacted fly ash and metakaolin particles, neo-formed geopolymer binder, and non-reactive impurities such as crystalline quartz and hematite inherited from the raw materials. In addition, randomly distributed spherical micropores and cavities as well as microcracks can be observed. In general, these pores are likely introduced into the sample by two possible sources: (1) the residual air bubbles that are entrapped into the geopolymer slurry during mixing and casting, and (2) the space that is previously occupied by water droplets (due to insufficient mixing) but then becomes a void after water evaporates. In fact, prior work also points out that the presence of macroscale pores in geopolymers is not unusual [102]. Microcracks may also have two potential origins: (1) shrinkage cracks during geopolymers curing and air-drying when upon water evaporation, and (2) loading-induced cracks during the UCT. These microstructural defects, including micropores and microcracks, can have detrimental influence on the mechanical performance of geopolymers.

Fig 3.7 shows selected SEM micrographs of the GC-1.78 samples cured in 0, 15, and 35 ppt saline solutions. All samples, regardless of the curing conditions, consist of unreacted and partially reacted components within the fully reacted, neo-formed geopolymer binder as the major matrix. At this length scale, there is not too much difference in the general bulk microstructure among the different samples cured in different salinities. Therefore, understanding of the origin of different mechanical properties among

these samples warrants further compositional and chemical analyses of these materials, which is discussed in the next two sections.

After the UCS measurements, careful examination of the cross-sectional surfaces of failed cylindrical samples found the color of the exterior layer is usually lighter than that of the interior layer for all the tested samples. Therefore, the microstructure and composition of the exterior and interior layers are worth separate discussion and comparison. As an example, Fig 3.8 compares the different visual appearance and microstructure of the exterior and interior layers of a 15 ppt saline water-cured GC-2.00 sample. Clearly, on the cross-sectional surfaces (Fig 3.8a-3.8b), the interior core is darker than the exterior layer, even though the change is transitional and progressive, and the boundary is not so well defined. Moreover, the circular boundary of color transition indicates that the radial change takes place starting from the outmost cylindrical surface of the samples. Fig 3.8c-3.8d present two typical SEM micrographs of the exterior layer and interior core of the same sample. Surprisingly, some pores of 80-400 μm in diameter are present in both the interior and exterior layers. However, it appears that the exterior layer contains relatively larger pores than the interior layer, mostly likely due to the fact that the exterior layer has direct contact with the curing solution and hence water can seep or permeate into this part of the geopolymer slurry before it hardens.

Fig 3.9 presents the SEM micrographs of the GC-2.00 samples cured in 0, 15, and 35 ppt saline solutions at much higher magnifications. Again, the interior and exterior layers are separated and compared in this figure. First of all, it appears that the exterior layer has relatively more unreacted or partially reacted components and more pores embedded in the neo-formed matrix. In contrast, the interior has a fairly homogeneous and

continuous matrix with more reacted components. In the meanwhile, among the samples cured in different salinities, higher salinities (e.g., 15 and 35 ppt) tend to generate more homogeneous matrix with a larger fraction of reacted binder than the one cured in freshwater. The homogeneous and continuous matrix reflects the formation of the geopolymer binder that contributes to the improved UCS. Overall, the saline solutions have more influence on the exterior than the interior of the samples, which is consistent with the pictures shown in Fig 3.8a-3.8b. In addition, other typical features include the presence of randomly distributed micro-pores and micro-cracks in all samples, and the majority of cracks occurs around pores and unreacted fly ash particles that obviously have weaker adhesion with or are relatively weaker than the neo-formed geopolymer binder.

In Fig 3.10, selected SEM micrographs show the different micromorphological features of residual fly ash particles in the geopolymer binder. In Fig 3.10a, an unreacted, broken hollow sphere of fly ash particles of 25-30 μm in size can be clearly seen, while Fig 3.10b shows a large cenosphere that is filled with many smaller spheres of unreacted fly ash particles. In general, completely reacted fly ash particles should fully dissolve and then transform into a homogeneous geopolymer binder. However, in the hardened geopolymer binder, fly ash particles may be partially reacted and thus maintain their spherical geometry. Fig 3.10c shows that a solid spherical fly ash particle has partially dissolved and reacted, leaving some empty space inside the spherical boundary. In addition, part of the external surface is still smooth, while the other part is replaced with rough and granular stuffing, indicating that this particle is definitely partially dissolved and reacted. Fig 3.10d shows a completely reacted fly ash particle, but the fly ash-to-geopolymer transformation is not so advanced that the reacted particle still maintains its spherical

geometry. Moreover, it seems the surface of the reacted sphere is highly porous, which is likely an indicator of the early termination of the ongoing geopolymerization reaction (e.g., possibly before the settling or hardening of geopolymer precursor). In addition, in all four micrographs, some smaller spheres that may be the unreacted fly ash particles can also be identified. These observations indicate that the final geopolymer products may not conform to the pre-designed Si/Al ratios, owing to a small fraction of raw materials not involved in the reaction. In fact, the change in the Si/Al molar ratio as well as the reduction in the relative content of pure geopolymer binder can directly affects the development of the UCS.

3.3.4 X-ray Fluorescence Analysis

In general, XRF yields the mass percentages of the compositional elements in a material, which are then by convention converted to the corresponding oxides, such as SiO_2, Al_2O_3, Fe_2O_3, TiO_2, MnO, CaO, Na_2O, K_2O, and P_2O_5, among others. Based on the elements' percentages, the average Si/Al molar ratios of all geopolymer samples cured in different saline solutions were calculated, and the results are presented in Table 3.2. For the GC-1.78 samples, the Si/Al molar ratio decreases from 1.83 to 1.79 when the salinity increases from 0 to 35 ppt. When compared with the air-cured samples, underwater casting and curing tends to increase the Si/Al ratio. For the air-cured GC-2.00 sample, the actual Si/Al ratio measured by XRF is 1.98, slightly lower than the pre-designed value of 2.00, which may be caused by the variability and nonhomogeneity of the raw materials. Similarly, underwater casting and curing causes an increase in the Si/Al ratio: i.e., 1.99 for 0 ppt, 2.09 for 15 ppt, and 2.04 for 35 ppt. The increase in the Si/Al ratio in the immediate water-cured samples suggests that a loss of Al^{3+} may take place, or the Al^{3+} may migrate from the

geopolymer slurry into the curing solutions. At this time, it is unclear why the Si^{4+} does not migrate out of the slurry. Nevertheless, the amount of lost Al^{3+} is still very small, when compared with other cations, as discussed later.

As an example, to illustrate the occurrence of chemical exchanges between the curing solutions and the being-cured geopolymer slurry, Fig 3.11 compares various Si-based elements' concentrations (i.e., in terms of the molar ratio of a specific element to Si) for the GC-2.00 sample cured in fresh water. For all of the considered major elements, including Si, Al, Na, Fe, Mg, Ca, and K, a dramatic decrease in the Na/Si ratio occurs, indicating that the major chemical exchange is the loss of Na^+, i.e., the permeation of the Na^+ from the geopolymer slurry to the curing solution, while other elements have little loss. Moreover, the exterior layer of the sample experiences more Na^+ loss than the interior core, which should be expected. In fact, since the curing mold is permeable, the being-cured slurry, which has a much higher Na^+ concentration than the curing fresh water, loses its Na^+ via mainly dispersion induced by differential concentration. However, upon immediate submersion of the slurry into water, geopolymerization reaction (mainly the polycondensation or hardening stage) occurs simultaneously with the chemical exchange between the being-cured geopolymer slurry and curing solution, and thus it competes with the dispersion process to retain the Na^+. If the geopolymerization occurs very fast, leaving little time to allow the migration or dispersion of Na^+ out of the slurry, then the majority of Na^+ cations remains in the cured geopolymer. This is mainly the case for the interior core of the sample. On the contrary, a slow geopolymerization reaction allows more Na^+ to leach into the curing water, which is the case for the exterior layer of the sample. As such, future

research may investigate the kinetics of the two competing reactions: chemical exchange or dispersion versus geopolymerization.

Prior discussion indicates that a major change in the Na/Si ratio occurs in the water-cured samples. As such, in the subsequent analysis, only Na or Na_2O is selected as an effective indicator to assess the degree of chemical exchanges between the being-cured geopolymer slurry and the curing saline solutions. Fig 3.12 compares the mass based Na_2O contents for the two geopolymer samples cured in different saline solutions. Again, for the GC-2.00 samples, results of the exterior layer and interior core are separate in this figure. In general, for both types of geopolymers, the Na_2O content increases with increasing the salinity of curing solutions. Moreover, for the GC-2.00 samples, the Na_2O content of all the exterior layers is less than that of the interior core, which is consistent with the visually observed color change (Fig 9a and 9b). When compared with the air-cured GC-2.00 sample, the exterior layer of 35 ppt cured sample possesses an even higher Na_2O content than the air-cured counterpart. Air-cured samples should have no loss of Na_2O content and hence can be used as a baseline reference. The Na^+ concentration in the 35 ppt saline solution may be even higher than that of the geopolymer polymer slurry, and hence during curing the Na^+ in the saline solution may disperse into the slurry, resulting in an increase in the Na^+ or Na_2O content in the final geopolymer products. For the samples cured in 0 and 15 ppt saline solutions, their Na_2O contents are all lower than that of the air-cured samples. This is of course caused by the dispersion of Na^+ in the geopolymer slurry into the curing solutions that have a relatively lower Na^+ concentration. In summary, during curing, Na^+ may disperse into the geopolymer slurry if the curing saline solution has a higher Na^+

concentration, or out of the geopolymer slurry if the curing solution has a lower Na^+ concentration.

3.3.5 pH Measurements

To further prove the exchange (i.e., either leaching or intrusion) of chemicals between the being-cured geopolymer slurry and the curing solution during the period of 28-day's curing, the pH values of different curing solutions for all samples were measured before and after the curing process. To ensure accuracy and comparability, the volume of each curing solution is exactly 150 ml. The 0, 15 and 35 ppt saline solutions have initial pH 6.97, 8.04, and 8.00, respectively, which remain the same within 24 hours. Fig 3.13a compares the curing solutions' pH values obtained before and after the curing process for the two types of geopolymers. Clearly, after 28-day's curing, the pH values of all curing solutions increase to different extents. At the same salinity, curing the GC-2.00 samples causes slightly higher increases than curing the GC-1.78 ones, obviously owing to the higher NaOH concentration used in the GC-2.00 synthesis. Fig 3.13b compares the pH increment (i.e., ΔpH) for the OWC, GC-1.78, and GC-2.00 samples. For the same curing solution (i.e., the same salinity), OWC induces the largest ΔpH, while the smallest ΔpH is caused by the GC-1.78, but the ΔpH difference between the GC-2.00 and GC-1.78 is not so significant. The most important feature is that the higher the curing solution's salinity, the lower the change in its pH (i.e., ΔpH). The increase in the curing solutions' pH manifests the leaching of OH^- and alkali metal cations from the geopolymer slurry into the solution [77,98], which is consistent with the XRF results discussed earlier. Therefore, according to the principle of chemical equilibrium, a curing solution with a higher salinity

or ionic strength can suppress the leaching of OH^- from the slurry into the solution, thusly preventing the further reduction in the strength of cured geopolymers.

3.4 Discussion

3.4.1 Difference from Prior Studies

As stated previously, much work has been conducted on the resistance of geopolymers to various chemical solutions. Such resistance involves the interactions between the chemical solutions and geopolymers that have been completely cured (e.g., after 28-day's curing) or pre-cured in air to some extent (e.g., the samples at least hardened so that demolding and handling become possible). For example, Giasuddin et al. [80] studied Class F fly ash-based geopolymers with a small fraction of ground granulated blast furnace slag as an additive cured in freshwater and NaCl solutions, and monitored the pH of the different curing media over time. They found that the pH increment was fast at the beginning 2 hours upon sample submersion and then became slower after 2 hours, but their samples had been first air-cured inside non-permeable molds at room temperature for 10-12 h and then placed in the liquids after demolding, or at least were not underwater casted with the curing started when the geopolymer was still in a slurry consistency. Thokchom et al. [77] studied the interactions between the Class F fly ash-based geopolymer mortars and 10% magnesium sulfate solution by exposing samples that had been air-cured for 28 days to the solution for up to 24 weeks, and found that the increase in pH was rapid during the initial 3 weeks and thereafter was not appreciable. However, a significant difference that distinguishes the current study from others is that the interactions between the

geopolymer and curing solutions start immediately after underwater casting. In other words, little or no air-curing/hardening is permitted prior to the submersion of the geopolymer slurry into the curing solution. Such a procedure realistically simulates the actual construction process such as injecting cement slurry into the borehole for well cementing or casting in situ concrete slurry under seawater. As such, it should be expected that more and faster chemical exchanges occur between the curing saline solutions and geopolymer slurry than the pre-hardened geopolymer, which is likely to affect the strength development of geopolymers and thus needs to be simulated in laboratory experiments.

3.4.2 Mechanisms for Strength Development

Based on the above results, casting and immediate curing in three saline solutions leads to a significant difference in the UCS of the geopolymer and OWC samples. In particular, the OWC's UCS decreases significantly with increasing the solution's salinity, while the geopolymer shows the opposite trend. It is well known that the strength of OPC can be negatively affected by the chemicals in seawater, such as the Cl^-, SO_4^{2-}, and Na^+. Detailed discussion of these effects is not the focus of this paper, but can be found in a plenty of publications, some of which are summarized earlier.

For geopolymers, although the above results show that curing in saline water can still cause the leaching of OH^- and Na^+, the amount of leached ions and other chemicals decreases with increasing salinity. As such, when compared with freshwater curing, increasing the curing solution's salinity actually results in an increase in the UCS. In other words, a higher salinity can suppress the leaching of alkali ions (i.e., Na^+, OH^-) from the slurry, which can influence the development of UCS. Moreover, a beneficial effect is that,

if the curing solution has a higher Na^+ concentration than the being-cured geopolymer slurry, Na^+ cations may intrude into the latter, resulting in a higher strength. In addition, geopolymers in general are not prone to chemical attacks or deterioration by Cl^-, SO_4^{2+}, among others. Therefore, the underlying mechanisms for the increase in the UCS of geopolymers cured in saline solutions, when compared with freshwater curing, include primarily the prevention and reduction of leaching of alkali ions from the slurry, and secondarily the ingress of some beneficial cations such as Na^+ into the slurry when the curing solution's salinity is very high.

3.4.3 Practical Implications

As discussed above, the increase in the UCS of saline water-cured geopolymers with curing salinity demonstrates that a higher salinity such as 35 ppt can bring beneficial effects on the mechanical properties. Moreover, such an effect of saline water curing on the rate and magnitude of strength is more pronounced for the geopolymer with a lower Si/Al molar ratio than the one with a higher Si/Al ratio. These findings have significant practical implications for underwater construction that requires in-situ casting concrete slurry directly underwater, particularly in chemically harsh environments such as offshore and underground brine formations. Although special Portland cements (such as the studied oil well cement) can fulfill the functional needs, they are prone to chemical attacks and deterioration, particularly by the high-salinity solutions. However, for geopolymers that have been proven to resist acid and sulphate chemicals, directly casting in high-salinity water actually favors the development of higher mechanical strengths, thusly eliminating

the need for extra functional additives typically used to improve the durability and resistance of OPC.

A particular noteworthy scenario is the potential application of geopolymers for oil well cementing in brine reservoirs. If OPC were used, the high salinity in the rock formations would require special additives to improve the resistance and durability of Portland cement to salt attacks, particularly at the construction stage when the cement slurry is injected into the gap between steel casing and borehole wall. Otherwise the Portland cement slurry may not reach the desired or designed strength upon curing in brine water. However, for geopolymer slurry, a higher salinity can be even beneficial to the strength development of geopolymer slurry. The higher the salinity, the better the strength development. Based on the above results, a higher Si/Al molar ratio within a certain range can lead to a higher UCS for underwater cast and cured geopolymers, due to the less leaching of alkali ions or the intake of some ions from the solution into the slurry.

3.5 Conclusions

Two types of geopolymers with different Si/Al molar ratios, synthesized from the mixture of Class C fly ash and metakaolin, were underwater cast and cured in saline solutions of varying salinity. Their mechanical properties, chemical and mineralogical compositions, microstructure, leaching behavior were characterized. Based on the analysis and comparison of the results, the following conclusions can be drawn:

- For the two studied geopolymers (i.e., two Si/Al molar ratios), their UCS increases with the curing solution's salinity, while the OWC exhibits the opposite behavior, and its UCS decreases with the salinity. Moreover, although

the GC-2.00 geopolymer has a higher UCS than the GC-1.78, the latter shows a higher UCS increment than the former.

- According to the compositional and microstructural analyses, the two completely cured products are both geopolymeric composites, but not pure geopolymers. The final materials comprise a gel-like geopolymer binder as the major matrix and include nonreactive crystalline phases from raw materials as well as un-reacted or partially reacted reactive phases. Moreover, immediate curing in saline water can slightly increase the porosity of the outer layer and leads to non-uniform coloration of the material.
- Upon underwater casting and immediate curing, geopolymer slurry starts to interact with the curing solution via primarily exchange of chemicals (i.e., leaching or intrusion), and the amount of chemical exchanges may depend upon the rate of geopolymerization reaction (i.e., the hardening or setting). In fact, the leaching out of or intrusion into the slurry and the hardening are two competitive processes that dominate the curing reactions and the performance of the final cured geopolymer.
- The major chemicals exchanged between the geopolymer slurry and curing saline solutions include Na+ and OH-, two key ions responsible for the mechanical properties of geopolymer.
- The findings of this study can shed light on the practical applications of geopolymer in chemically harsh environments with additional benefits, such as resistance to chemical attack and enhanced strength resulting from high salinity.

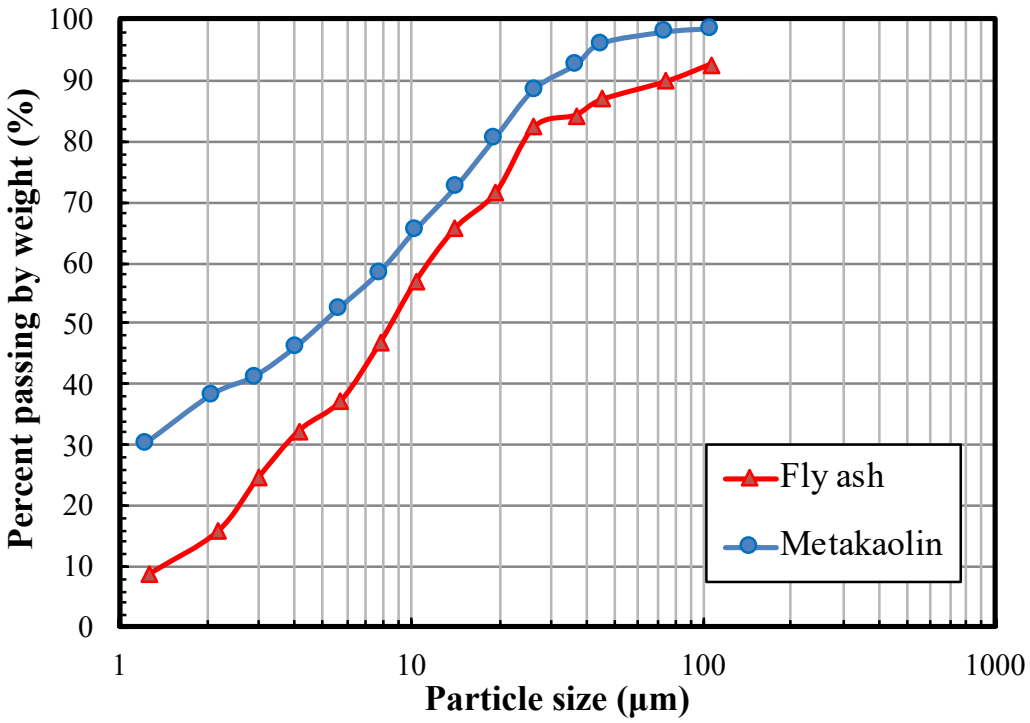

Figure 3.1: Particle size distribution of two raw materials, fly ash and metakaolin, used for geopolymer synthesis.

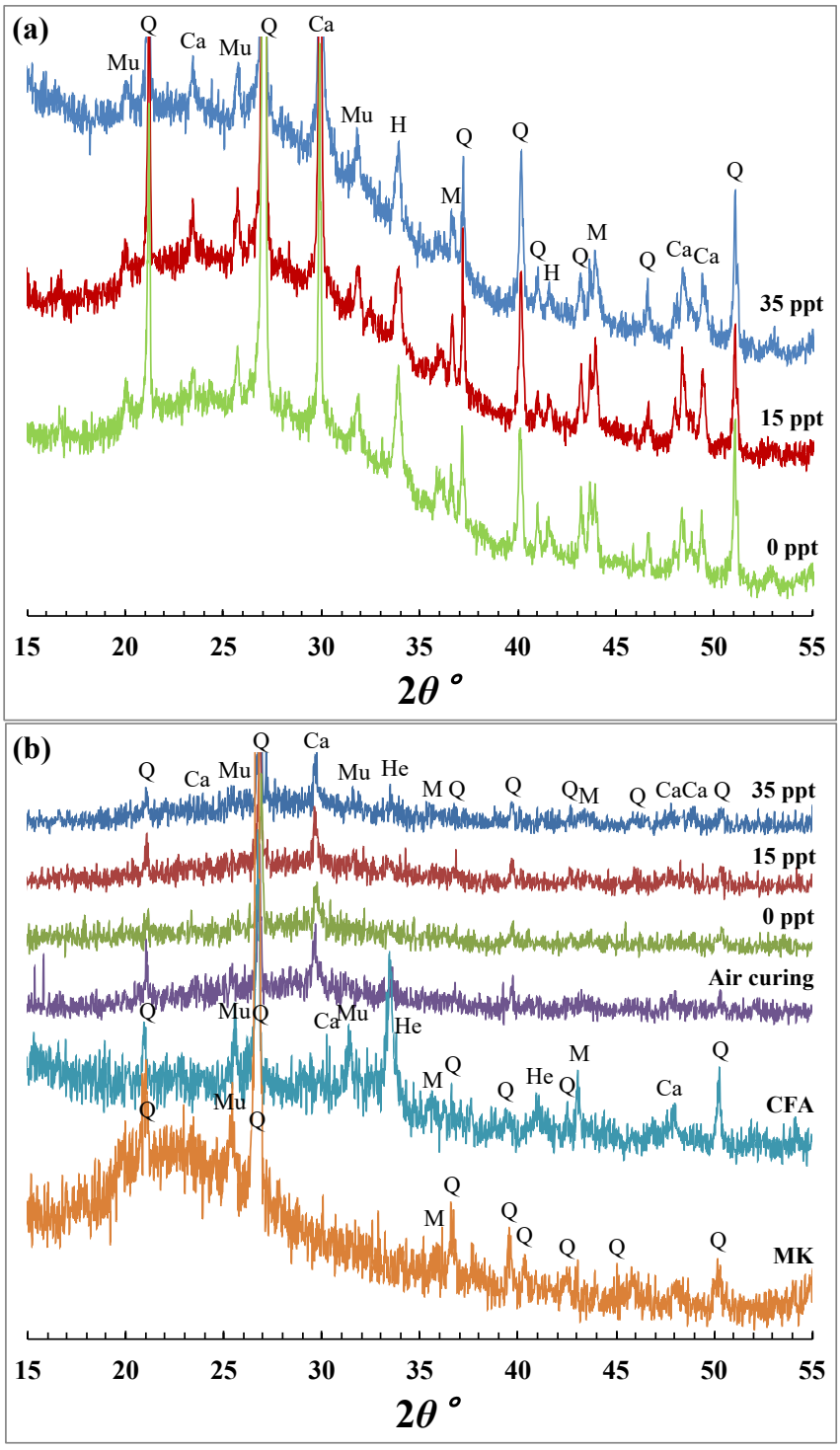

Figure 3.2: XRD patterns of raw materials and geopolymer samples cured in different saline solutions: (a) GC-1.78; (b) GC-2.00 (MK = metakaolin, CFA = Class C fly ash, Mu = Mullite, Ca = Calcite, He = Hematite, M = Magnetite, Q = Quartz).

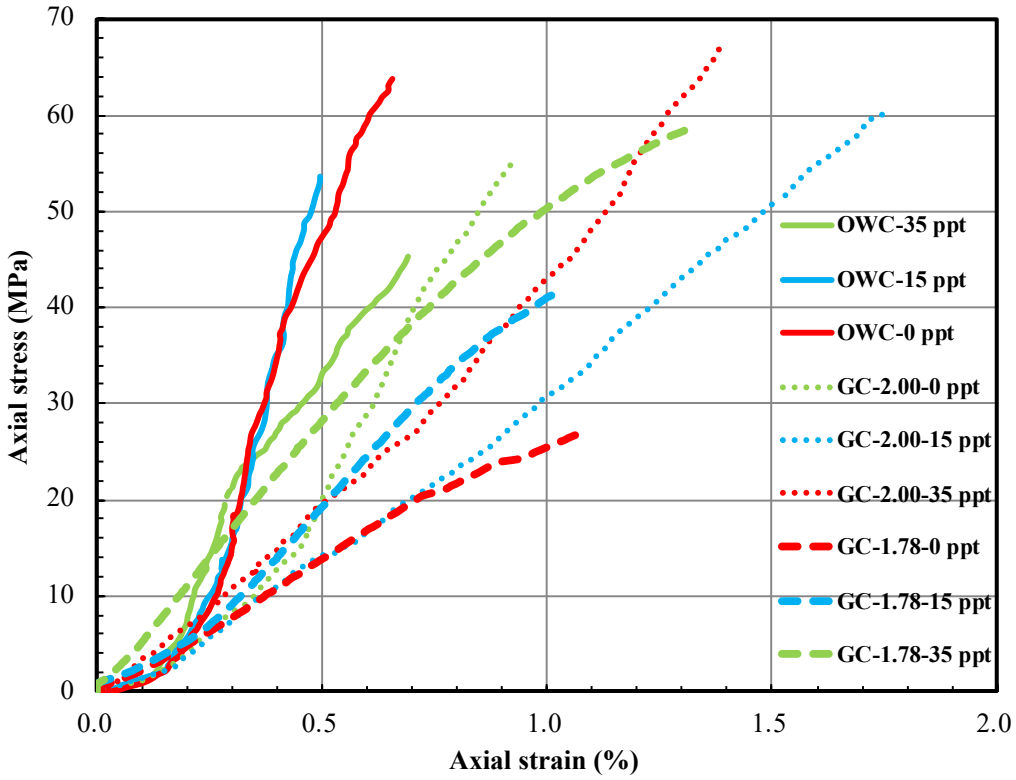

Figure 3.3: Example stress-strain curves of Class G oil well cement and geopolymer samples.

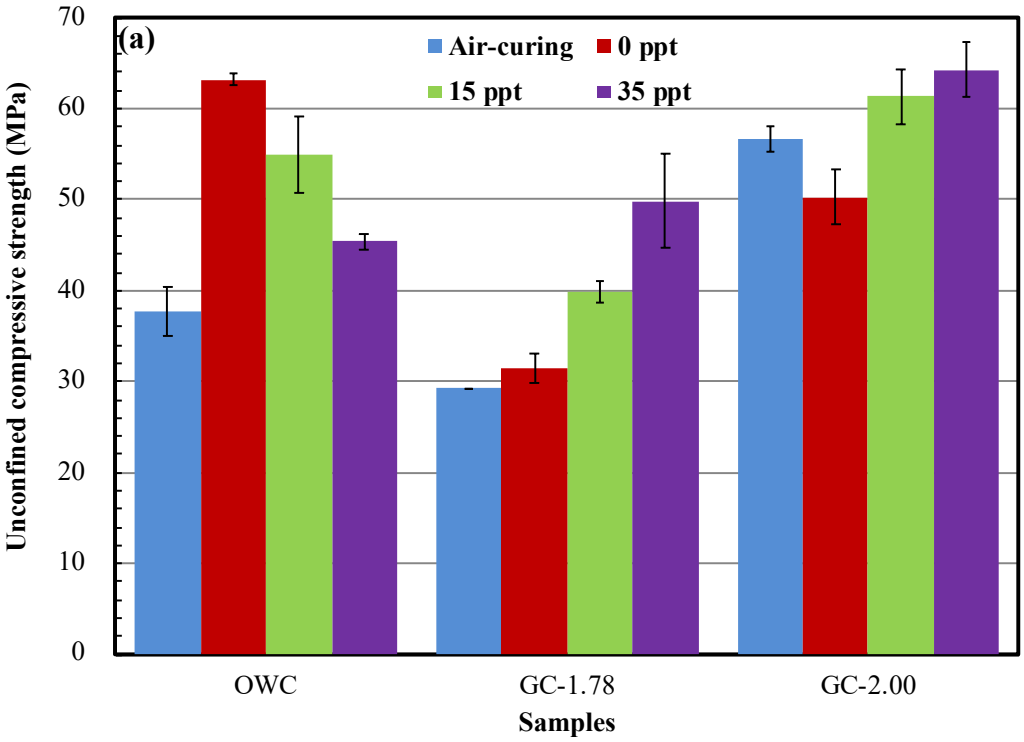
(a)
Air-curing
0 ppt
15 ppt
35 ppt
Unconfined compressive strength (MPa)
70
60
50
40
30
20
10
0
OWC
GC-1.78
GC-2.00
Samples

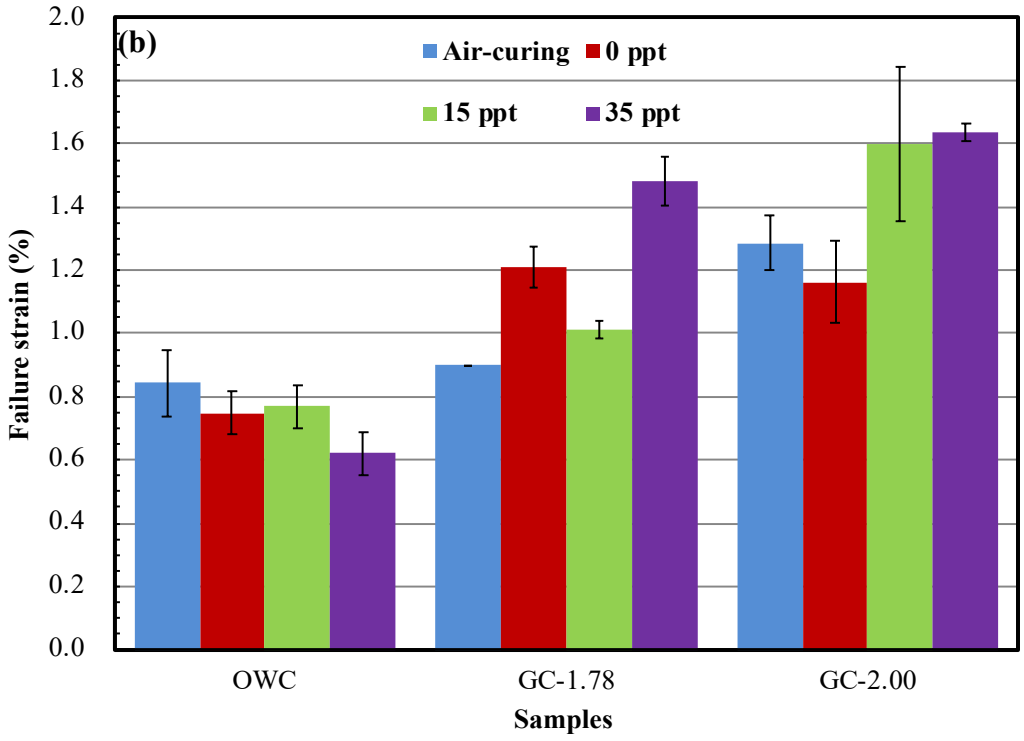
(b)
Air-curing
0 ppt
15 ppt
35 ppt
Failure strain (%)
2.0
1.8
1.6
1.4
1.2
1.0
0.8
0.6
0.4
0.2
0.0
OWC
GC-1.78
GC-2.00
Samples

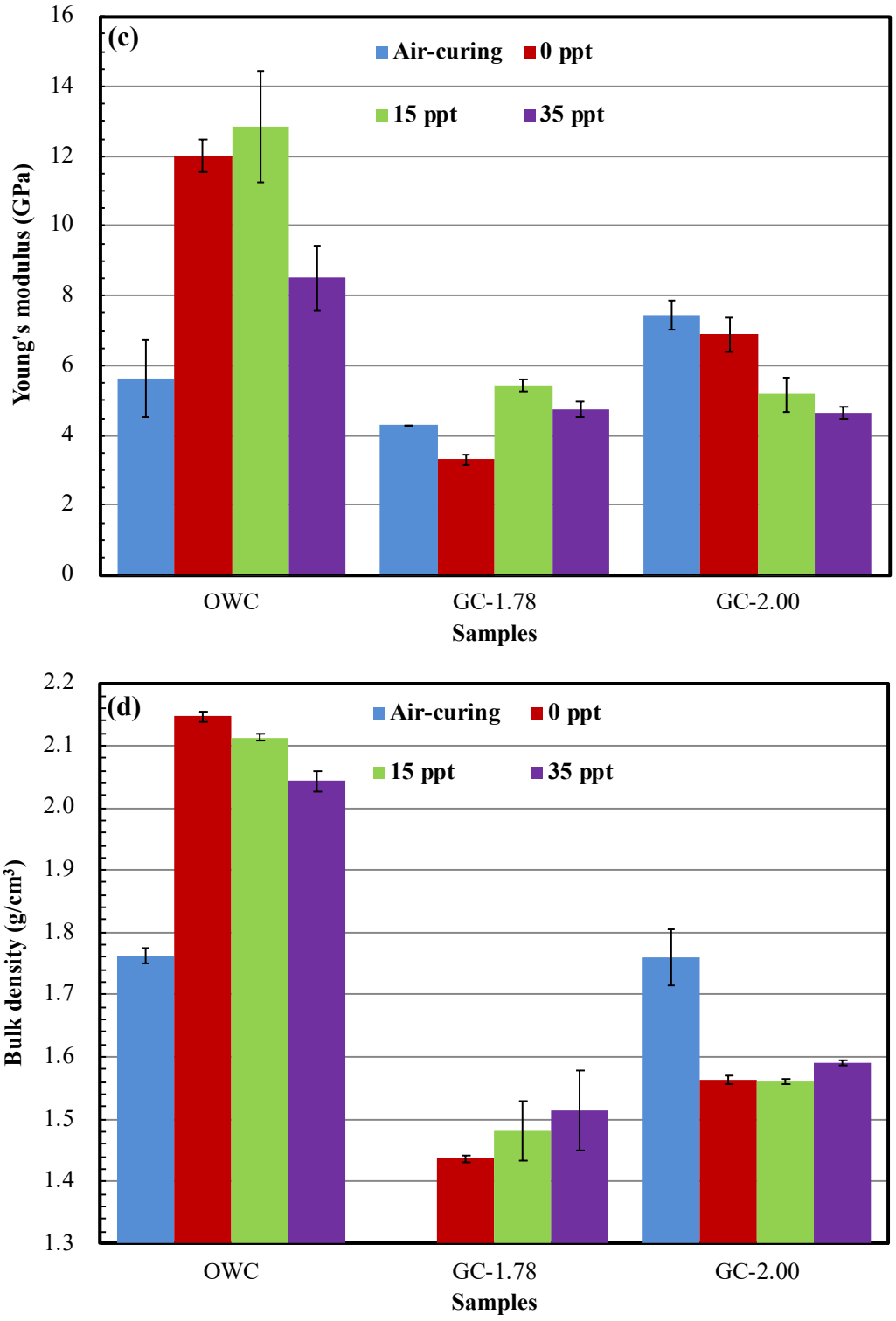

Figure 3.4: Mechanical and physical property indexes of Class G oil well cement and geopolymer cement samples after 28 days curing: (a) unconfined compressive strength; (b) failure strains; (c) Young's modulus; (d) bulk densities (the error bars represent one standard deviation, which applies to other figures as well).

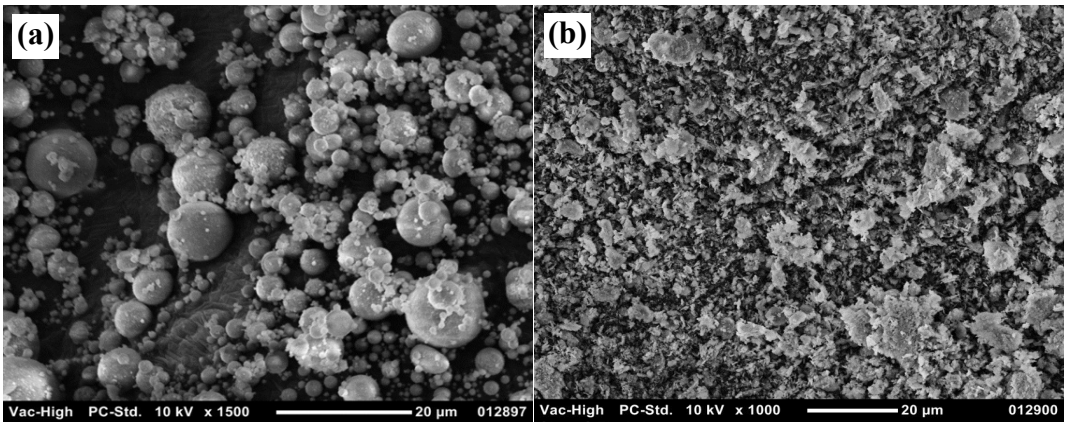

Figure 3.5: SEM micrographs of raw materials: (a) Class C fly ash; (b) metakaolin.

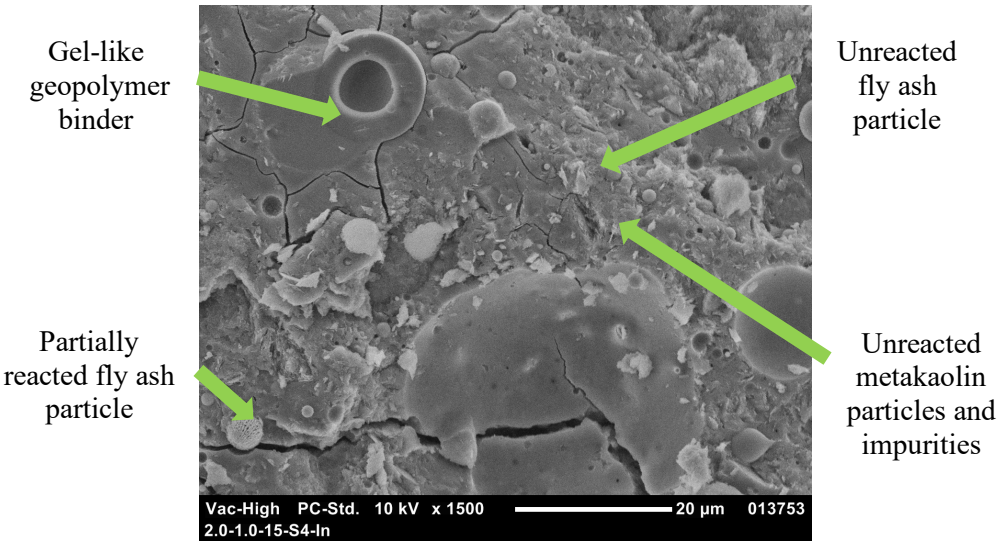

Figure 3.6: An SEM micrograph showing the overall microstructure and composition of the geopolymer samples.

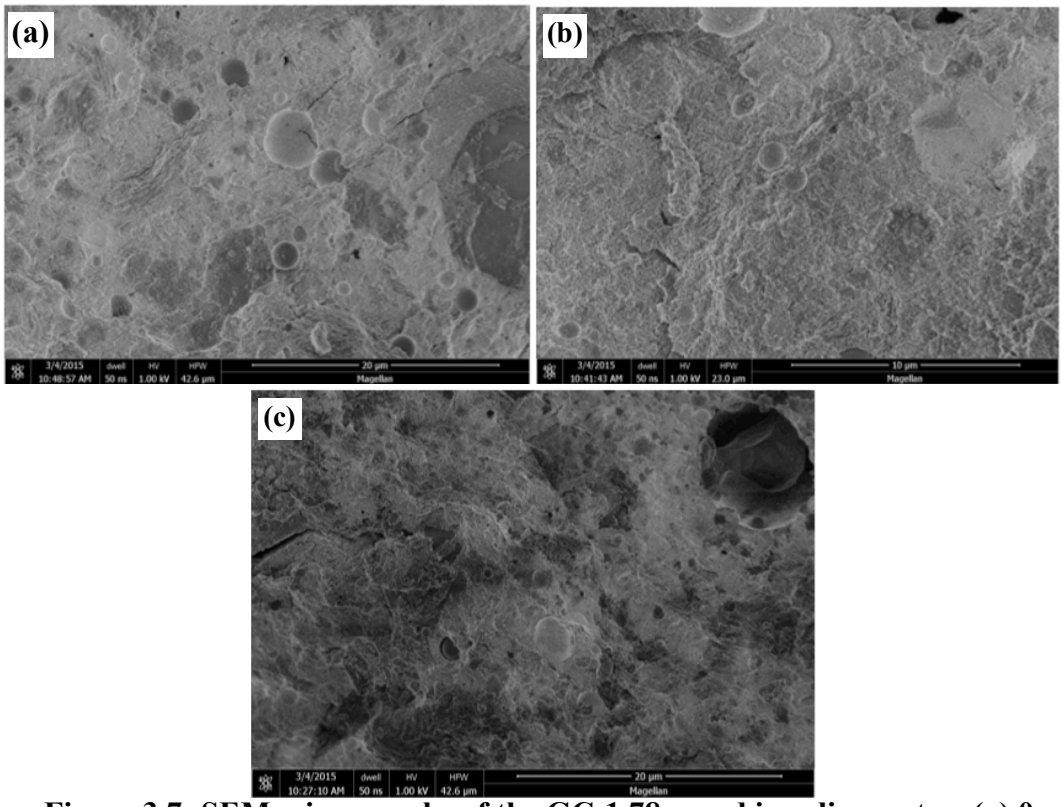

Figure 3.7: SEM micrographs of the GC-1.78 cured in saline water: (a) 0 ppt; (b) 15 ppt; (c) 35 ppt.

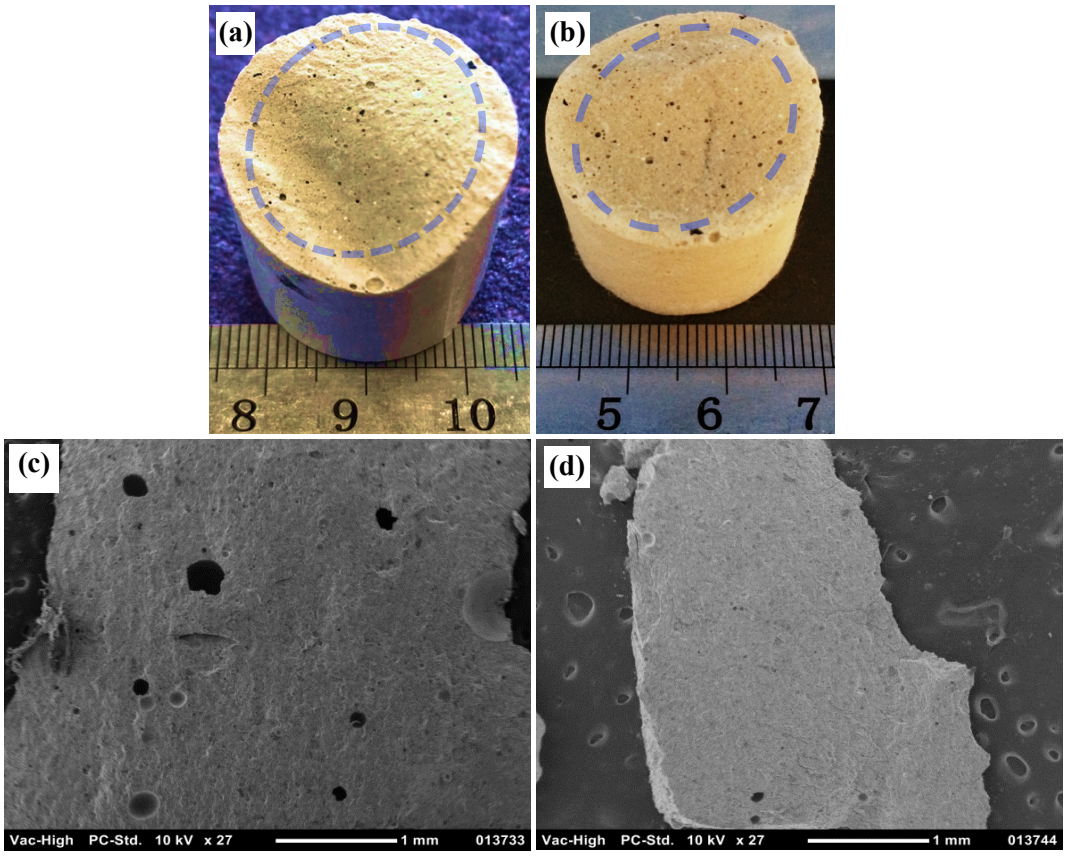

Figure 3.8: Different appearance and microstructure of the exterior and interior layers of 15 ppt saline water-cured GC-2.00 samples: (a) and (b) optical images of the cross-sectional surface of two different cylindrical samples; (c) SEM micrograph of the exterior layer; (d) SEM micrograph of the interior layer.

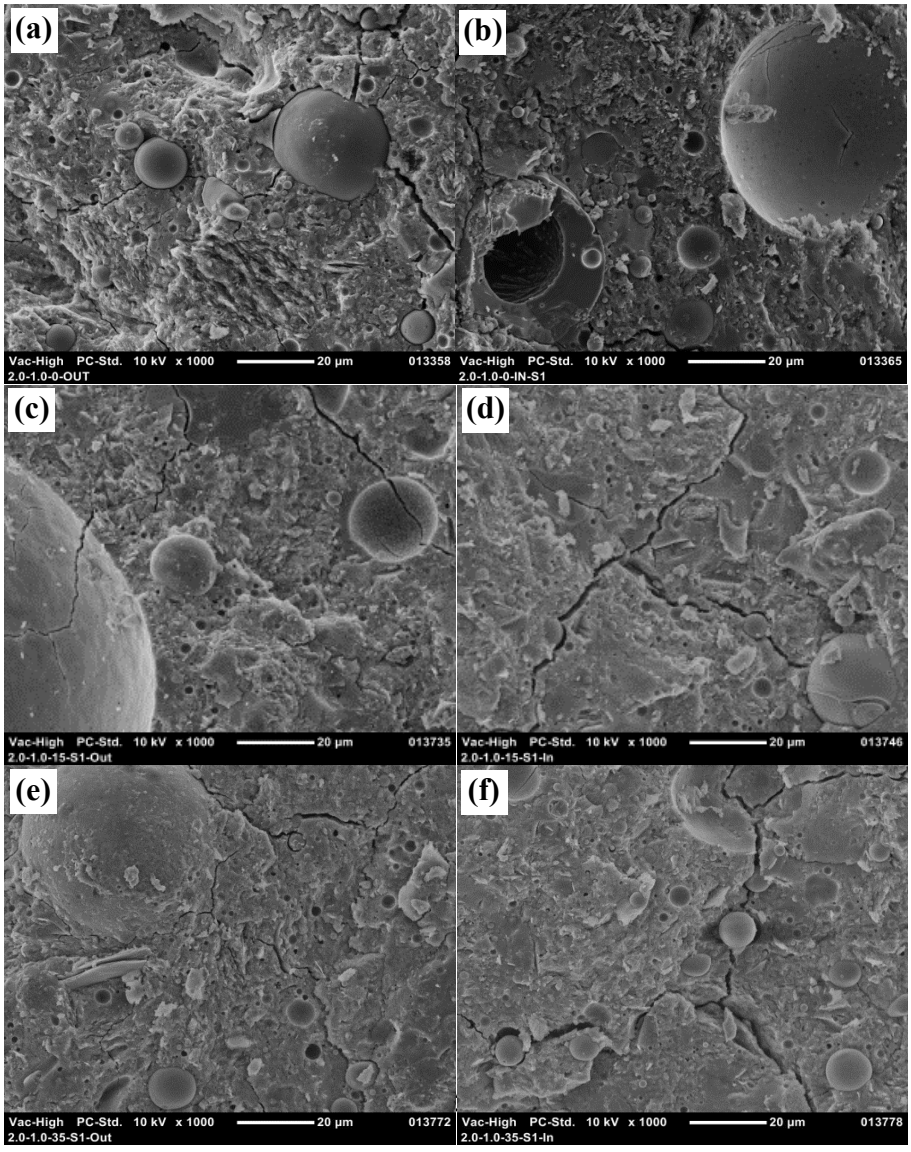

Figure 3.9: SEM micrographs of the GC-2.00 samples cured in different saline water: (a-b) 0 ppt; (c-d) 15 ppt; (e-f) 35 ppt; (a), (c), and (d) are from the exterior layer; (b), (d), and (f) are from the interior layer.

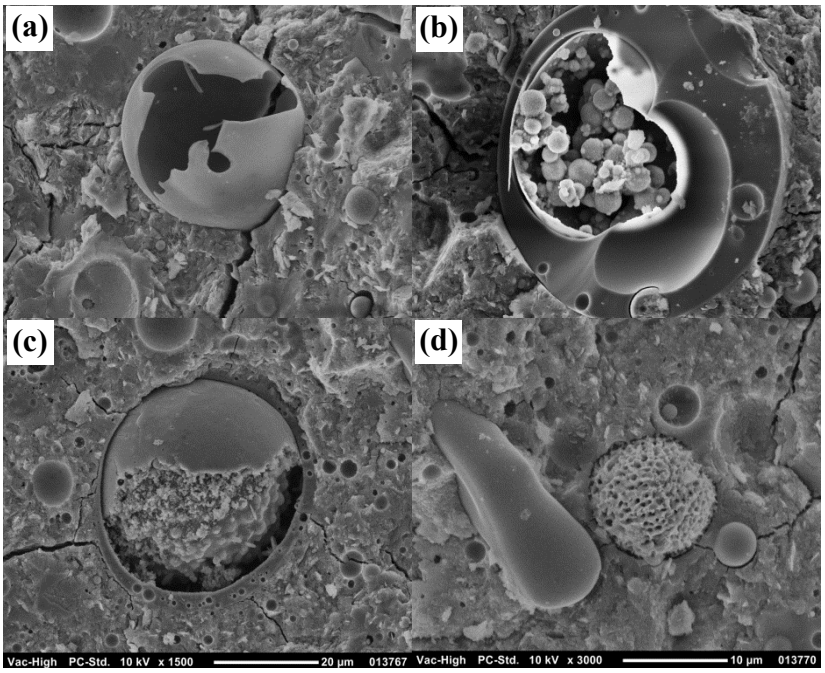

Figure 3.10: SEM micrographs showing the different micromorphological features of fly ash particles: (a) unreacted hollow sphere; (b) unreacted cenosphere; (c) partially reacted solid sphere; (d) completely reacted solid sphere.

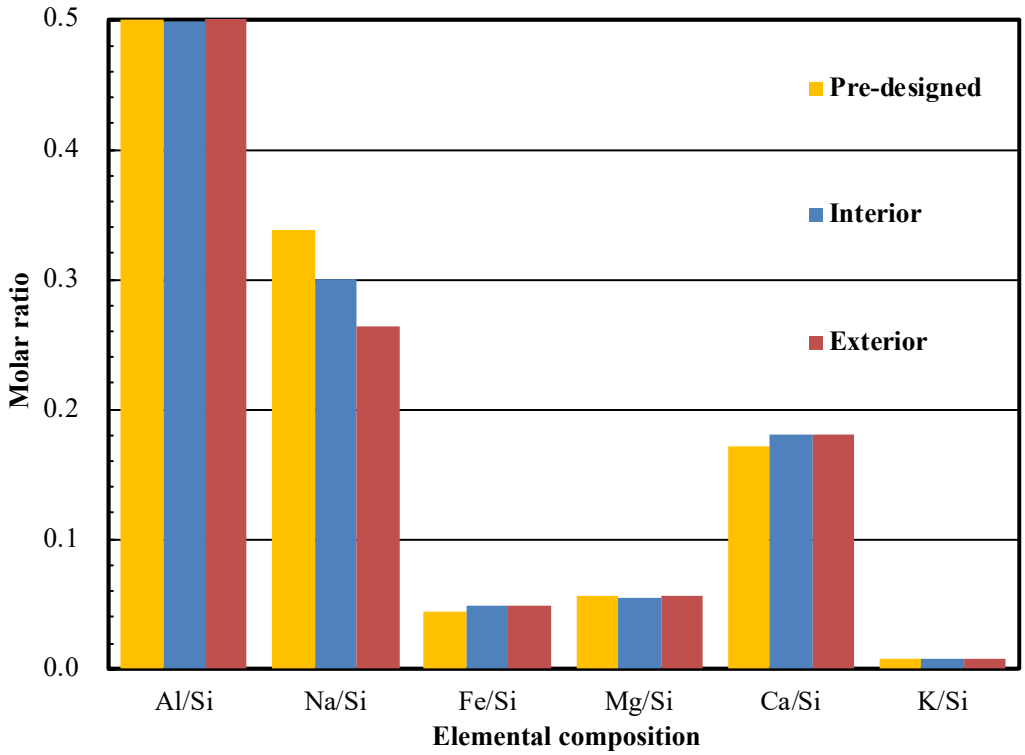

Figure 3.11: Molar ratio of elemental composition of GC-2.00 (0 ppt) among Al, Na, Fe, Mg, Ca, K, and Si.

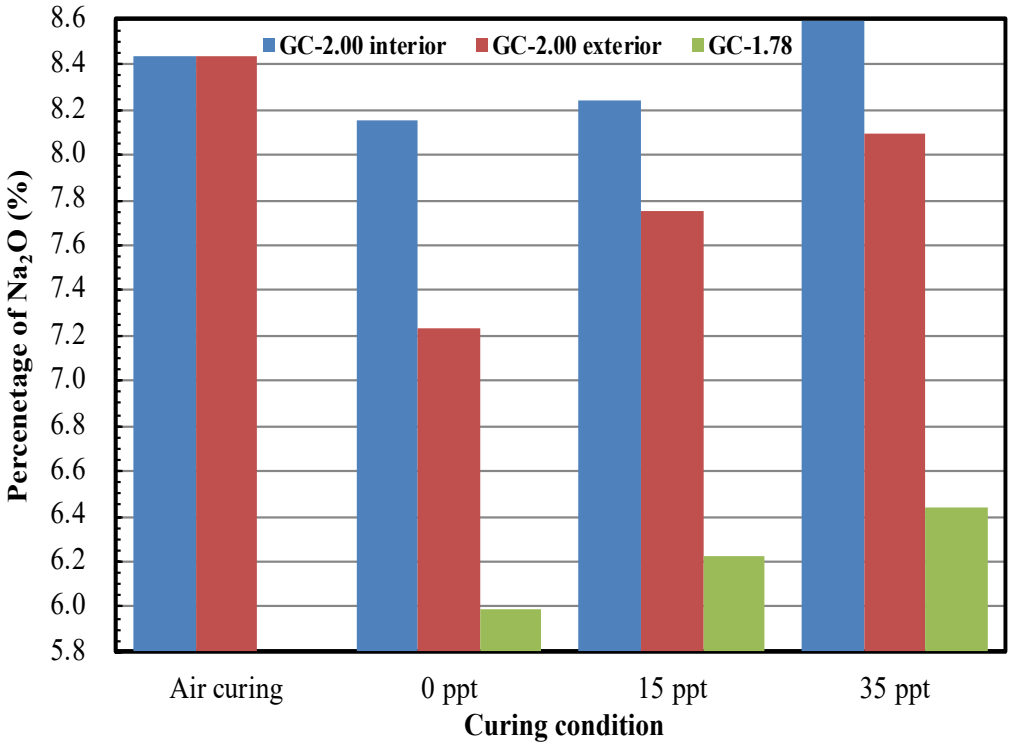

Figure 3.12: Percentage of Na_2O of geopolymer samples under different curing conditions.

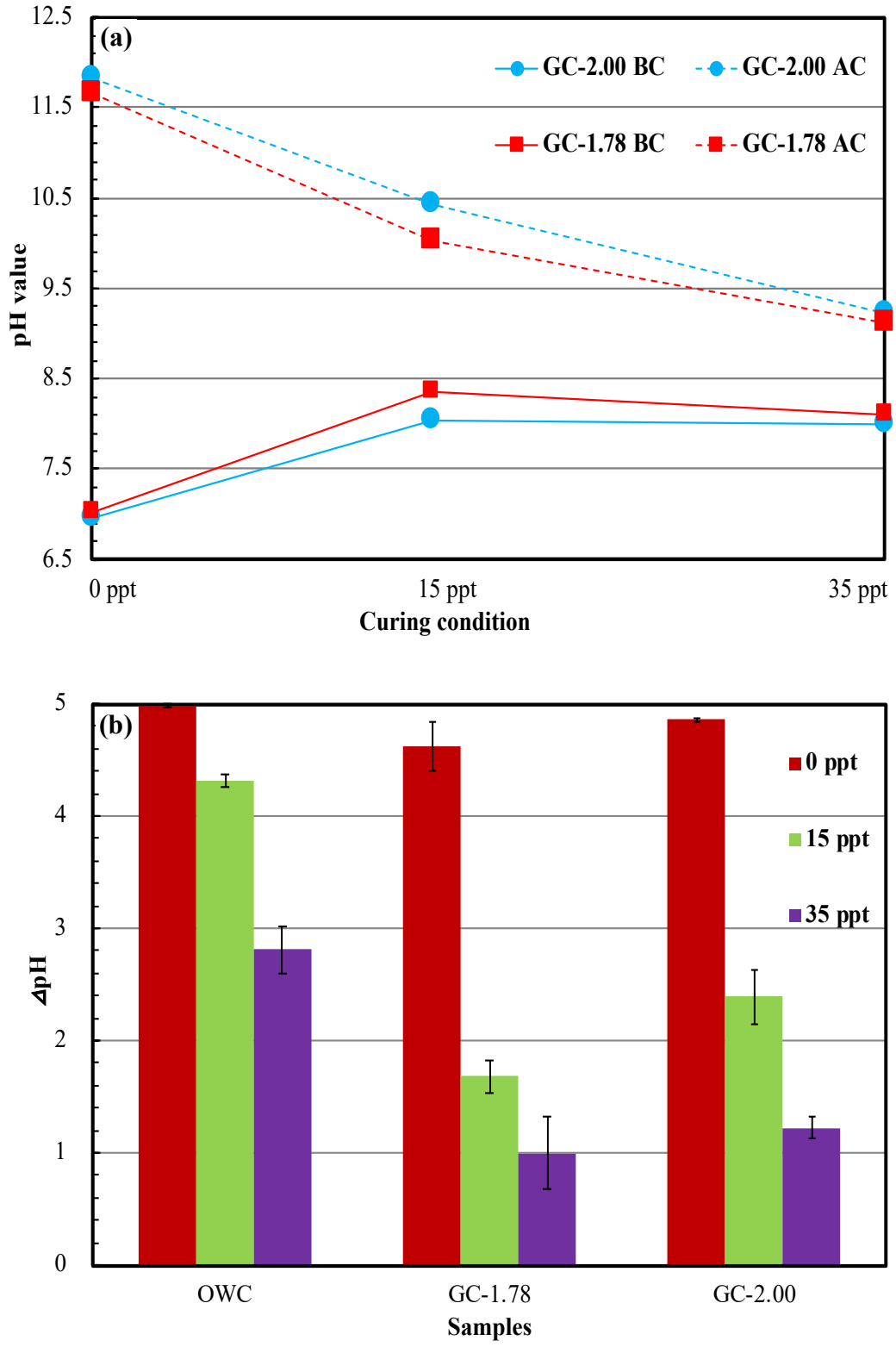

Figure 3.13: Average pH value (a) and increment (b) of pH (*Δ*pH) of curing water (BC = before curing process; AC = after curing process).

Table 3.1: Size fractions and chemical compositions[a] of the Class C fly ash and metakaolin.

Composition	Class C Fly ash (wt.%)	Metakaolin (wt.%)
Clay-sized fraction (≤ 2 μm)	14.70	38.30
Silt-sized fraction (2 – 75 μm)	74.10	58.90
Sand-sized fraction (> 75 μm)	11.20	2.80
SiO_2	38.56	56.61
Al_2O_3	19.80	39.16
Fe_2O_3	6.26	1.87
MgO	5.15	0.09
CaO	22.28	0.05
SO_3	1.72	0.05
K_2O	0.61	0.30
Na_2O	1.58	0.01
Moisture	0.11	0.13
LOI	0.41	0.19
Total	96.48	98.46

[a] Chemical composition data provided by the supplier.

Table 3.2: The average Si/Al molar ratios of all geopolymer samples cured in different saline solutions.

Curing solution concentration (ppt)	Si/Al molar ratio	
	GC-1.78	GC-2.00
0	1.83	1.99
15	1.81	2.09
35	1.79	2.04
Air-curing	1.78	1.98

CHAPTER 4

SALINE WATER CURED GEOPOLYMER: EFFECT OF NA TO AL RATIO

4.1 Introduction

Geopolymers, as an alternative binder material especially for current popular calcium silicate hydrate binder [14,15,23,93], are attracting continuous increasing enthusiasm of research. It is well-known for the prominent characteristics, such as super compressive strength, low permeability, excellent chemical resistance, exceptional fire resistance, and high durability as well as low energy consumption and low carbon emission during manufacture [14,15,103–106]. In addition, the reusing of solid wastes, such as fly ash, granulated blast furnace slag, rice husk ash, or red mud, is another widespread concern [44,95–97,107].

Geopolymers are inorganic synthetic materials produced through the reaction between aluminosilicate materials and alkaline solutions, forming an amorphous to semi-crystalline chains or network structures of aluminosilicate mineral in tetrahedral coordination linked with co-valent bonds (oxygen bridges) [32–34]. The general formula is as follows: $M^{+}_{n}\{-(SiO_2)_z\text{-}AlO_2\text{-}\}_n$ where M is an alkali cation such as K^+ or Na^+, n is the degree of polymerization, and z is the Si/Al molar ratio, which can be 1, 2, 3, or >> 3 [42–44].

It is known that geopolymers have a good performance in the field of resistance to salts corrosion. Thokchom et al. [77] studied the performance of Class F fly ash based geopolymer mortar specimens with three different Na_2O contents in magnesium sulphate solution. After 28-days' air-curing in room temperature (including 2 days in an oven), specimens were immersed in 10 wt.% solution of magnesium sulphate up to another 24

weeks. Mechanical experiments showed that all the samples display decrease in strength (up to 56% loss), when higher Na_2O contents brings a greater strength. This result indicated that magnesium sulphate solution curing causes the negative influence on the mechanical properties of geopolymers although high Na_2O contents of samples can relatively improve the strength to some extent. Nasvi et al. [81] examined the mechanical characteristics of Class F fly ash-based geopolymer, cured in freshwater and saline water (5% and 15% NaCl solution). They found geopolymer samples experience a reduction of strength in freshwater and saline water and the reduction rate is almost half of that of OPC-based oil well cement. In Addition, the reduction rate was less for samples cured in higher saline solution, due to the lower alkali leaching rates from geopolymers into the brine water. Giasuddin et al. [80] found that fly ash-based geopolymers cured in saline solutions (8 and 15 wt.% NaCl) display higher strength than that cured in freshwater, but still lower that the air-cured counterparts. It illustrated that the decrease of strength is directly related to the leaching of alkali and metal cations from the sample.

Some studies were also conducted to investigate the effect of activator on the mechanical performance of geopolymers. Hou et al. [108] investigated the influence of concentration and the SiO_2/Na_2O molar ratios (1.0-2.5) of alkaline activator solution on mechanical performance of Class C fly ash-based geopolymers, and found that the UCS increases with the increasing SiO_2/Na_2O molar ratios, while it is opposite with SiO_2/Na_2O molar ratio exceeded 1.4. Gao et al. [109] and Rattanasak and Chindaprasirt [110] also obtained the similar results that the metakaolin-based or fly ash-based geopolymers with the SiO_2/Na_2O molar ratio of 1.5 exhibits the better mechanical performance as well as lesser porosity. Lyu et al. [91] discovered that the mechanical properties of metakaolin-

based geopolymer with various SiO_2/Na_2O molar ratios (1.27-1.91) are correlated with the different constituents and structures such as silicon $Q^4(4Al)$ and silicon $Q^4(2Al)$.

As mentioned before, most of the research aimed at studying the effect of saline solution curing started from the time when the geopolymers have hardened, and hence the relatively less chemical exchange. In other words, they didn't consider the most important period of the first several curing days, in which the ions exchange should be the most active. Therefore, in this study, the cast geopolymer slurry in the mold will be dipped into the curing solution with no time interval between these two-step operations, which can supply the appropriate opportunity and sufficient time for the chemical exchanges between the geopolymer slurry and curing water. This design is to furthest simulate the current process of well cementing that oil well cement slurry is injected into the well where chemical exchanges between cement slurry and permeable rock formations take place before and during the hydration reaction. In addition, in order to realize such design, kind pf porous molds were used to permit the chemical exchanges. In prior studies, little research was done to apply the compounded salts (e.g., not a pure NaCl or $MgSO_4$) to prepare the curing saline water. To differentiate this study from others that only submerge the pre-hardened geopolymer samples into saline solutions prepared with homogeneous type of salt, one kind of commercial sea salt (salt-mixture) was used to simulate the chemistry of the brine fluids, and customer-built, porous, permeable molds for underwater casting and curing of geopolymer slurry. In summary, the research on two aspects will be carried out in presented work: (1) to investigate the influences of casting and immediate curing in saline solutions on the characteristics of geopolymers in terms of mechanical properties, microstructure, and chemical and mineralogical compositions; (2) to discuss the effects of four different

Na/Al molar ratios on the geopolymers' performance under the function of saline water curing.

4.2 Materials and Methods

4.2.1 Materials

The geopolymer formulation was based on the aluminosilicate components of Class C fly ash [52] and metakaolin, purchased from Headwater Resources, Inc., USA and Advanced Cement Technologies, LLC, USA, respectively. The particle size distributions [28] of the dry fly ash and metakaolin are shown in Fig 4.1, while Table 4.1 presents the chemical compositions and size fractions, which are provided by the suppliers. Median particle size (D_{50}) of 8.7 (fly ash) and 5.0 (metakaolin) μm illustrate that metakaolin particle is much finer and may has better reactivity. The raw materials are activated by mixture of sodium hydroxide with purity quotient >95% and sodium silicate solution with a specific gravity of 1.4, consisting of 9.1 wt.% Na_2O, 29.2 wt.% SiO_2, and 61.7 wt.% H_2O, both of which are from Fisher Scientific, Inc., USA. For benchmarking purpose, Class G oil well cement (OWC), supplied by LafargeHolcim, USA, is conducted to complete the parallel testing. To simulate the real ocean water as far as possible, the research chooses the Instant Ocean sea salt (Spectrum Brands, Inc., USA) to prepare curing solutions of different salinities (0, 15, 35 ppt), because of its chemical composition and concentration much closest to the natural seawater [67].

To build a system of function similar to opening contact between cement slurry and surrounding environment (i.e., saline or acid solution) in the underground oil well, the high-

density polyethylene (HDPE) porous molds (Fig 2.6) are used to guarantee the chemical exchange between geopolymer slurry and curing solution and enable the process of cast and curing process. The HDPE is a highly stable material not reacting with chemical substances in saline water and geopolymer slurry. The size details of such mold: 1.0 inch (2.54 cm) and 1.32 inch (3.35 cm) in inner and outer diameter, respectively, and 2.5 inch (6.35 cm) in height with pore size of 30 μm. In the research, another type of plexiglass split molds (2.0 × 5.0 cm in inner diameter and height) are used to fill the corresponding air-curing geopolymer slurry without any exchange. Two kinds of molds keep the aspect ratio (i.e., height to diameter ratio) of 2.5 to minimize the end effects encountered in UCT. Non-porous end caps made of polyvinylidene fluoride (PVDF) are used to avoid potential chemical reactions.

4.2.2 Geopolymer Syntheses

Four different contents of NaOH were used to reach four Na/Al molar ratios of geopolymers for study the effect of Na/Al ratios on geopolymers' mechanical properties, labeled as "GC-0.67", "GC-0.80", "GC-0.84", and "GC-1.0", where GC is geopolymer; Number is the Na/Al molar ratio. To ensure the Na/Al ratio as a single variable in recipe of the geopolymer, other main governing factors, such as Si/Al molar ratio and water content (i.e., mass ratio of water to powder materials), were kept constant for all the geopolymers as 2.00 and 50%, respectively, which showed the great compressive strength in previous working experience [61]. Given the fact that Class C fly ash alone reacts too fast with the alkali activator solution, Metakaolin was added to Class C fly ash at a mass ratio of 1:1.

NaOH pellets were used together with sodium silicate solution to prepare the activator solutions, which were allowed to stay overnight in a sealed container. Next, the powder mixture of fly ash and metakaolin was blended for 2 min, after which the mixture was mixed with the activator solutions for 15 min at least to guarantee the homogeneity and sufficiency of geopolymerization reaction. Before the cast, a thin layer of vacuum grease was smeared on the inner side of non-porous molds and the seam surface and two end caps of both two molds for two functions: (a) easy demolding; (b) encapsulation. In addition, a piece of pre-wetted Whatman filter paper with a general pore size of 20 μm was pasted on the inner wall of porous molds to stop the leaching of big size particles from the geopolymer slurry and hence block the porous wall. Meanwhile, this filter paper still allows the chemical exchange between the geopolymer slurry and curing solution. The step of a thin layer of film stuck on the inside surface of caps was conducted to ensure better sealing. Then the made geopolymer slurry were cast into the aforementioned two types of molds (the porous and non-porous). The trapped air bubbles were removed by hand-vibrating. Afterwards, the assembled porous molds were immediately immersed in the curing solutions (constant volume of 150 ml) with three different salinities, 0, 15, and 35 ppt, while non-porous molds stay in the air, which were then placed in the ambient laboratory environment for 28 days. To realize the repeatability, 4 samples as a group for each curing condition were cast and cured. For the comparison, similar process of sample preparation was conducted to the OWC with the same water content of 0.5. After 28 days-curing, all samples were demolded and dried in the air for 7 days at least. The last step before subsequent mechanical measurements is to level the two ends of samples with the Plaster of Paris and then ensure that the vertical axis is perpendicular to undersides of samples by

polishing and level gauges. All the corresponding curing solutions were stored in the sealing condition for pH and salinity measurements.

4.2.3 Mechanical, Microstructural, and Chemical Characterization

Ions exchange between geopolymer slurry and curing solution was performed with pH and salinity measurements by measuring the change of curing solutions before and after the 28 days' curing process. A SevenCompact S220 pH meter (Mettler-Toledo, LLC., Columbus, OH, USA) was in charge of collect pH values, which was pre-calibrated by the standard buffer solutions of pH 4.00, 7.00, and 10.00. The salinity measurements were completed applying YSI model 30 electrical conductivity meter [30].

In order to carry out the UCT, Geotest loading frame with load capacity of 10,000 lb was used to measure the UCS of all the samples at a constant strain rate of 0.5%/min [99]. The raw materials and fracture pieces picked from the interior core and exterior layer of geopolymer samples were studied using a Neoscope JCM-5000 (JEOL, Ltd., Japan) SEM with an accelerating voltage of 10 kV. Before SEM measurements, samples were sputter-coated by a thin layer of gold in order to obtain high-quality micrograph by improving surface's electrical conductivity.

The phase and mineralogical compositions of raw materials and grounded geopolymer powder samples were determined by XRD using Philips X'Pert-MPD diffractometer, whose instrument parameter includes Cu Kα radiation (40 mA and 45 kV), step size of 0.02° 2θ, collection speed of 0.02°/s, and scan range of 15-55° 2θ (diffraction angle). And the random powder sample mount was prepared by the razor-tamped surface (RTS) method [61], which can minimize preferred orientation of platy particles such as

clays in the sample mount. XRF was conducted to detect the chemical composition of all the geopolymer samples to supply the data for analysis of ions exchange between geopolymer slurry and curing solution, through using Siemens MRS 400 MP and Philips PW2400 XRF spectrometer. The powder samples (particle sizes of ≤ 45 μm) for XRD and XRF were manufactured by wet grounding with isopropyl alcohol for 2 min in a McCrone micronizing mill.

4.3 Analysis of Results

4.3.1 Compositional Analysis by XRD

Fig 4.2 shows the XRD patterns of all the air-cured and wet-cured geopolymer samples and the raw materials (Class C fly ash and metakaolin). The existence of broad hump affirms that both Class C fly ash (20-36° 2θ) and metakaolin (15-35° 2θ) belong to kind of amorphous phases, while the sharp peaks represent the crystalline phases, such as quartz, mullite, calcite, hematite, and magnetite, which are non-reacted (as discussed later) and hence are treated as impurities in the final geopolymers.

First of all, the pronounced broad humps between 15-40° 2θ have testified all the final products as the amorphous geopolymers [34,60,80]. Moreover, the sharp peaks and their position on the XRD patterns of geopolymers are in accordance with those of the raw materials, indicating that these crystalline phases do not take part in the geopolymerization reactions and hence are regarded as inert fillers in the geopolymer matrix [44,60,100]. However, there are not emblematic distinctions among the patterns of different geopolymer samples cured in various conditions. Therefore, the XRD only tests and verifies the

identification of amorphous geopolymer (not purely one) but is ineligible to analyze and manifest the differential strength presented in the following section.

4.3.2 Mechanical Properties

Fig 4.3 exhibits the representative unconfined compression stress-strain curves of wet-cured geopolymer samples as well as the OWC samples for comparison. It shows the well-defined linear elastic regime and brittle failure of all the geopolymer and OWC samples. However, several curves are still non-linear most likely due to the irregular end surfaces of samples. Nevertheless, it is available to gain the peak strength, failure strain, Young's modulus through reading data or calculation.

The OWC samples play the role of the reference and their average UCS are shown in Fig 4.4a. The air-curing sample has an UCS of 37.75 MPa, which is visibly lower than other ones probably due to the lack of enough water for hydration reaction. The UCS of sample cured in freshwater is the highest one of 63.16 MPa, and then decreases with the increasing curing salinity. Such result verifies again that saline water curing has the definitive, negative influence on the mechanical properties of OWC, which refers to a series of complicated chemical reactions between OWC and saline water.

Compared to the performance of OWC, GC-0.67 and GC-0.80 geopolymers exhibit the totally antipodal results: UCS increases with an increase in the salinity of curing water. The highest UCS of two geopolymers are up to 64.27 MPa and 58.60 MPa, respectively, when salinity of curing solution is the largest one of 35 ppt. For the same curing condition, the performance of GC-0.80 in the strength is weaker than that of GC-0.67. In fact, UCS of air-curing GC-0.67 is only slightly lower than the GC-0.80. After considering the other

two air-curing geopolymers (GC-0.84 and GC-1.00) together, the result shows there is little difference among four air-curing geopolymer samples, indicating that the increasing Na/Al ratio has little effect on the development of strength in dry-curing condition. The dramatic hardly found character is that the GC-0.67 and GC-0.80 samples cured in 15 and/or 35 ppt have the greater UCS than corresponding air-curing samples. It means the discussion to geopolymers with such design mixes has exceeded the scope of only resistance to high salinity situations. Nevertheless, a reversal happens again to GC-0.84 and GC-1.00 geopolymer samples. The UCS of GC-0.84 decreases with the increasing salinity of curing water, while GC-1.00 presents the similar bad performance in the strength in the different wet-curing conditions. For GC-0.84, it is weaker than GC-0.67 and GC-0.80 in the same curing condition, except for samples cured in 0 ppt solution. And GC-1.00 owns the lowest UCS compared to other three geopolymers. In summary, for the geopolymers with high Na/Al molar ratio, higher salinity of curing solution has the negative influence on the development of strength. And the turning point of Na/Al molar ratio is between 0.80 and 0.84 in this case.

Except for the strength, other indicators such as failure strain, Young's modulus, and bulk density of all the samples are presented in Fig 4.4b-4.4d, respectively. Among the different geopolymers, GC-0.67 samples have the highest failure strains and lowest Young's modulus. For the same salinity, failure strain of samples basically has a continuous decrease, while Young's modulus keeps increasing trend, except for very few cases. It indicates that GC-0.67 geopolymer samples may be better in the resistance to tensile cracking. Compare to the OWC samples, geopolymers' Young's moduli are smaller than the OWC under the same salinity, while the failure strains of geopolymers generally

almost are greater or fair to that of OWC samples. Therefore, under the saline water curing, geopolymer samples become more ductile, especially for the GC-0.67 and GC-0.80 cured in higher salinity (i.e., 15 or 35 ppt) owning the higher strength meanwhile, while saline water curing causes negative influences on the mechanical properties of OWC. Fig 4.4d shows the detail of bulk densities of OWC and geopolymer samples. It is clear that the increasing salinity causes the downtrend to OWC but uptrend for geopolymers. Moreover, the bulk densities of wet-curing geopolymers are far less than those of OWC samples. In general, a structural material with a lower bulk density but higher UCS can bring multiple benefits to the design and construction, such as a smaller dead load but higher resistance.

4.3.3 Microstructure

Fig 4.5 displays the clear micromorphology of fly ash and metakaolin, which contributes to the identification and comparison of the final geopolymer's microstructure through the particle size and shape. The fly ash is generally composed of microspheres with diameter from 1 to 20 μm (Fig 4.5a), while the metakaolin particles are platy in shape with 10-30 μm in size (Fig 4.5b), which is born of platy kaolinite crystals. To better explain the similarity and difference of SEM micrographs of all the geopolymer samples in the latter, an example graph of final geopolymer piece picked up after the strength testing is shown in Fig 4.6. It is a visible mixture mainly including neo-formed geopolymer binder, partially reacted and unreacted fly ash and metakaolin particles [60]. Naturally, it also contains the unobservable non-reactive crystalline based on the XRD analysis, such as quartz, calcite, and mullite. Another feature is the randomly distributed micropores and microcracks. In general, these pores are likely introduced into the sample by two possible

sources: (1) the residual air bubbles that are entrapped into the geopolymer slurry during mixing and casting, and (2) the space that is previously occupied by water droplets (due to insufficient mixing) but then becomes a void after water evaporates. Microcracks may also have two potential origins: (1) shrinkage cracks during geopolymers curing and air-drying when upon water evaporation, and (2) loading-induced cracks during the UCT. These microstructural defects, including micropores and microcracks, can have detrimental influence on the mechanical performance of geopolymers. In addition, macropores (Fig 4.7) also go against the development of strength. Meanwhile, Fig 4.7 announces one important proof that the color of interior part is darker than the exterior layer, indicating the exterior layer of geopolymer sample is affected more and demonstrating it is worthy to separately do analysis and comparison to the exterior and interior layers in the subsequent sections.

The SEM micrographs with 1000 magnification times are applied to all the wet-cured geopolymer samples. Fig 4.8 and Fig 4.9 show the surfaces of GC-0.67 and GC-0.80 samples in detail. Firstly, for the samples cured in different salinities, it seems that geopolymers cured in 15 and 35 ppt solutions perform better in the uniformity on the whole and consecutiveness of geopolymer binder than that cured in 0 ppt solution. Compared to the exterior layer, the interior seems to be more homogeneous and continuous matrix, while the exterior has relatively more unreacted and partially reacted raw materials and more pores inlayed in the binder. Nevertheless, it is hard to recognize the particular place of GC-0.67 samples apart from GC-0.80 samples cured in the same salinity. In summary, the curing water have more effect on the exterior than the interior, which conforms to the color difference obtained from Fig 4.7. Moreover, greater performance in homogeneous and

continuous matrix with less micropores is equal to more generated geopolymer binder, which directly contributes to the development of UCS.

Fig 4.10 shows the SEM micrographs of the GC-0.84 samples cured in 0, 15, and 35 ppt saline water. As the same above, the interior has a homogeneous and continuous matrix with less unreacted or partially reacted components and less pores than the exterior. However, compared the samples cured in different salinities, it is found that higher salinities (e.g., 15 and 35 ppt) tend to own less homogeneous matrix with a smaller fraction of reacted binder than the one cured in the freshwater. For GC-1.00, as shown in Fig 4.11, according to the visual contrast, there is little difference between the interior and exterior layers, and the performance among different salinities is as poor as each other. When compared to GC-0.67 and GC-0.80 samples, more unreacted or partially reacted components and more micropores embedded in the GC-1.00 geopolymer matrix, which indicates that its micromorphology is worse than the other geopolymer samples, corresponding to its worst mechanical performance. Overall, for the geopolymer samples with Na/Al molar ratio more than 0.80, higher salinities tend to have a negative influence on the formation of geopolymer binder and directly affect the development of UCS.

4.3.4 X-ray Fluorescence Analysis

XRF usually perform the elemental analysis in the form of offering oxide which is described in the mass percentages. Table 4.2 shows the average Na/Al and Si/Al molar ratios of all geopolymer samples cured in different saline solutions. In general, compared to the pre-designed Si/Al ratio of 2.00, GC-0.80 and GC-1.00 presents the relative stable Si/Al ratio, while GC-0.67 and GC-0.84 have the relative larger Si/Al ratio gaps. The

difference between the real and pre-designed is basically kept in the range of 4.5% (i.e., the largest different value of 2.09 is from GC-0.67 cured in 15 ppt saline solution). The Si/Al ratios of air-cured samples expectably conform to the pre-designed value of 2.00 except with GC-0.67 (Si/Al ratio = 1.99). There are two possible reasons causing Si/Al ratio's inconsistent. The one is the variability and non-homogeneity of the raw materials. Another is the leaching of Al^{3+} or Si^{4+} from geopolymer slurry into the curing water. For the Na/Al ratios, an obvious feature is that all of the actual measured data are lower than the corresponding pre-designed ones. Taking air-cured geopolymer samples for examples: the difference between the real and pre-designed Na/Al ratio is larger when the pre-designed Na/Al ratio is bigger. At this time, the reason explaining such case is unclear. The discussion about the change in the Na/Al ratios of wet-cured geopolymer samples will be presented in the later section.

When considering the influence of ions exchanges on the strength, first of all, it is necessary to figure out which element's content is varied. Therefore, as an example, the GC-0.67 sample cured in 0 ppt solution is chosen to compare its different kinds of Si-based elements' concentrations (i.e., in terms of the molar ratio of a specific element to Si), as shown in Fig 4.12. The result displays that only Na among six elements occurs distinct fall, indicating that Na^+ is the major ion participating in the process of ions exchange between geopolymer slurry and curing solution. The possible reason is that Na^+ mainly exists in the dissociation form in the geopolymer slurry, while other ions mostly in non-free form. In addition, the concentration of Na^+ appears obvious gap between the interior layer and exterior layer, while other ions have little one. In fact, there are two process causing the leaching and gap: (a) the differential concentration forces Na+ to move into the low

concentration side; (b) the rate of geopolymerization reaction (mainly the polycondensation or hardening stage) decides which part will be hardened firstly and hence drastically reduce the movement of ions.

As shown in Fig 4.12 that Na/Si ratio occurs the major change, therefore, Na or Na_2O is chosen as the indicator to judge the degree of chemical exchanges between geopolymer slurry and curing water in the following analysis. Fig 4.13 presents the mass-based Na_2O contents of all the wet-cured geopolymer samples. The interior layer's GC-0.67 and GC-0.80 samples reveal the increasing Na_2O content with the curing salinity, even finally higher than that of the air-cured samples (as a reference since it should have no chemical exchange with any medium) when salinity of curing solution is up to 35 ppt. Since the exterior layer of geopolymer sample is affected more by the direct contact with the curing water, its Na_2O content is observably lower than that of the interior layer. In summary, when the Na^+ concentration of curing solution is inferior to that of the geopolymer slurry, the flow direction of Na^+ should be from a high concentration of geopolymer slurry to a low one of curing solution. And it is opposite to the case between 35 ppt curing solution and geopolymer slurry. Compared to the GC-0.67 and GC-0.80, the tendency of Na_2O contents of GC-0.84 and GC-1.00 is opposite, which decrease with the increase in the salinities of curing water. However, the common ground is that the Na_2O content of all the exterior layers is less than that of the interior core. For all the wet-cured samples, their Na_2O contents are lower than that of the air-cured samples. This is still caused by the intrusion of Na^+ in the geopolymer slurry into the curing solutions. However, the increasing salinities of curing solutions should have reduced the leakage of Na^+ in the geopolymer slurry. There are two possible reasons to explain the decrease of Na_2O content.

The first is the higher concentration of NaOH, which prevents the process of reaction of geopolymerization to some extent and hence leaves lots of existing unused Na^+ in the geopolymer slurry. Another possible reason is based on the facts of white sediments [77] found in the curing process. It is possible that high salinity triggers certain chemical reaction related to the Na^+ in the solution. And such action leads to the dispersion of Na^+ in the geopolymer slurry into the curing solutions. In summary, during curing, Na^+ may disperse into the geopolymer slurry if the curing saline solution has a higher Na^+ concentration, or out of the geopolymer slurry if the curing solution has a lower Na^+ concentration.

Since the change in the Na^+ or Na_2O content is related to the formation of geopolymer binder, which contributes to the improvement of UCS, the data of average Na_2O content and UCS are compared together, as shown in Fig 4.14. As expected, there is a good correlation between UCS and Na_2O content. For GC-0.67 and GC-0.80 cured in solutions, UCS increases with increasing Na_2O content (Fig 4.14a and 4.14b). In a meanwhile, for samples cured in 35 ppt solutions, both UCS and Na_2O content are larger than those of air-cured samples. The only difference is the growth rate between UCS and Na_2O content. For GC-0.84 and GC-1.00, UCS decreases with decreasing the Na_2O content, except for the GC-1.00 cured in 35 ppt solution (Fig 4.14c and 4.14d). In summary, besides the role of Na^+ as the metal ion to balance the negative charge mentioned by many researchers, the Na^+ or Na_2O content can also represent the degree of geopolymerization or the percent of geopolymer binder in the final products, to some extent.

The above analysis can be reviewed from another point: the difference in the real measured Na/Al molar ratios, as shown in Table 4.2. The results and their tendency are

greatly similar to the percentage of Na_2O of geopolymer samples under different curing conditions shown in Fig 4.13. The UCS increases or decreases with the change in the Na/Al ratios. It means, for the G-0.67 and GC-0.80 under the influence of salty curing water, a higher salinity results in the increment of Na/Al ratio of geopolymer samples and hence increase in the UCS, while it is opposite to GC-0.84 and GC-1.00.

4.3.5 pH Measurements

The pH values of different curing water for all the samples were measured before and after the 28-day's curing process in order to understand and compare the ions exchange between the geopolymer slurry and the curing solution among the samples. The volume of every curing solution is kept constant as 150 ml for the reason of data comparison. In fact, the pH measurements during the period of the curing process displays that most of the change in the pH has completed in the first two days and there was little change in the remaining 26 days. This also indicates that the vast majority of the ions exchange happens before the harden (finished in 1 to 2 days) of the geopolymer slurry. As shown in the Fig 4.15a, all the pH values after 28-day's curing have increase to varied extent. And probably because of higher NaOH concentration, samples with higher Na/Al ratio own a greater pH value under the same salinity. Fig 4.15b presents the pH increment (i.e., ΔpH) for OWC and four geopolymer samples. The phenomenon of higher Na/Al ratio bringing higher ΔpH illustrates that leaching of OH^- and alkali metal cations from the geopolymer slurry should directly cause the change in the pH of curing solution [77]. In general, for OWC and geopolymer samples, ΔpH decreases with the increasing salinity, due to the mechanism of

keeping chemical equilibrium. In other words, the leaching of OH^- from the geopolymer slurry is prevented by the high salinity of curing solution.

4.3.6 Salinity Measurements

pH measurements are mainly to monitor the concentration of OH^- leached from the geopolymer slurry. In order to obtain the change of concentration of other ions in the curing solution after 28-day's curing, salinity of curing solution is measured before and after the curing process, which also is useful to judge and hence prove the ions exchange in geopolymer samples. The same as pH measurements, the volume of each curing water is 150 ml. Fig 4.16 compares the salinity increment (i.e., Δsalinity) for the OWC and four geopolymer samples. For different geopolymer samples in the same curing conditions, Δsalinity increases with the higher Na/Al molar ratio. Another trait is that the higher the curing solution's salinity, the lower the Δsalinity. The increase of salinity affirms the leaching of cations and anions from the geopolymer slurry into the solution. It is worth noting that the minus Δsalinity for the GC-0.67 and GC-0.80 in 35 ppt solutions represents the intrusion of ions from curing solution into the geopolymer slurry, which certifies the accuracy of the XRF results discussed before. Therefore, based on the data shown in Figure 4.16, a conclusion is obtained that, for certain design mix of geopolymer such as GC-0.67 and GC-0.80, the intrusion of saline ions has the motivated influence on the development of UCS, while it is opposite for OWC.

4.4 Conclusions

Subsequence conclusions were drawn on the basis of analysis and results obtained in this study:

SEM and XRD testing prove that all the final cured products can be defined as the geopolymers, meanwhile including other impurities, such as nonreactive crystalline phases from raw materials, unreacted or partially reacted fly ash and metakaolin. Compared to the air-curing geopolymers, saline water curing causes adverse impact on the microstructure of wet-curing ones, especially the exterior layer.

At the same curing condition, the increased Na/Al molar ratio has little effect on the UCS of air-curing samples but causes the negative influences on the wet-curing ones. For the geopolymers with low Na/Al molar ratios, higher salinity improves the development of UCS, while it is opposite for geopolymers with high Na/Al molar ratios.

The major chemical exchanges between the geopolymer slurry and curing solution are the Na^+ and OH^-, which are obtained from XRF and pH measurements, respectively. Moreover, the experiments of XRF and salinity measurements verify that both of leaching and intrusion are existed, which depends on the differential concentration between geopolymer slurry and curing water. The fact the varied Na content of geopolymer samples is closely related to the performance in the UCS illustrates that Na^+ is the key factor for the mechanical properties of geopolymers.

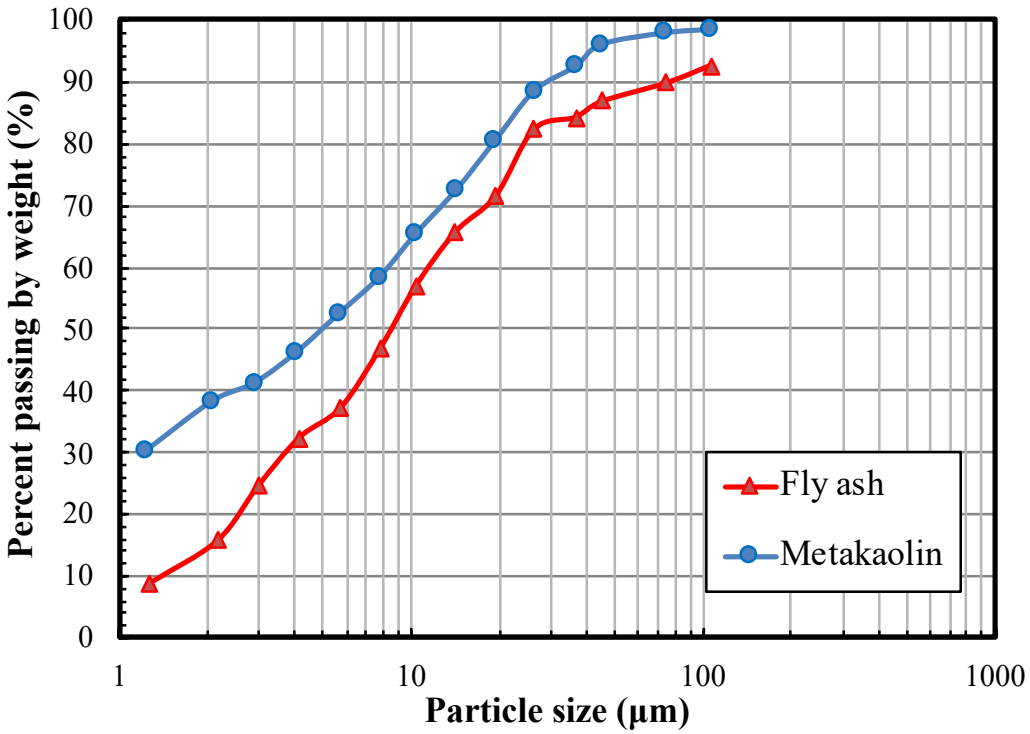

Figure 4.1: Particle size distribution of raw materials used for geopolymer synthesis.

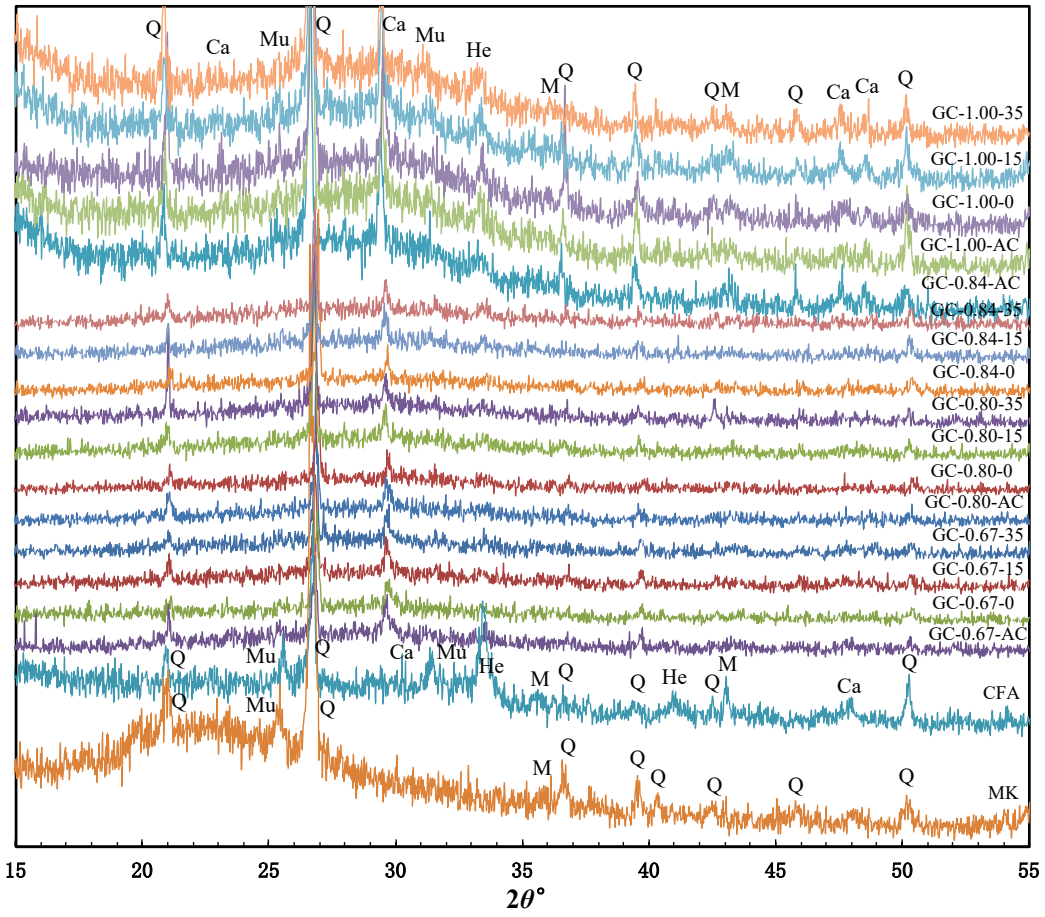

Figure 4.2: XRD patterns of raw materials and geopolymer samples (GC-0.67, GC-0.80, GC-0.84 and GC-1.00) cured in different salinity solutions (MK = metakaolin, CFA = Class C fly ash; AC = air-curing, Mu = Mullite, Ca = Calcite, He = Hematite, M = Magnetite, Q = Quartz).

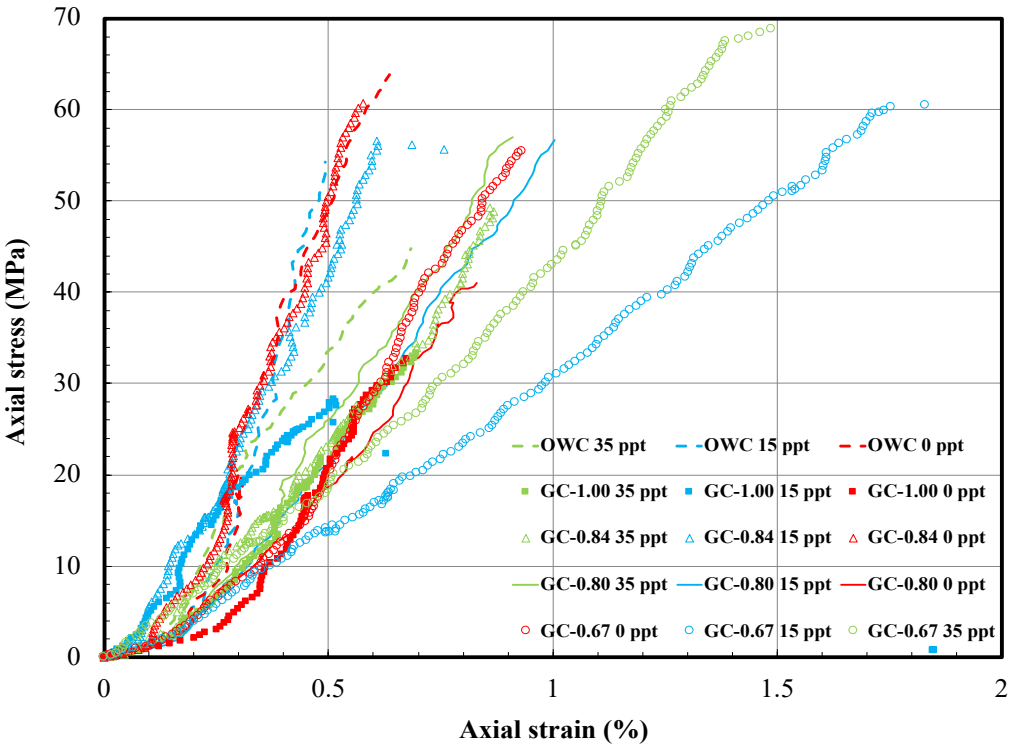

Figure 4.3: Example stress-strain curves of Class G oil well cement and geopolymer samples.

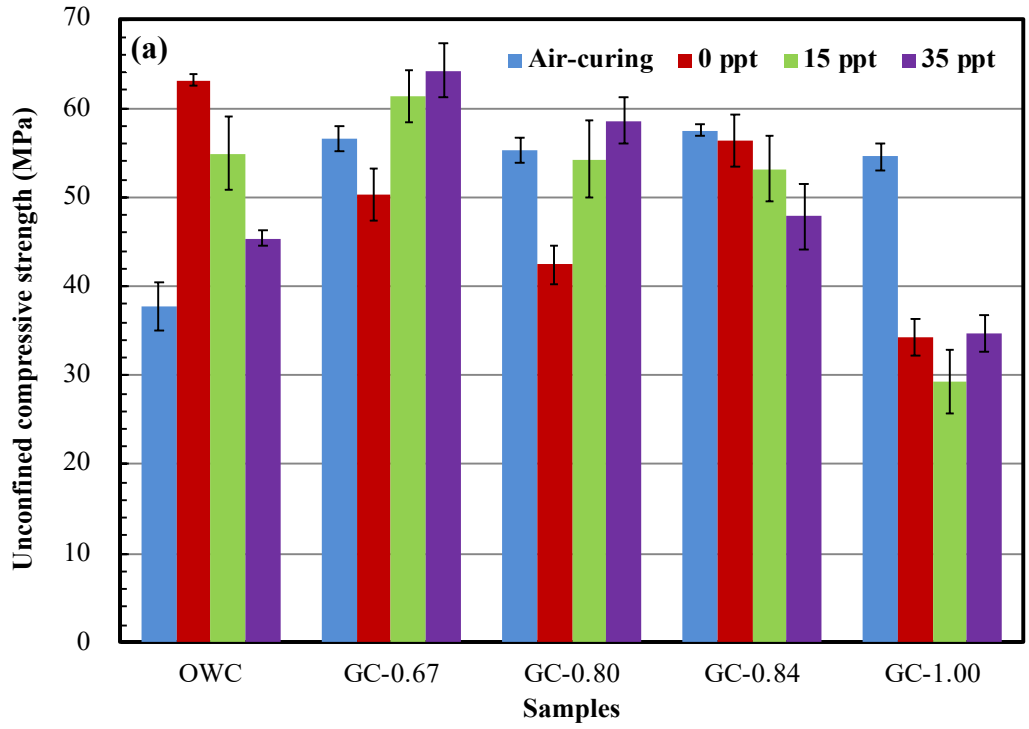
(a)
Air-curing
0 ppt
15 ppt
35 ppt
Unconfined compressive strength (MPa)
70
60
50
40
30
20
10
0
OWC
GC-0.67
GC-0.80
GC-0.84
GC-1.00
Samples

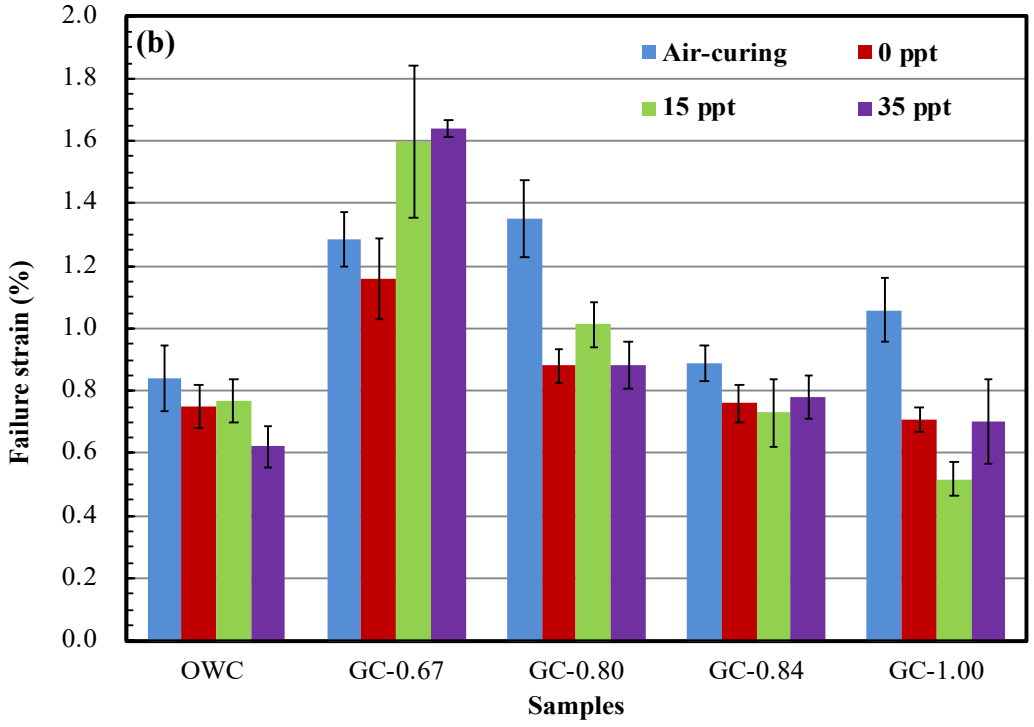
(b)
Air-curing
0 ppt
15 ppt
35 ppt
Failure strain (%)
2.0
1.8
1.6
1.4
1.2
1.0
0.8
0.6
0.4
0.2
0.0
OWC
GC-0.67
GC-0.80
GC-0.84
GC-1.00
Samples

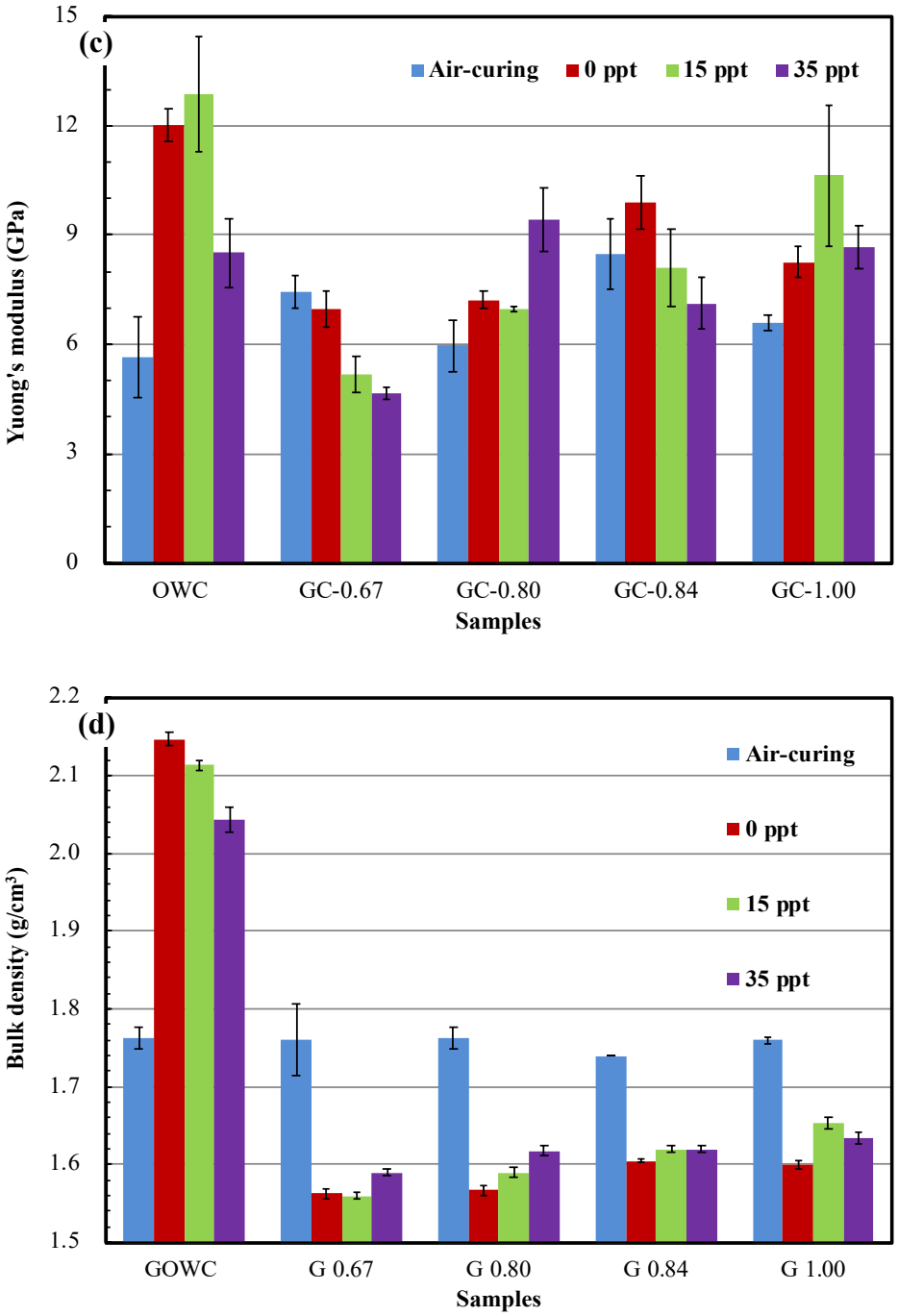

Figure 4.4: Mechanical and physical property indexes of Class G oil well cement and geopolymer samples after 28 days curing: (a) unconfined compressive strength; (b) failure strains; (c) Young's modulus; (d) bulk densities (the error bars represent one standard deviation, which applies to other figures as well).

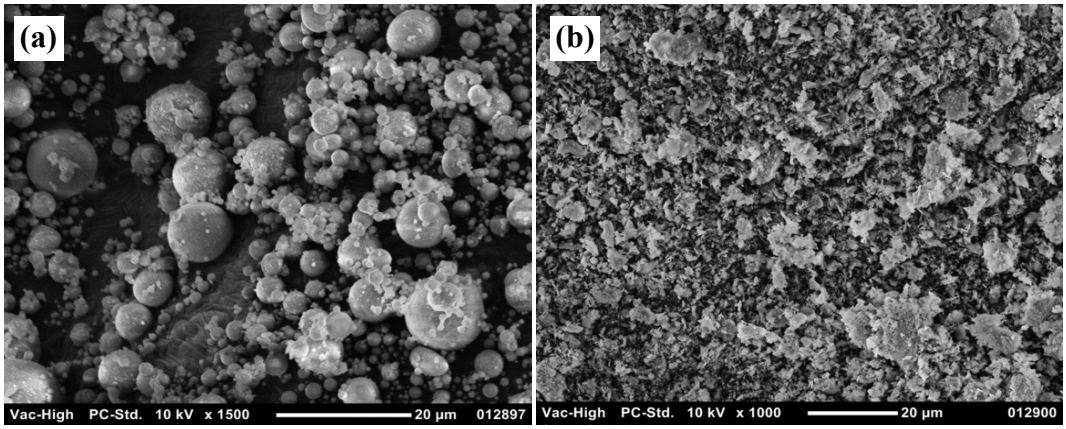

Figure 4.5: SEM micrographs of raw materials: (a) Class C fly ash; (b) metakaolin.

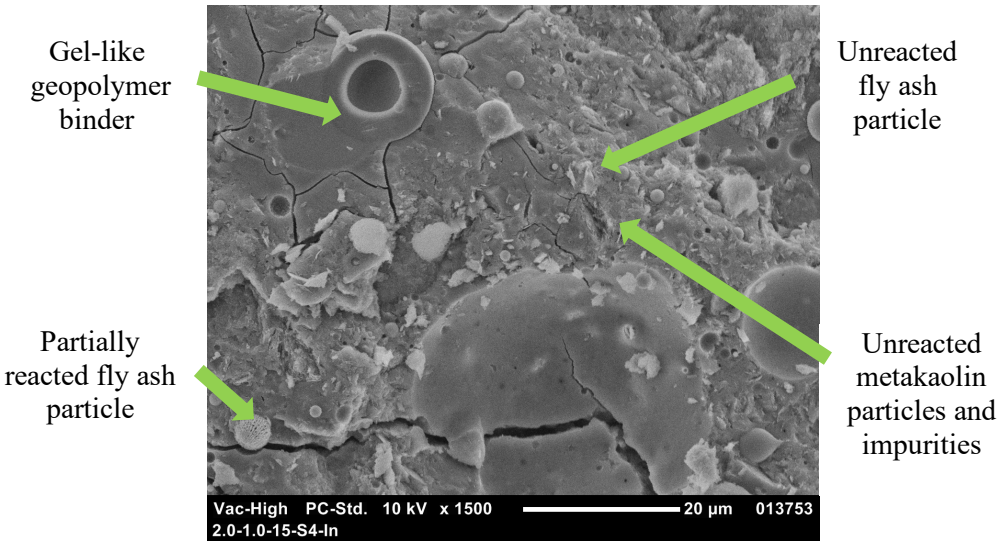

Figure 4.6: An SEM micrograph showing the overall microstructure and composition of the geopolymer samples.

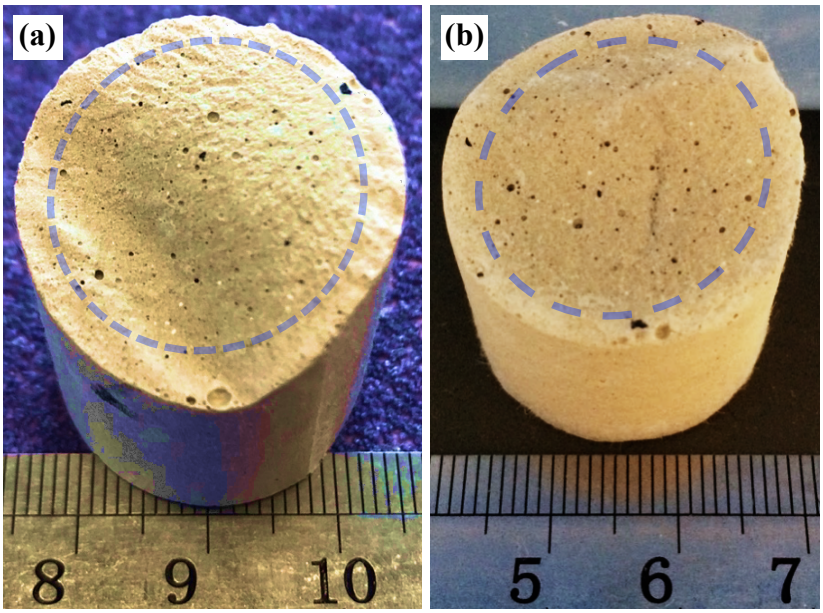

Figure 4.7: optical images of the cross-sectional surface of two different cylindrical samples.

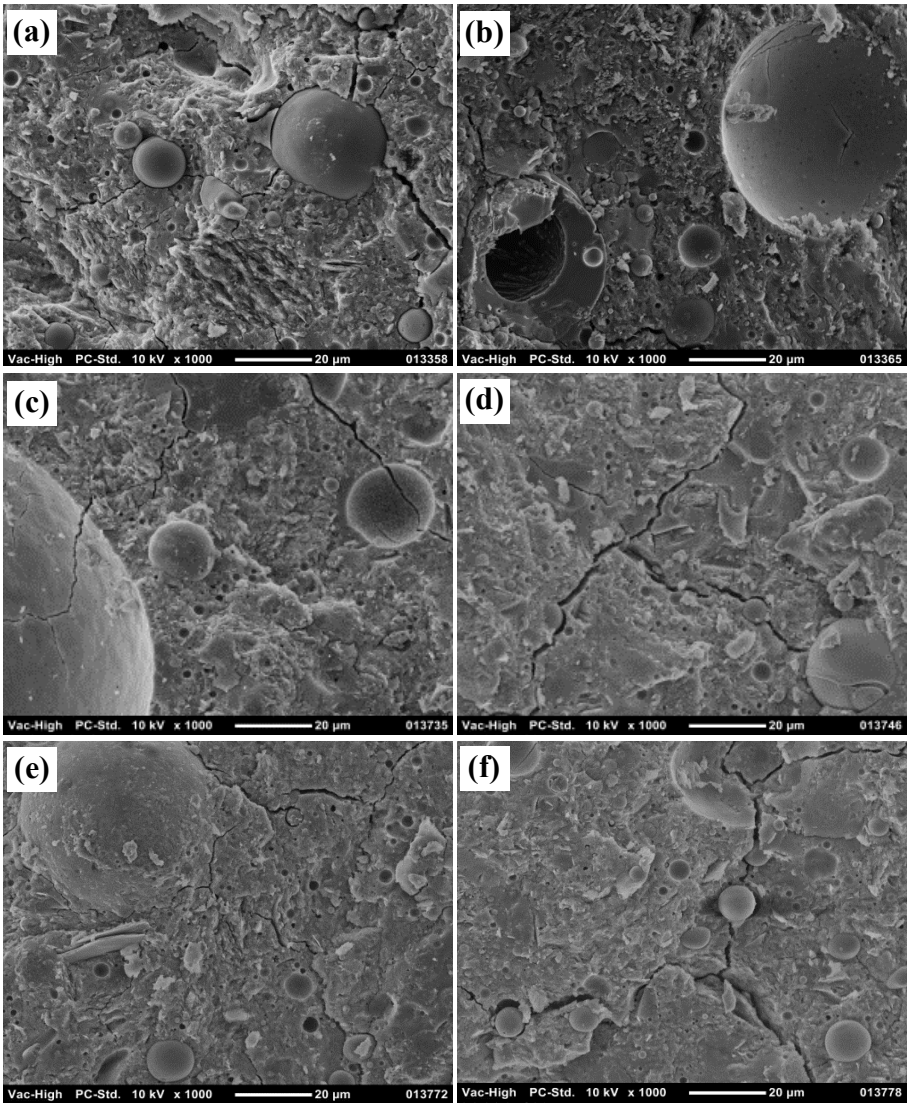

Figure 4.8: SEM micrographs of the GC-0.67 samples cured in different saline water: (a-b) 0 ppt; (c-d) 15 ppt; (e-f) 35 ppt; (a), (c), and (d) are from the exterior layer; (b), (d), and (f) are from the interior layer.

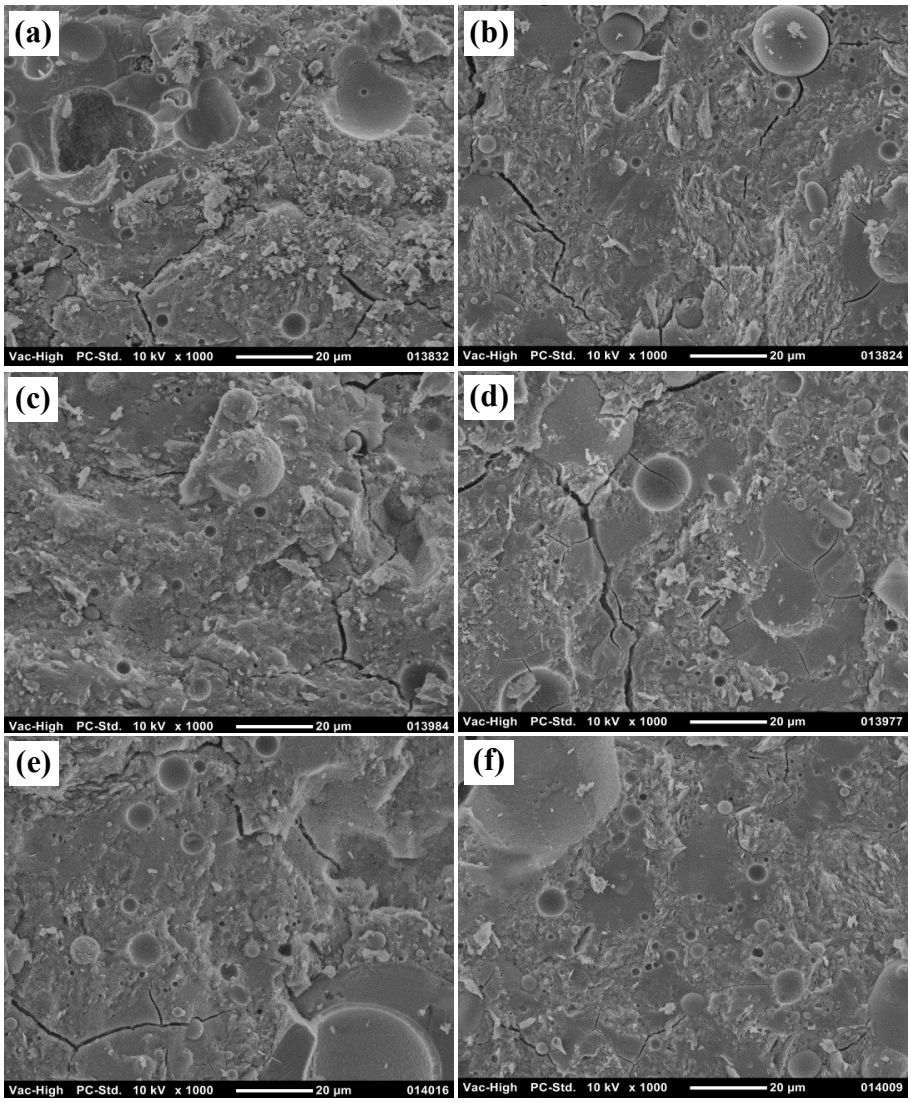

Figure 4.9: SEM micrographs of the GC-0.80 samples cured in different saline water: (a-b) 0 ppt; (c-d) 15 ppt; (e-f) 35 ppt; (a), (c), and (d) are from the exterior layer; (b), (d), and (f) are from the interior layer.

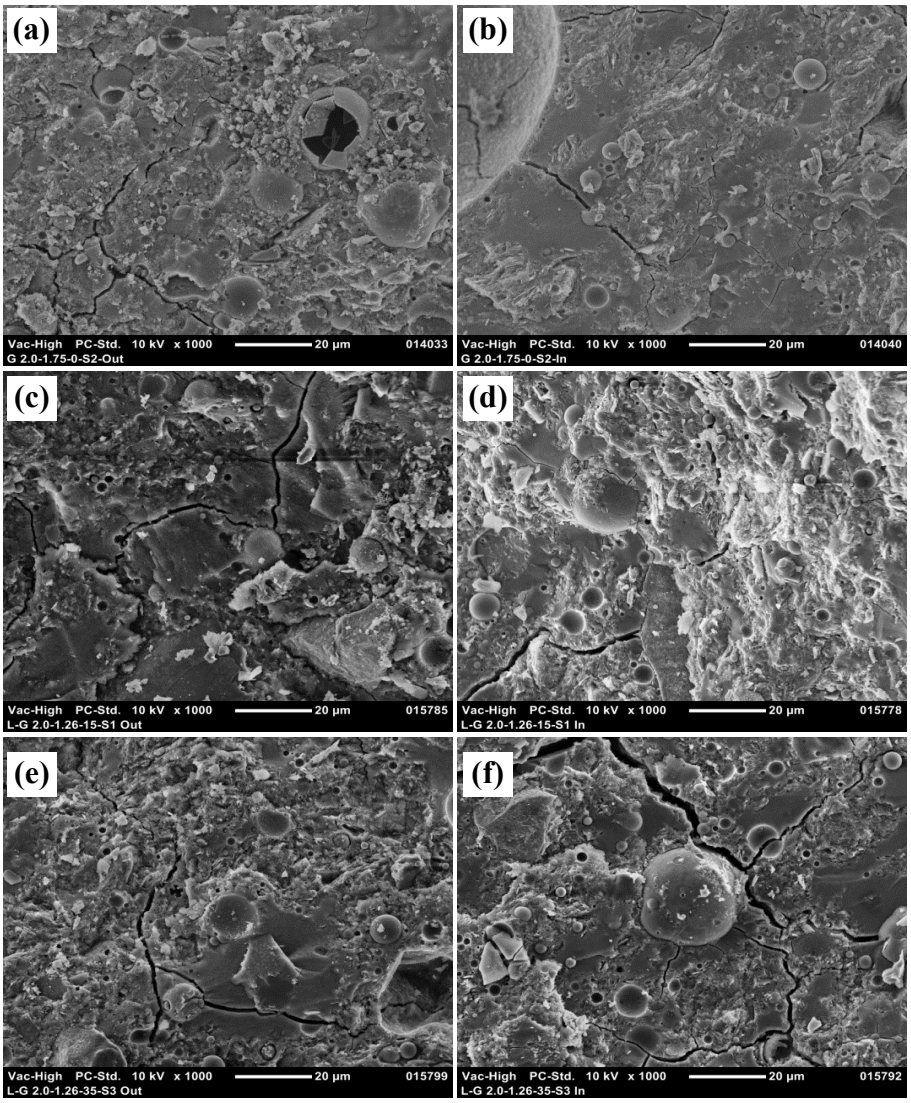

Figure 4.10: SEM micrographs of the GC-0.84 samples cured in different saline water: (a-b) 0 ppt; (c-d) 15 ppt; (e-f) 35 ppt; (a), (c), and (d) are from the exterior layer; (b), (d), and (f) are from the interior layer.

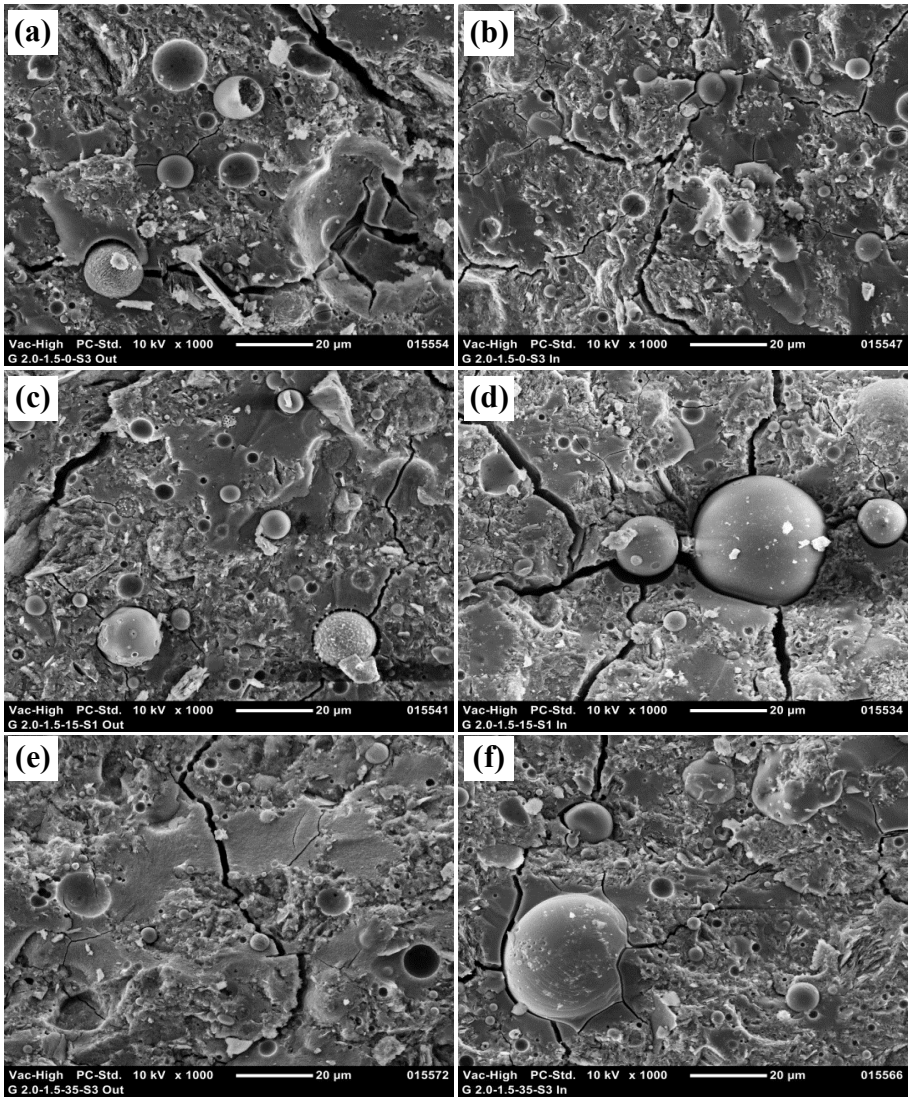

Figure 4.11: SEM micrographs of the GC-1.00 samples cured in different saline water: (a-b) 0 ppt; (c-d) 15 ppt; (e-f) 35 ppt; (a), (c), and (d) are from the exterior layer; (b), (d), and (f) are from the interior layer.

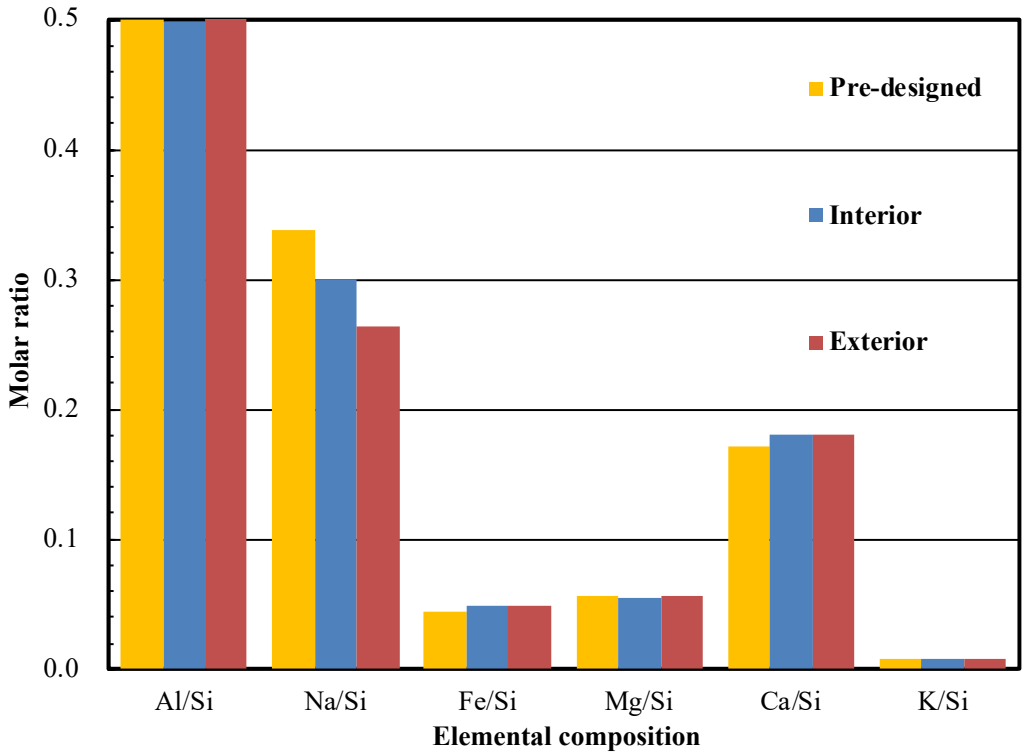

Figure 4.12: The elemental composition of GC-0.67 sample cured in fresh water.

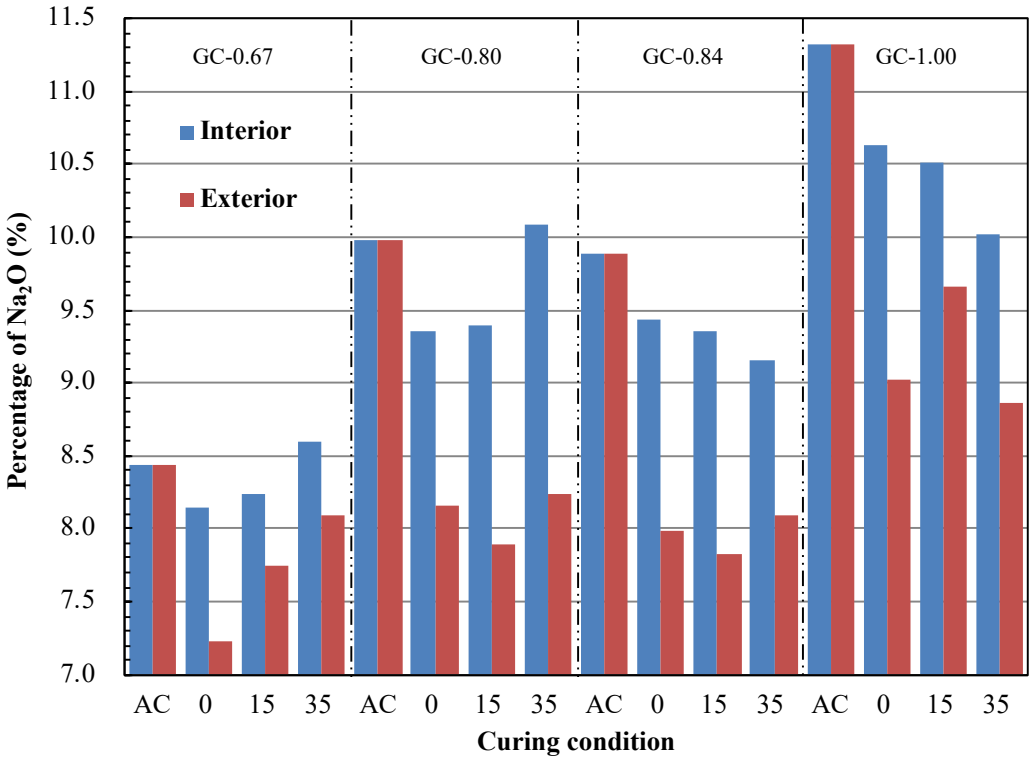

Figure 4.13: Percentage of Na_2O in the final geopolymer samples cured under different conditions.

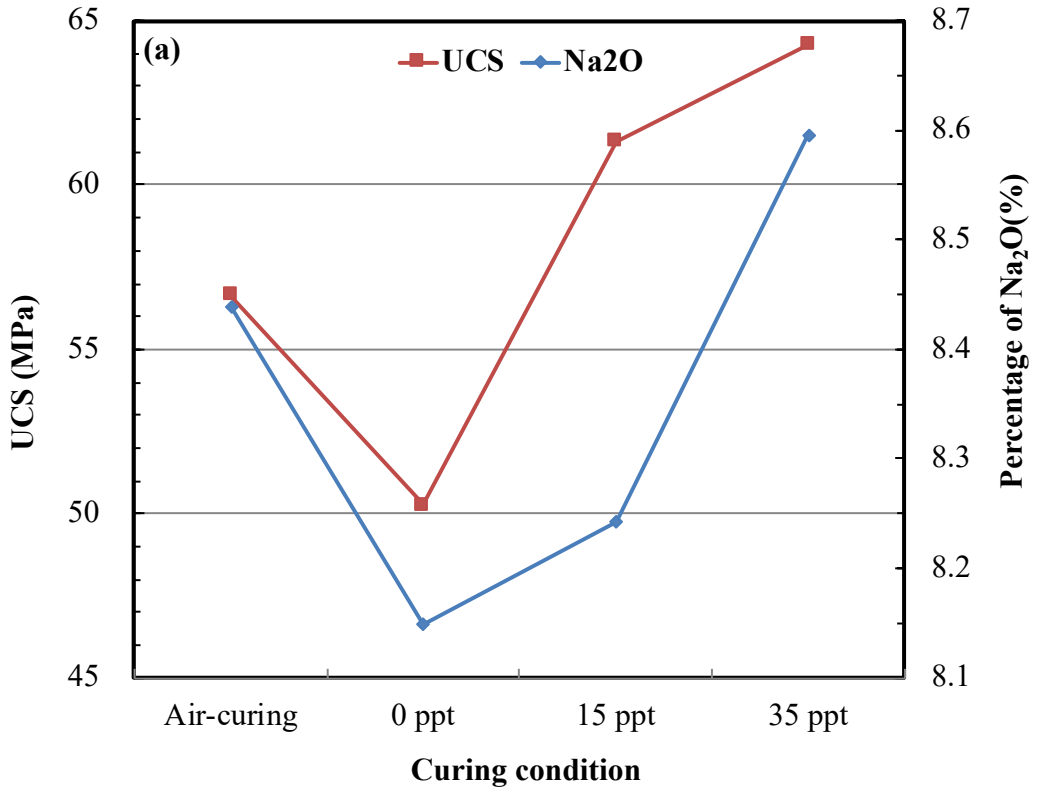
(a)
UCS
Na2O
65
60
55
50
45
8.7
8.6
8.5
8.4
8.3
8.2
8.1
UCS (MPa)
Percentage of Na2O(%)
Air-curing
0 ppt
15 ppt
35 ppt
Curing condition

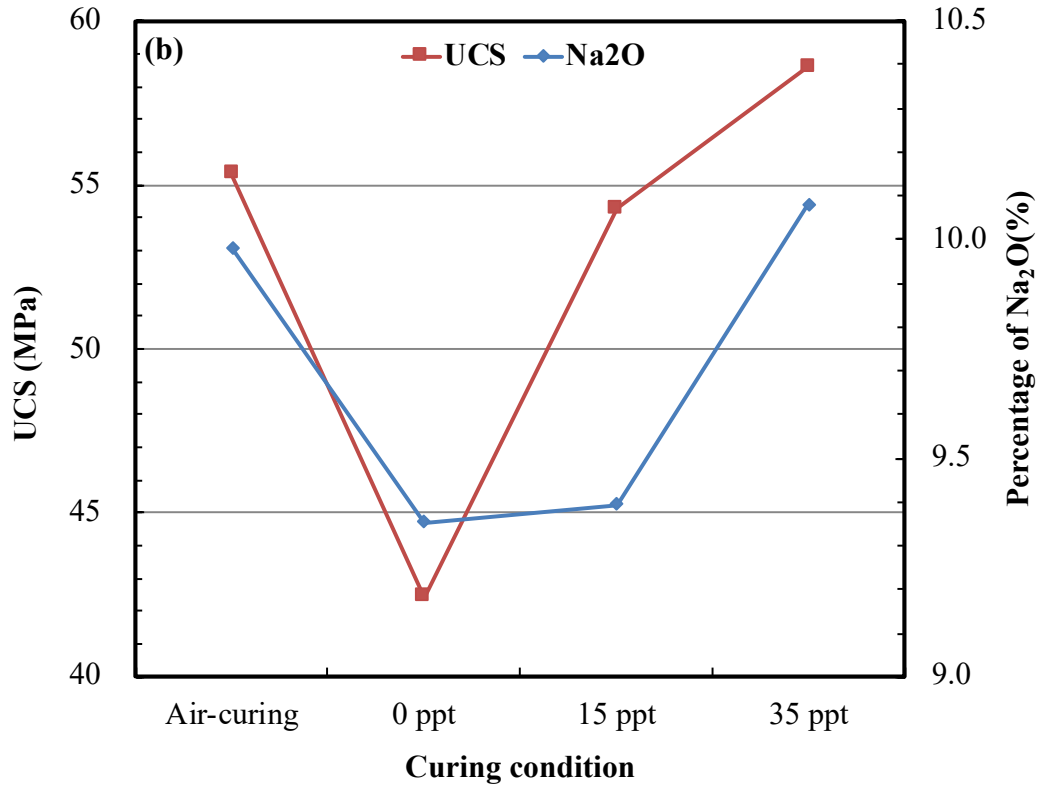
(b)
UCS
Na2O
60
55
50
45
40
10.5
10.0
9.5
9.0
UCS (MPa)
Percentage of Na2O(%)
Air-curing
0 ppt
15 ppt
35 ppt
Curing condition

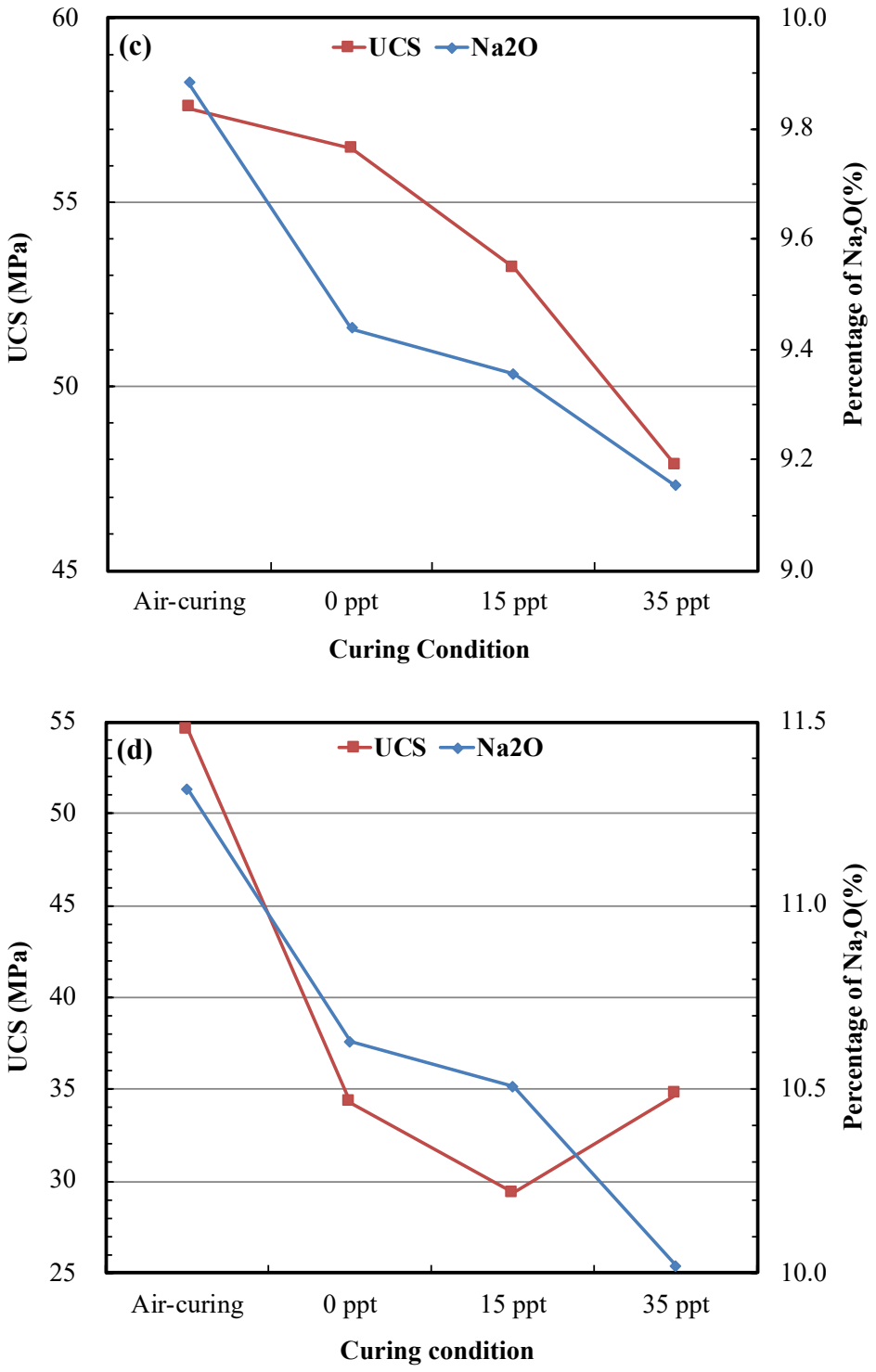

Figure 4.14: Relationship between percentage of Na_2O of the interior layer and unconfined compressive strength: (a) GC-0.67, (b) GC-0.80, (c) GC-0.84, (d) GC-1.00.

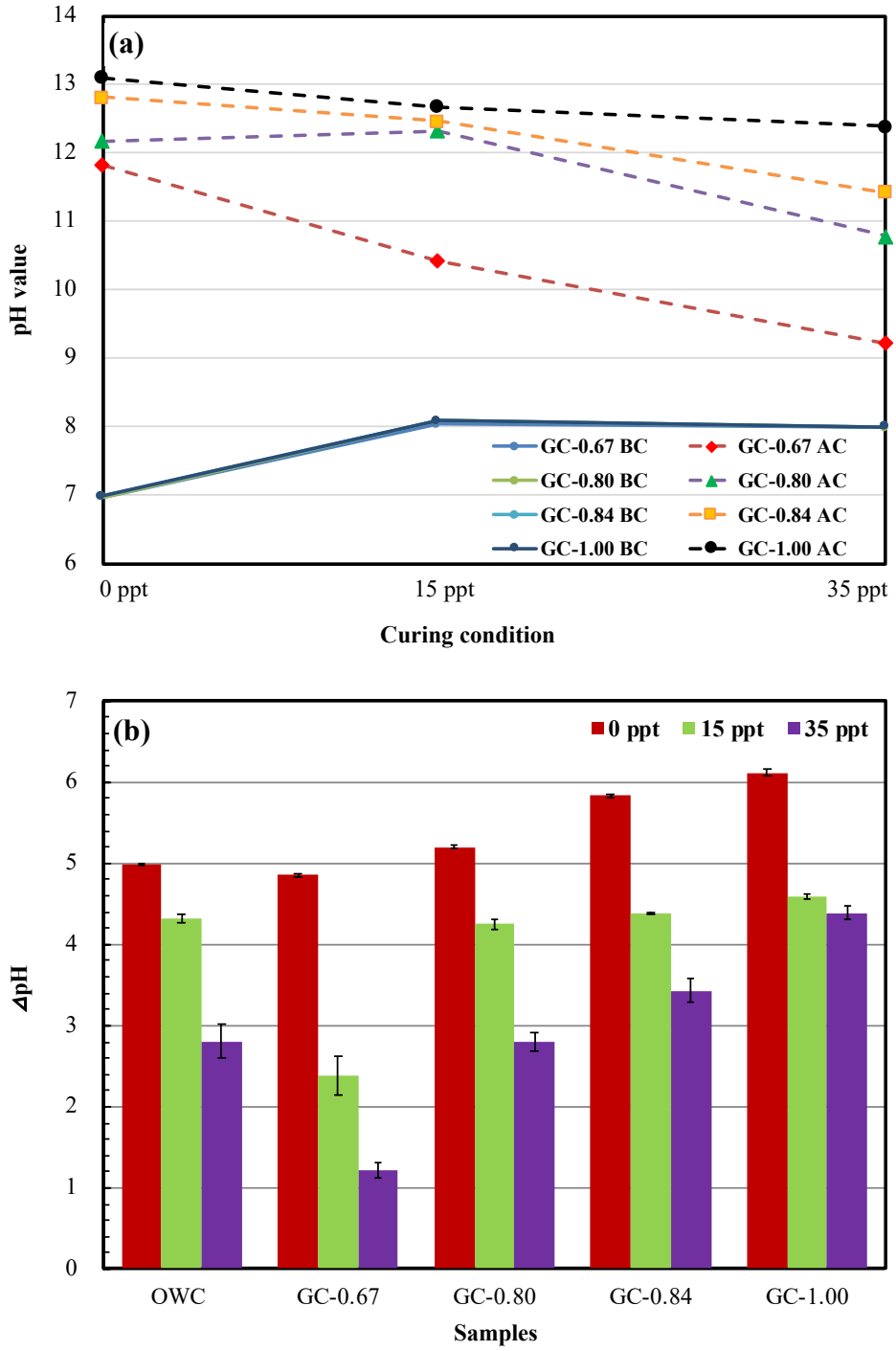

Figure 4.15: pH measurements of different curing solutions: (a) pH values before and after curing process; (b) the change in the pH (*Δ*pH) of the curing solutions (BC = before curing; AC = after curing).

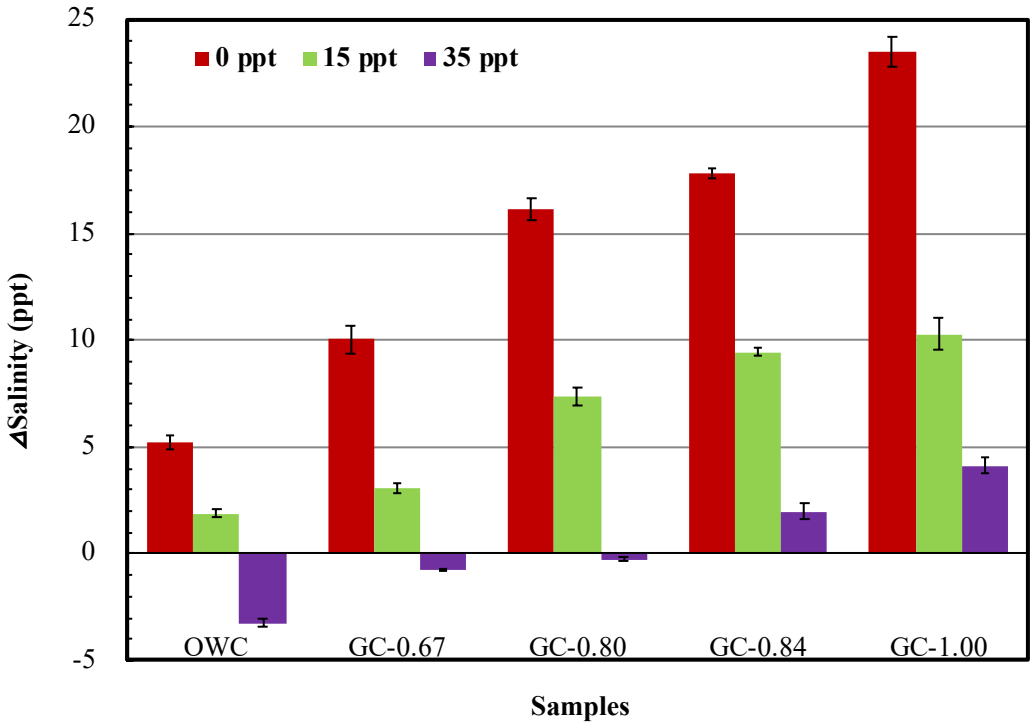

Figure 4.16: The change in the salinity (*Δ*salinity) of curing solutions.

Table 4.1: Size fraction (wt.%) and chemical composition[a] (wt.%) of fly ash and metakaolin.

Composition	Class C Fly ash (wt.%)	Metakaolin (wt.%)
Clay-sized fraction (≤ 2 μm)	14.70	38.30
Silt-sized fraction (2 – 75 μm)	74.10	58.90
Sand-sized fraction (> 75 μm)	11.20	2.80
SiO_2	38.56	56.61
Al_2O_3	19.80	39.16
Fe_2O_3	6.26	1.87
MgO	5.15	0.09
CaO	22.28	0.05
SO_3	1.72	0.05
K_2O	0.61	0.30
Na_2O	1.58	0.01
Moisture	0.11	0.13
LOI	0.41	0.19
Total	96.48	98.46

[a] Chemical composition data provided by the suppliers.

Table 4.2: The actual average Na/Al and Si/Al molar ratios of all geopolymer samples cured in different saline solutions.

Curing solution concentration (ppt)	Na/Al molar ratio (Si/Al molar ratio)			
	GC-0.67	GC-0.80	GC-0.84	GC-1.00
Air-curing	0.62 (1.99)	0.75 (2.00)	0.75 (2.00)	0.86 (2.00)
0	0.60 (1.99)	0.70 (2.01)	0.72 (2.05)	0.79 (1.97)
15	0.64 (2.09)	0.70 (2.01)	0.71 (2.03)	0.79 (1.99)
35	0.65 (2.04)	0.76 (2.02)	0.71 (2.07)	0.75 (1.99)

CHAPTER 5

THE POTENTIAL APPLICATION OF FLY ASH-BASED GEOPOLYMER CEMENT

5.1 Introduction

OPC, a typical cementitious binder, is the most common type of cement used in general around the World as an elementary constituent of mortar, concrete, stucco, and grout. OPC shows excellent strength and is considered as an adaptable and affordable material widely used in construction. However, the universal application of OPC also brings many issues including carbon dioxide (CO_2) emissions and large quantities of consumption of the natural resources, such as limestone and clay, and energy associated with the process of production. The quantity of CO_2 released in the manufacturing of cement is around one ton for one ton of cement clinker [33,50]. Lots of studies have been done to alleviate the problem in the cement industry [88,111,112].

Fly ash is a coal combustion product that is composed of the particulates (fine particles of burned fuel) that are driven out of coal-fired boilers together with the flue gases, processed by the dust collection system, either mechanically or by using electrostatic precipitators before they are discharged to the atmosphere. The effect of fly ash on the environment can vary based on the thermal power plant where it is produced, as well as, the proportion of fly ash to bottom ash in the waste product [113]. This is due to the different chemical make-up of the coal based on the geology of the area the coal is found and the burning process of the coal in the power plant. When the coal is combusted, it creates an alkaline dust. This alkaline dust can have a pH ranging from 8 to as high as 12 [114]. The effect of fly ash on soils and microorganisms in the soils are influenced by the

pH of the ash and trace metal concentrations in the ash. These contaminated soils can be detrimental or beneficial to plant development [115]. Coal contains trace levels of trace elements (such as arsenic, barium, beryllium, boron, cadmium, chromium, thallium, selenium, molybdenum and mercury) many of which are highly toxic to humans and other life. Therefore, fly ash obtained after combustion of this coal contains enhanced concentrations of these elements and the potential of the ash to cause groundwater pollution is significant.

Based on the two problems mentioned above, fly ash-based geopolymer cement will be a highly potential solution, especially with the superior compressive strength, low permeability, excellent chemical resistance, and exceptional fire resistance, among others [14,15]. This developing class of cementitious material has many advantages over the traditional OPC, such as low energy consumption and hence more sustainable, and low carbon footprint. The term "geopolymer" was firstly proposed by Davidovits in 1978 and has been developed greatly in the next decades.

For geopolymer synthesis, fly ash as industrial byproduct has been studied as raw materials, including fly ash [96,97,110,116], fly ash and kaolinite mixture [96], fly ash and metakaolin mixture [15,117], red mud and fly ash mixture [44], and metakaolin, fly ash and red mud mixture [60]. NaOH in alkali activator solutions plays a substantial role in the dissolution of Si and Al oxides. The Na/Al molar ratio (identical in meaning to the SiO_2/Na_2O molar ratio) has a substantial outcome on the UCS of the geopolymers [98]. However, there might be a loss of the mechanical properties as the concentration of NaOH solution beyond certain bound, because of the existence of OH^- in the alkali-activated matrix that could alter the geopolymer structure [118,119]. The curing environment is

another vital factor impacting the mechanical properties of the geopolymers, such as temperature.

Lots of research have been done to verify the feasibility of fly ash as the main source material for synthesizing the geopolymer. The alkali activation of one low calcium hard coal fly ash and four high calcium lignite coal fly ashes was studied by Winnefeld et al. [120] to make assessment of phase formation in fly ash-based geopolymer pastes and mortars in building materials. The results showed that the optimum concerning mortar strength development was reached with the help of heat curing as 80℃ and high activator concentration, up to 70 MPa. Guo et al. [121] studied the compressive strength of Class C fly ash-based geopolymer paste, which can be up to 65 MPa when curing in the room temperature. The paper published by Li et al. [97] presented the workability, compressive strength, and microstructure for Class C fly ash-based geopolymer pastes and mortars at mass ratios of water-to-fly ash from 0.30 to 0.35. The highest strengths of paste and mortar were 58 MPa and 85 MPa when they were cured at 70℃ for 24 h. Diaz et al. [122] investigated the suitability of five different fly ashes as source materials for geopolymers. The compressive tests revealed a wide range of performance from 40 MPa to 80 MPa, which can satisfy the typical construction application requirement of 28-day compressive strength of 25-40 MPa.

Although so much research have been done, due to the difference of chemical compositions of coal and the processes of combustion, it is still necessary to design the experiments to test the fly ash from different regions, especially when the final purpose is to apply it in the real construction. This chapter presents the experimental work on fly ash-based geopolymer paste and mortar. Since the purpose is to apply it in the regular

environment, all of samples would be cured at room temperature in the whole process without any heat curing. Fly ash is the only source material of aluminosilicate, activated by a mixture of sodium hydroxide and sodium silicate solution (analytical and industrial). The compressive strength property of geopolymer paste and mortar were mainly studied. Chemical and mineralogical compositions analyses, including SEM, XRD, and XRF, were conducted to acknowledge the basic information of raw materials.

5.2 Materials and Methods

5.2.1 Materials

Fly ash was the main source materials of aluminosilicate for synthesizing the geopolymer paste and mortar specimens, which was collected from two different power stations, Jincheng, Shanxi Province, China. Jinmeinengyuan (JMNY) Power Station is employing circulating fluidized bed boiler, which produces Class F fly ash [52]. And only one batch of the fly ash was supplied in 2016. Yangcheng (YC) Power Station is applying pulverized coal boiler whose fly ash is classified as Class F fly ash. Three different batches of fly ash were used: the first batch arrived in February 2017; the second batch was obtained in January 2018. Table 5.1 and Fig 5.1 presented the chemical composition and particle size distribution of the fly ash from different power station, respectively.

Since the fly ash used by two local Power Stations (JMNY and YC) came from the same source of coal, there was little difference in chemical composition. However, the color of these fly ashes was different visually. As shown in Fig 5.2, the color of fly ash from JMNY was dull-red, while the color of fly ash from YC was still gray. The reason of

difference might be the different technology of two furnace. It also can be seen that the color of fly ash (YC - batch 2) is darker than the ash from YC - batch 1, due to the change of burning temperature. A main difference between fly ashes (YC) from two batches is the specific gravity. The values of batch 1 and batch 2 are 1.61 and 2.91, respectively. The difference between fly ash (JMNY) and fly ash (YC) is also indicated from their particle size distributions presented in Fig 5.1. The mean particle sizes (D_{50}) of the fly ash (YC) was 6.5 μm, which is finer than that of fly ash from JMNY (17 μm).

The SEM images of two kinds of fly ashes are shown in Fig 5.3. Generally speaking, the particle shape of fly ash was spherical ranging in variety of size. However, the most of particles of JMNY fly ash in Fig 5.3a were flocculent, whose size are larger than that of YC fly ash. Such phenomenon is consistent to the results of particle size distributions.

A combination of sodium hydroxide and sodium silicate solution was used as the activator. Sodium silicate solution was supplied by a chemical industrial company in Tsingtao, China. The chemical composition of sodium silicate solution in industrial grade was 8.39 wt.% Na_2O, 26.94 wt.% SiO_2, and 64.67 wt.% H_2O with specific gravity of about 1.4. And one company in Hebei province, China, offered the analytical grade sodium hydroxide flakes with purity of ≥ 95.0%.

5.2.2 Sample Preparation

The fly ashes were dried in the oven before experiments. The geopolymer were prepared with different Si/Al molar ratios and various Na/Si molar ratios (activators) by regulating the amount of NaOH. The slurry was prepared by using water to mixture powder mass ratios ranging from 0.55 to 0.20. The NaOH and RO water were firstly mixed by a

glass stirring rod and left to cool down to the room temperature. After this the sodium silicate solution was added to the NaOH solution, followed by mixing for at least 5 min and allow them to rest overnight with covering in order to fully blend and non-contact with air. The blended solution was combined with dry fly ash powder, followed by mixing for a minimum of 15 min to ensure thorough mixing among the powder and solution, resulting in the formation of the geopolymer precursor in the form of slurry. The detailed mixture designs of pastes and mortars for the fly ash-based geopolymer are presented in Table 5.2.

Two shapes of molds were used in this part of work, including cylindrical mold with an inner diameter of 1 inch and height of 2.5 inch (i.e., an aspect ratio of 2.5 to minimize the end effects) and cubic mold with length of 2 inch. The prepared geopolymer paste or mortar were cast into preassembled molds, vibrated by hand to remove the trapped air, followed by placed in a laboratory ambient environment for 28 d. Prior to assembling, the interior of mold was coated with a thin layer of vacuum grease for easy removal of specimens after 28 d curing duration. There was another 7 more days for air drying after demolding. The details of preparation of geopolymer paste and mortar samples were introduced in section 2.2.2 of chapter 2. To ensure repeatability, normally 3-4 samples were prepared for each type of geopolymer. After 28 d, each specimen was de-molded.

5.2.3 Characterization

Cured samples were tested for their UCS [31] using an automated GeoTAC loading frame (Trautwein Soil Testing Equipment, Inc., USA) with 50,000 lb load cell at a persistent strain rate of 0.5%/min. Before compression testing, a very thin coating of lubricant was applied to the two ends of each sample in order to decrease the friction and

hence shear stress development among the sample end surfaces and stainless-steel end plates of the loading frame. Details of the test methods are explained in section 2.2.3.5 of chapter 2.

The microstructure of fly ashes was tested using the JEOL Neoscope JCM-5000 SEM at an accelerating voltage of 10 kV. In order to prepare appropriate samples for XRF and XRD, the fly ash samples were conducted by wet crushing with Isopropyl alcohol in McCrone Micronising Mill for 2 min, which made the fine powder with particle sizes ≤ 45 μm. The chemical element analysis was performed using a Siemens MRS400 MP and a Philips PW2400 XRF. The mineralogical composition of fly ash was characterized by XRD using Philips X'Pert-MPD diffractometer. All XRD scans used Cu Kα radiation, a step size of 0.02°, a scan speed of 0.02° per 1 s, and a scan range of 15-55° 2θ (diffraction angle).

5.3 Analysis of Results

The paste and mortar mixture of geopolymer were designed to investigate the effect of Si/Al molar ratio, Na/Si molar ratio in activator, water/fly ash mass ratio, fly ash from different combustion system, and fly ash/sand mass ratio on the compressive strength of those geopolymer samples cured in ambient environment. The results were compared for the variation of one parameter at a time while other parameters were constant.

5.3.1 Measurement of Feasible Range of Si/Al and Na/Si Molar Ratios

When facing to one new fly ash without any data supporting designing mixture, it is necessary to judge the approximate range of mixture design from which the range of compressive strength would be obtained. Since some references mentioned that the Si/Al

molar ratio of 1.6 to 2.0 is available for the requirement of compressive strength. The chapter 3 and 4 have showed corresponding data of geopolymer samples with the Si/Al molar ratio of 2.0. Therefore, in this chapter, the upper limit of Si/Al ratio can be affirmed as 2.0. Another reason of choosing the value 2.0 is that the cost of geopolymer paste material compared to OPC is extremely high, while Si/Al ratio is larger than 2.0. Thus, based on the consideration of cost, it is not necessary to study the compressive strength of geopolymer with Si/Al molar ratio bigger than 2.0, even though their mechanical performance is excellent. Besides, in order to refer to the results from chapter 3 and 4, the cylindrical mold with same size was firstly used to cast and cure the samples, as shown in Fig 5.4. As for the selection of lower limit of Si/Al, similarly because of the consideration of cost, it is worthy to attempt lower ratio to find the possibility of practicable design mixture of geopolymer paste. Therefore, the Si/Al ratio of 1.5 was chose to start the testing.

5.3.1.1 Effect of Si/Al Molar Ratio

Fig 5.5, 5.6, and 5.7 showed the graphs of geopolymer paste samples cured after 28 d when the Si/Al ratio is 1.5; Na/Si ratios are 1.25, 1.5, 2.0; water/fly ash ratio is 0.55. Based on the appearance, the shape was more integrated when the Na/Si ratio was greater. Fig 5.5 showed the worst case, in which the sample is almost totally composed of the powder without any strength. Samples in Fig 5.6 was better, but it is still able to find the stive by touching their surfaces. Through the compression testing, the average strength of samples in Fig 5.7 was only 0.51 MPa. Therefore, when the water/fly ash ratio was 0.55, the Si/Al ratio of 1.5 was useless whatever Na/Si ratio is from 1.25 to 2.0. This also

indicated that the designed Si/Al molar ratio of 1.5 cannot totally satisfy the requirement of generating the geopolymer material.

In the next step, the larger Si/Al ratios (as shown in Table 5.1 with Mix No. From 1-1 to 1-9) were conducted in the experiments to verify the compressive strength. The results were presented in Fig 5.8. The clear increasing trend was found in Fig 5.8a, when the Si/Al ratio increased with the constant Na/Si ratio of 1.25. However, it was the step-style growth which means the effect of Si/Al ratio is not obvious during some small range such as 1.8 to 1.9. When the Na/Si ratio was 1.5 (Fig 5.8b), the strength indeed increased with the increasing Si/Al ratio except Si/Al ratio of 1.8, which is a saltation compared to the around data. Such data would be checked again in the following sections. For the Na/Si ratio of 2.0 in Fig 5.8c, all of data was waved around 30 MPa, which would be checked again in the following experiments. But if only based on the existing data, it indicated that the Si/Al ratio from 1.65 to 1.80 doesn't have positive influence on the growth of strength. In order to directly contrast the data, design mix of Si/Al 2.0 and Na/Si 1.0 was tested, and the samples was shown in Fig 5.9. It is found that there are some cracks on their surface, which directly results in the lower strength, compared to the reference. These results indicated that, under such situation, it is better to choose the Si/Al ratio smaller than 2.0.

Besides the analysis of data, another factor also should be considered: precision of mold. Its size was same to that used in the chapter 3 and 4, but technology of manufacturing the mold was not as good as that, which is possible to affect the results of mechanical properties. Therefore, the standard mold (cubic with 50 mm length) for cement and mortar samples would be used in the following testing and the results were showed in the corresponding sections later.

5.3.1.2 Effect of Na/Si Molar Ratio

The results of average UCS for samples with same Si/Al ratio and different Na/Si ratios were presented in Fig 5.10. For Si/Al molar ratios from 1.65 to 1.95 except 1.8, the strength increased with the increasing Na/Si ratio from 1.25 to 1.5. However, as for Si/Al ratios of 1.75, 1.8 and Na/Si ratio of 2.0, the decrease of strength was found. Such results were similar to several published paper [119,123]. It was reported that a weak chemical reaction occurs with a low alkaline solution [124]. And the compressive strength of samples will increase with the increasing NaOH concentration because of the more generated silica and alumina in a highly concentrated alkaline solution [125]. Thus, high concentrated NaOH solution should accelerate the dissolution of fly ash and bring a better geopolymerization. But another fact is that the higher NaOH concentration will also prevent the increase of strength. Somna et al. [123] found that the Si/Al ratio decrease as concentration of NaOH increased. At low NaOH, leaching of Si was higher than of Al, while rates of Al leaching were improved at higher NaOH concentration which lead to the geopolymer paste with lower Si/Al ratio [110]. Therefore, the NaOH concentration beyond one special point will result in a decrease in the strength due to early precipitation of aluminosilicate products [123]. In this research, it is confirmed that the Na/Si molar ratio from 1.25 to 2.0 is good enough for the formation of geopolymer, especially the 1.5.

5.3.2 Effect of Water/Fly Ash Mass Ratio

In section 5.3.1, the water/fly ash ratio of 0.55 was chosen based on the design mix in Chapter 3 and 4. After testing above, it was found that the flow of geopolymer paste with such water/fly ash ratio is still workable to a great extent. In order to obtain the better

mechanical properties, decreasing the water/fly ash ratio is a great option. Patankar et al. [126] investigated the effect of water/geopolymer binder ratio on the production of fly ash based geopolymer concrete, in which six water/geopolymer binder ratios (0.40, 0.35, 0.30, 0.25, 0.20, and 0.16) were tested. It is found that water/geopolymer binder ratio of 0.25 is corresponding to the best mechanical performance. Extra water/fly ash ratio were also studied to verify the effect of initial water content on the development of fly ash-based geopolymer [127,128].

In this research, the water in water/fly ash ratio contains two parts: the water in activator and extra water. The water in activator is from the water in sodium silicate solution which is not able to change. Therefore, water/fly ash ratio can only be designed by adjusting the amount of extra water. After calculation, it was found that its lower limit is around 0.2. But the lower limit will change with different Si/Al and Na/Si molar ratios. Thus, the experiments were designed to attempt different water/fly ash ratios until their lower limits. And as so was said in section 5.3.1, it started to employ the standard mold (cubic with 50 mm length) from this part research. Fig 5.11 presents such mold and corresponding sample. According to the results shown in section 5.3.1, the design mixture such as Si/Al ratio of 1.65, 1.80, and 1.90 with Na/Si ratio of 1.5 was selected to be tested. And all of the data was presented in Fig 5.12. After testing, the water/fly ash ratio for Si/Al ratios of 1.8 and 1.9 can be down to 0.35 and 0.45, respectively. 0.35 was not the lower limit for Si/Al ratio of 1.65. However, it was probable for geopolymer slurry that there is no workability when water/fly ash is lower than 0.35. For 1.65-1.5, the decrease in water/fly ash ratio had noteworthy effect on the increasing of compressive strength. The optimal performance of mechanical property (43.57 MPa) appeared at water/fly ash ratio

of 0.40. The lower water/fly ash ratio still had a positive influence on strength for higher Si/Al ratio, in which 0.45 is the best choice. However, for the highest Si/Al ratio in this experiment, the negative effect was conducted on the strength. This indicated that the lower water/fly ash ratio would play an active role while Si/Al ratio was lower. And furthermore, the greatest strengths in three groups were close to each other. Under the consideration of cost, the direction of research should develop to the lower Si/Al ratios. Finally, the conclusion is that the decrease in water/fly ash ratio is really to increase the concentration of NaOH solution without change of Na/Si ratio which affects the chemical reaction discussed in section 5.3.1.2; But at the same time, the flow become to be another important factor to decide the mechanical properties. Therefore, the next objective is to find out the balance between Si/Al and Na/Si molar ratio and flow situation.

Another discovery is that, compared to results in Fig 5.8b, there is a strength difference for Si/Al ratio of 1.65, 1.80, and 1.90 with 0.55 water/fly ash ratio when using two different molds. It verified that the cubic mold can bring the more accurate data so that it is necessary to doing remaining testing by using standard mold.

5.3.3 Confirmation of Optimal Proportions

As described in section 5.3.1, the feasible range of design mixes include Si/Al ratio of 1.65-2.0, Na/Si ratio of 1.25-2.0, while water/fly ash ratio is 0.55. The results from section 5.3.2 showed that the water/fly ash ratio of 0.4 probably results in the better mechanical properties of geopolymer designed with lower Si/Al ratio. Therefore, the water/fly ash ratio of 0.4 was constant for all of design mixes in this part research. There was some change in the chosen of Si/Al and Na/Si ratios. Since the employment of less

water is equal to improve the concentration of NaOH solution, the lower Si/Al ratio possibly became available. Thus, the Si/Al ratios as shown in Table 5.1 (3-1 to 3-6) were selected to study. Based on the conclusion from section 5.3.1.2 that Na/Si ratio of 1.5 was a wonderful choice, in order to explore the greater performance of geopolymer, the Na/Si ratios as 1.5, 1.75, and 2.0 were investigated. And standard mold (cubic with 50 mm length) was used. Fig 5.13 exhibits the whole data of this part. As expected, the geopolymer samples with Si/Al ratio lower than 1.65 showed orderly strength under the function of both lower water/fly ash ratio and standard mold. For samples with Na/Si ratio of 1.5, the compressive strength increased with increase in Si/Al ratio and climbed to the top at 1.70-1.5 with 54.94 MPa. Samples with Na/Si ratio of 2.0 showed the best mechanical performance at 1.6-2.0 with 61.01 MPa. Finally, the optimal range of design mix was fixed in the Si/Al ratio of 1.5-1.6 and Na/Si ratio of 1.5-2.0.

5.3.4 Effect of Fly Ash from Different Combustion Systems

The fly ash used above was from JMNY power station. Its chemical composition, particle size distribution, SEM image, and color were detailly described in section 2.2.1. However, it is easy to find the difference compared to another type of local fly ash owing the same source/chemical composition and different producing process. This is the fly ash from YC power station. This sort of fly ash is whiter, finer, and possesses more microscopic pellets, which indicates that it is more active and is able to theoretically promote the geopolymerization. According to the results from last section, the optimal range of design mixes will be used in this part of study to investigate different performance of geopolymer making of different fly ash. But there is one uncertain factor should be tested during the

experiment: water/fly ash ratio. Preliminary judgement is that it needs less extra water. Therefore, extra water (or water/fly ash ratio) would be added step by step: 0.05, 0.1, 0.15, 0.2, 0.25, 0.3, 0.35, and 0.4, until the slurry can be blended successfully. The result was shown in Fig 5.14. the standard mold was still used.

After testing, it is found that water/fly ash ratio of 0.20 is enough to obtain good flow. The geopolymer slurry would become into the solution when water/fly ash ratio was up to 0.40. Therefore, the results of compressive strength of geopolymer samples using two different fly ash cannot be directly compared because of the changed control variable. But relatively speaking, YC fly ash really led to the higher mechanical performance in Fig 5.14. The strength for 1.5-1.5 and 1.6-1.5 was greater than the highest value in Fig 5.13 and have better flow at the same time. While Na/Si ratio was up to 2.0, the strength decreased because of more concentration of NaOH solution. The immediate reason is that there are several clear cracks on samples. Although the mechanical performance of this batch YC fly ash was excellent, the results of geopolymer samples made from other batches fly ash never reached this standard again. It indicated that the quality of such fly ash from YC power station is unstable. On the contrary, the quality of JMNY fly ash was always stabilized based on a mass of experimental data.

5.3.5 Effect of Sand/Fly Ash Mass Ratio

The addition of sand in geopolymer can improve the strength, which is not only economically favorable but also reduces pore density [129]. Kuenzel et al. [130] studied the influence of sand on the mechanical properties of geopolymers and discovered that adding sand aggregate also means adding strong particles to the geopolymer matrix.

Kotwal et al. [131] studied the influence of temperature and activator composition on the physical properties of ambient cured fly ash-based geopolymer mortar. Results displayed that the temperature increased with higher levels of NaOH and Na_2SiO_3 due to the caustic nature of the strong chemical base, which can efficiently improve the compressive strength. It also showed that, compared to the geopolymer mortar with sand/fly ash ratio of 1.0, higher sand/fly ash ratio up to 3.0 caused a little decrease in the strength and great drop in the flow. Li et al. [97] presented the workability, compressive strength and microstructure for geopolymer mortar made of Class C fly ash at mass ratios of sand/fly ash of 2.75 and found that fluidity increases with a decreasing concentration of sodium hydroxide; strength of mortar was much higher than paste with the same water/fly ash ratio under the temperature of 70 ℃.

Table 5.1 has given the design mixes of testing for effect of sand/fly ash ratio (5-1 to 5-3). In order to assure the workability of geopolymer mortar in flow, the water/ fly ash of 0.55 was chosen. The source of fly ash is from JMNY power station. The testing results were shown in Fig 5.15. The reference means the geopolymer paste samples with the corresponding same design mixes. For proportion of 1.65-1.5, strength increased with the increasing sand/fly ash ratio and then turned down after 2 to 1 ratio. But all of mortar samples had the better performance in mechanical properties than paste. However, geopolymer mortar of 1.90-1.5 showed totally different trend. The strength of all of mortar samples were lower than paste. And the situation geopolymer mortar of 1.80-1.5 was between other two cases. The strength of mortar samples was higher or lower than paste and the highest strength appeared at ratio of 2 to 1. In conclusion, it is found that the lower Si/Al ratio was, the better relative strength of mortar sample was. And the optimal ratio of

sand/fly ash should be around 2 to 1. This result was applicable to such fly ash at water/fly ash ratio of 0.55. it is still necessary to verify this conclusion when type of fly ash and water/fly ash ratio changed.

5.4 Conclusions

This study intended to figure out the optimal design mixes of geopolymers based on the fly ash supplied from JMNY and YC power stations by investigating Si/Al molar ratio, Na/Si molar ratio, water/fly ash mass ratio. Fly ash based geopolymer paste mixtures were designed without additives and heat curing in ambient curing condition. The fly ash was activated using the mixture of sodium silicate solution and sodium hydroxide with Na/Si molar ratio of 1.0 to 2.0. Extra water was added to the mixture to adjust the water/fly ash mass ratio. Si/Al molar ratio was tested from 1.5 to 2.0 by adding the sodium silicate solution. Test specimens were measured for compressive strength. The results of the study are summarized below:

When water/fly ash ratio was 0.55, the Si/Al ratio was confirmed as 1.65-2.0 with Na/Si ratio of 1.0-2.0. The range of compressive strength was from 17 to 55 MPa. When water/fly ash ratio reduced to 0.40, the range of Si/Al ratio amplified to 1.5-2.0. And at the same time, compressive strength changed from 9 to 62 MPa. The workability and setting time increased with the increase in Si/Al and Na/Si ratios. Although the decrease in water/fly ash ratio resulted in the increasing strength, workability dropped quickly. Considering both of mechanical performance and cost, the greatest potential design mixtures were Si/Al ratio of 1.5-1.6; Na/Si ratio of 1.5-2.0; water/fly ash ratio of 0.2-0.4.

The variation in technology of producing fly ash resulted in the big difference in the quality of fly ash, which would affect the process of geopolymerization. The results of geopolymer mortar showed that the optimal sand/fly ash ratio should be around 2.0 in this study. However, there are other factors will affect the sand/fly ash ratio such as water/fly ash ratio, concentration of NaOH solution, which were not considered in this research.

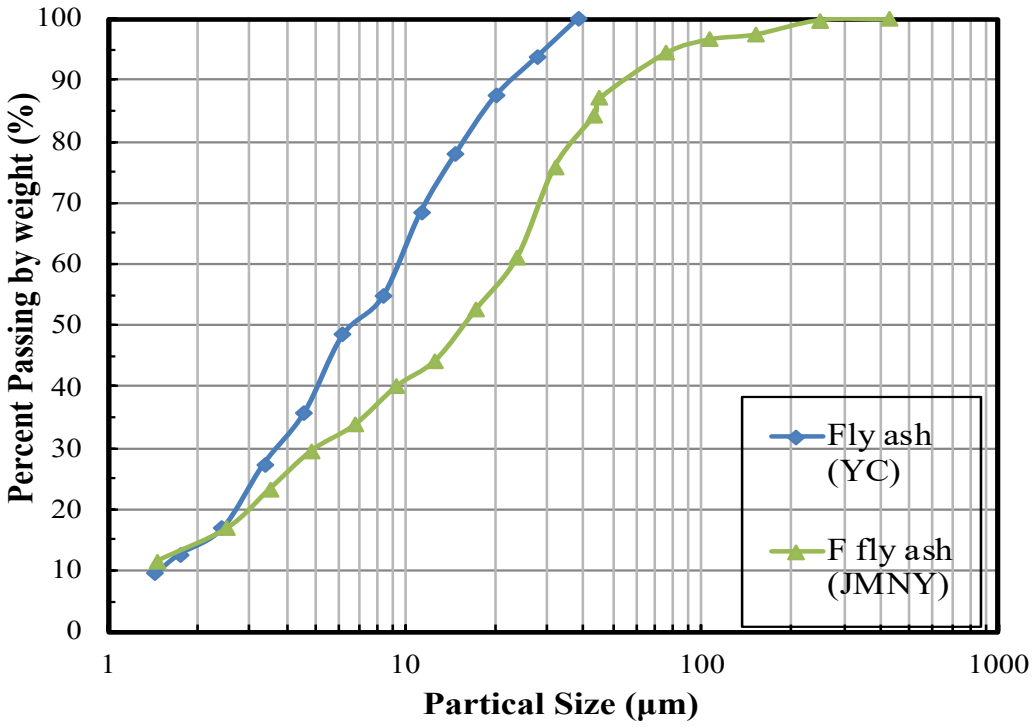

Figure 5.1: Particle size distribution of fly ash (YC) and fly ash (JMNY).

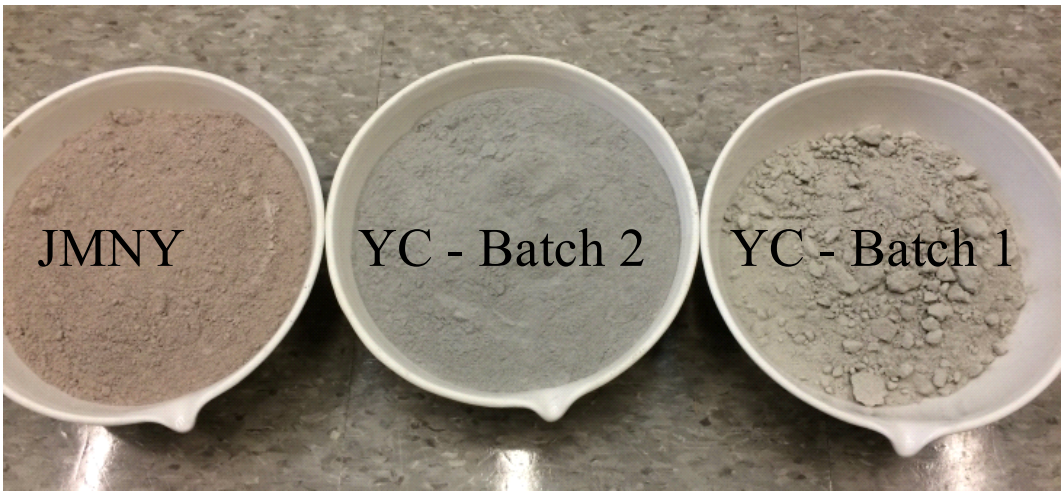

Figure 5.2: The color of fly ash (JMNY and YC).

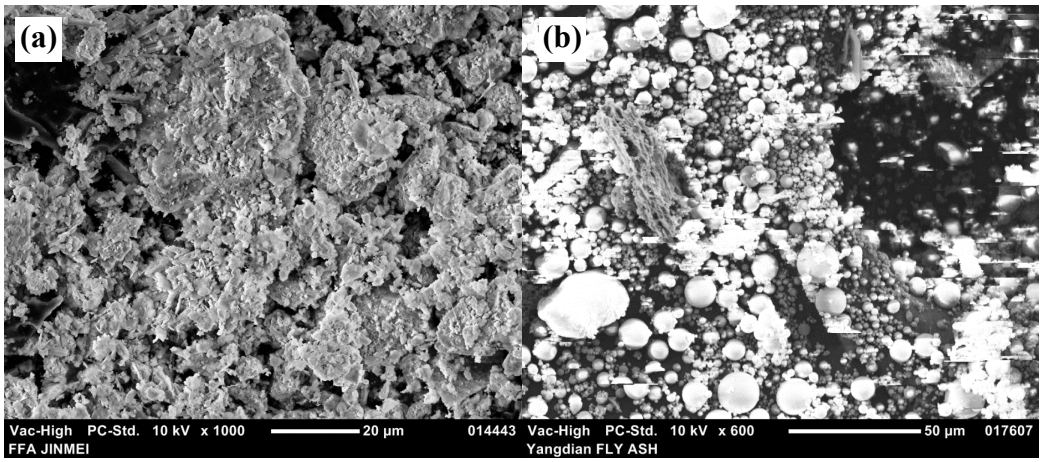

Figure 5.3: SEM images of fly ashes: (a) JMNY, (b) YC.

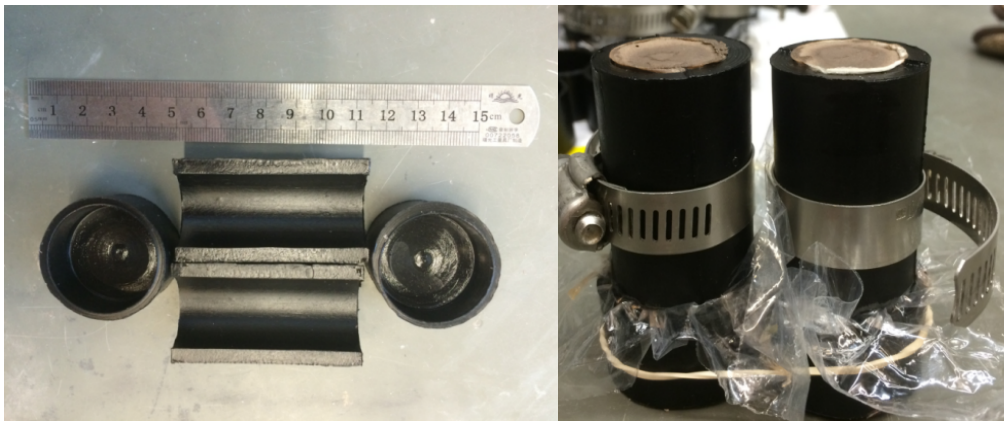

Figure 5.4: The mold of geopolymer sample (1”-inside diameter, 2.5”-height).

Figure 5.5: Samples of geopolymer paste (Si/Al = 1.5, Na/Si = 1.25).

Figure 5.6: Samples of geopolymer paste (Si/Al = 1.5, Na/Si = 1.5).

Figure 5.7: Samples of geopolymer paste (Si/Al = 1.5, Na/Si = 2.0).

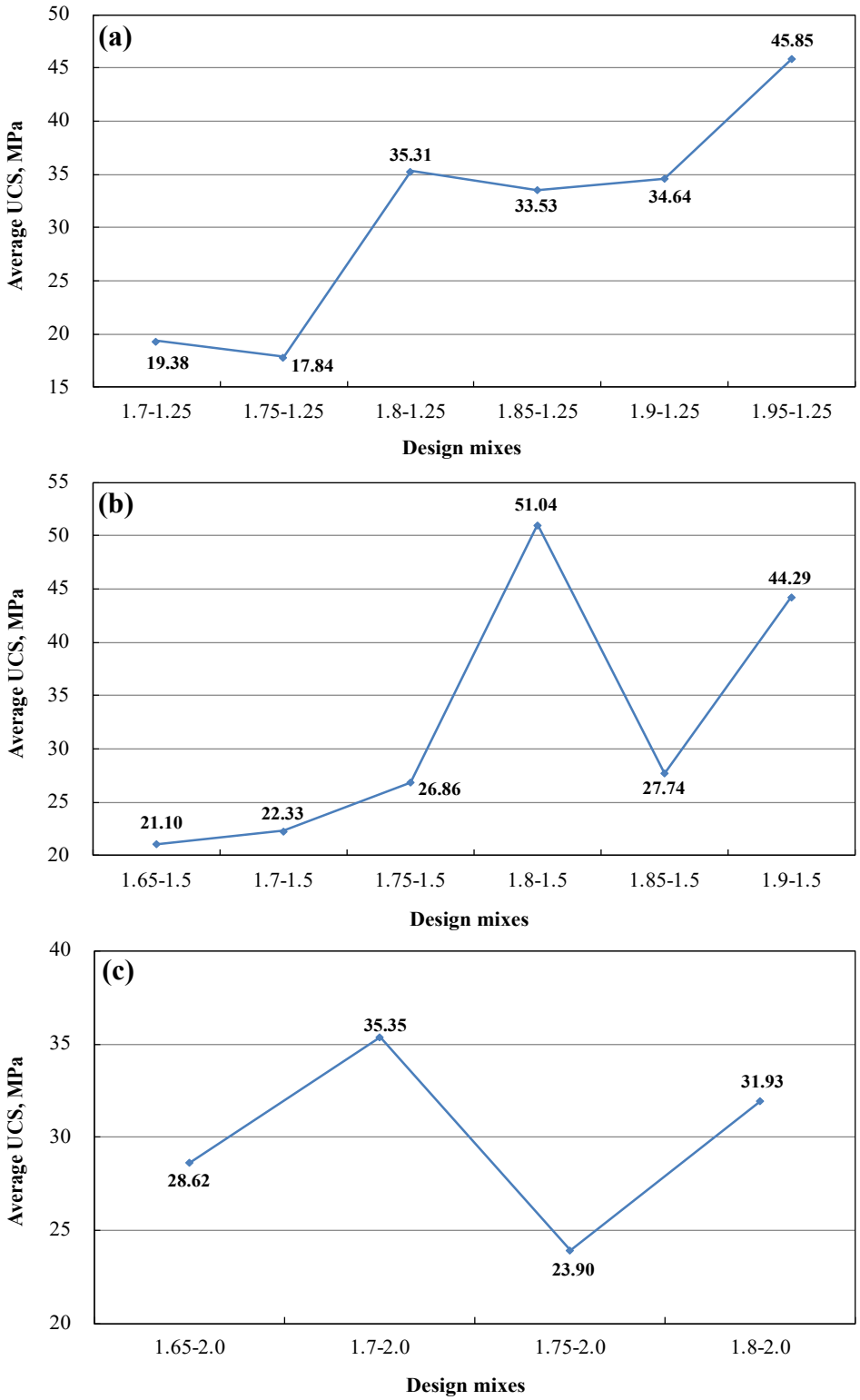

Figure 5.8: Average UCS of geopolymer samples with different Si/Al molar ratios: (a) Na/Si ratio of 1.25, (b) Na/Si ratio of 1.5, (c) Na/Si ratio of 2.0.

Figure 5.9: Samples of geopolymer paste (Si/Al=2.0, Na/Si=1.0).

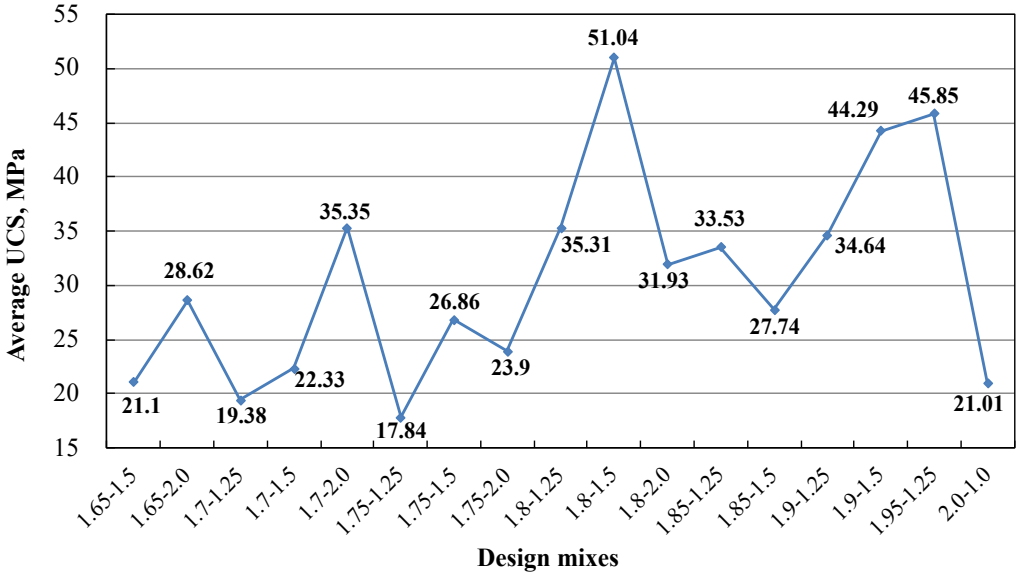

Figure 5.10: Summary of average UCS of geopolymer samples: Si/Al ratio of 1.65 to 2.0; Na/Si ratio of 1.25 to 2.0; water/fly ash ratio of 0.55.

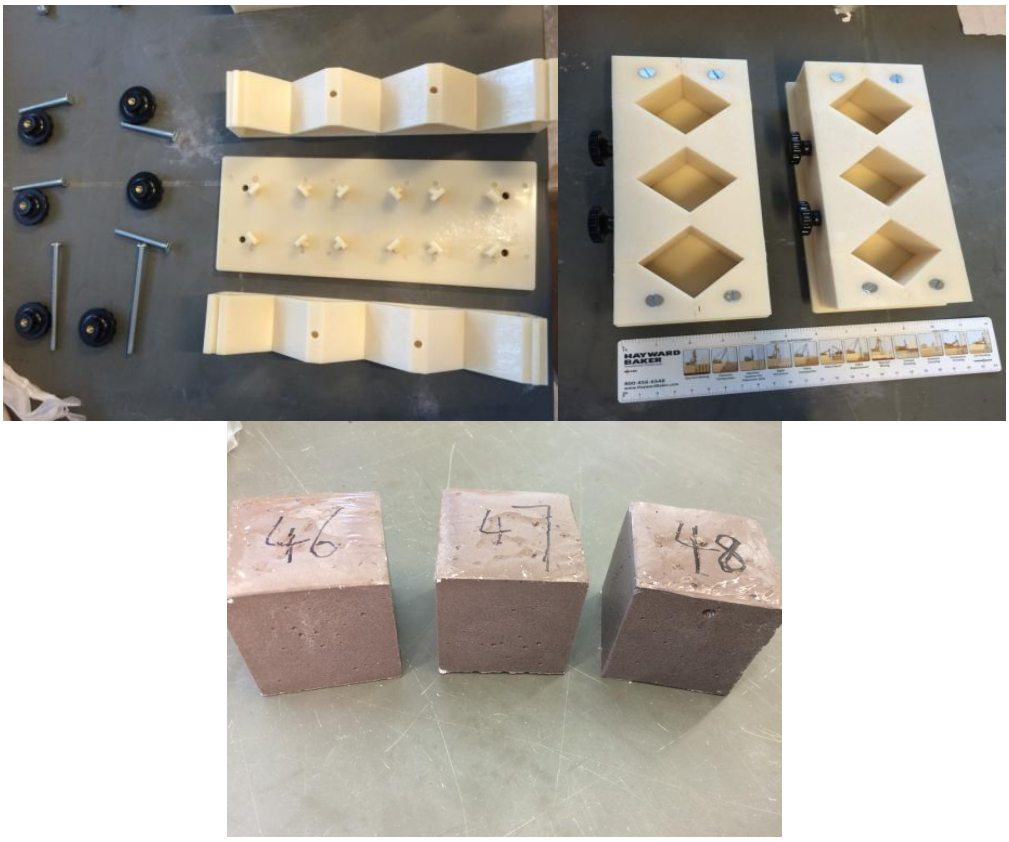

Figure 5.11: Mold of geopolymer sample (cube with 50 mm length).

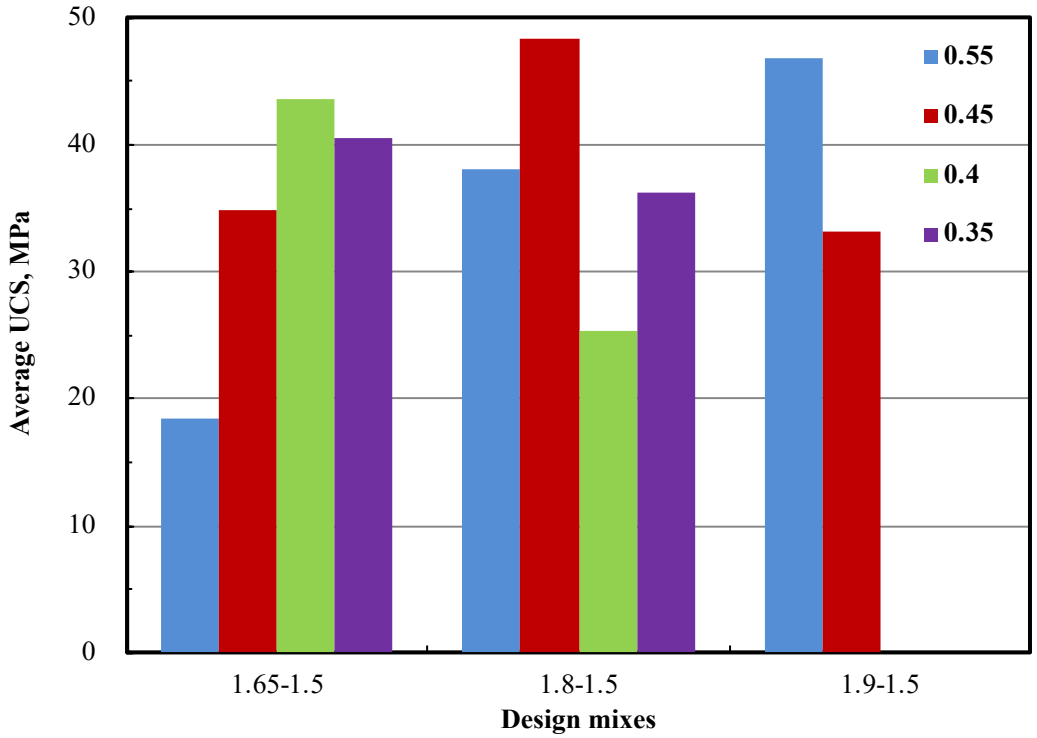

Figure 5.12: Average UCS of geopolymer samples for different water/fly ash ratios.

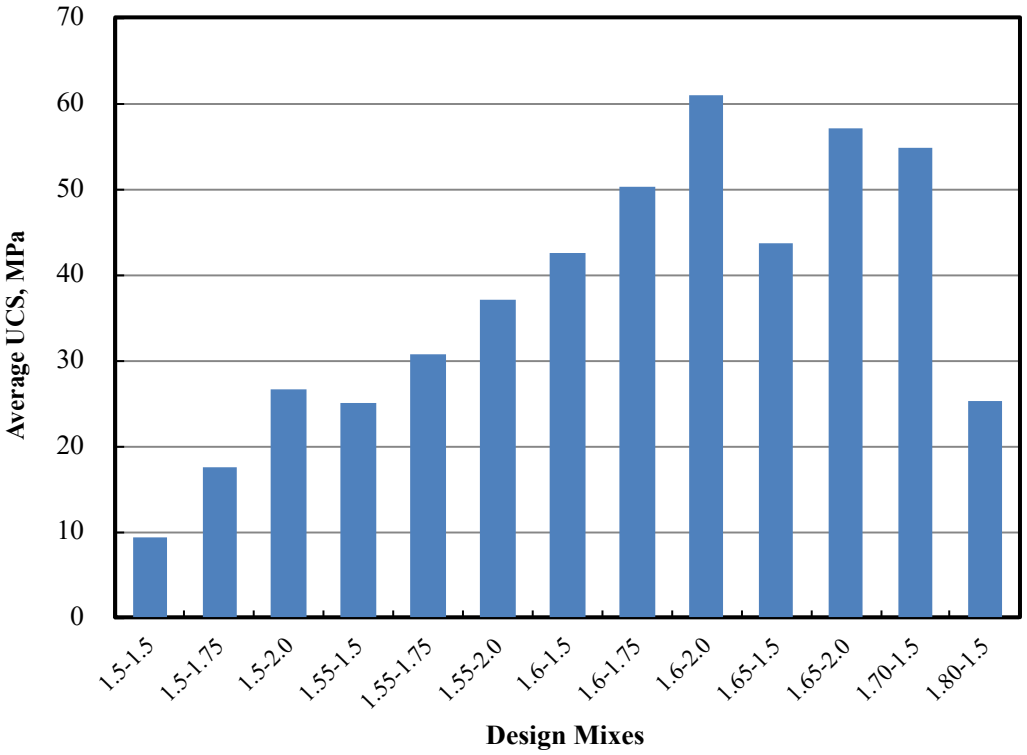

Figure 5.13: Summary of average UCS of geopolymer samples: Si/Al ratio of 1.5 to 1.8; Na/Si ratio of 1.5 to 2.0; water/fly ash ratio of 0.4.

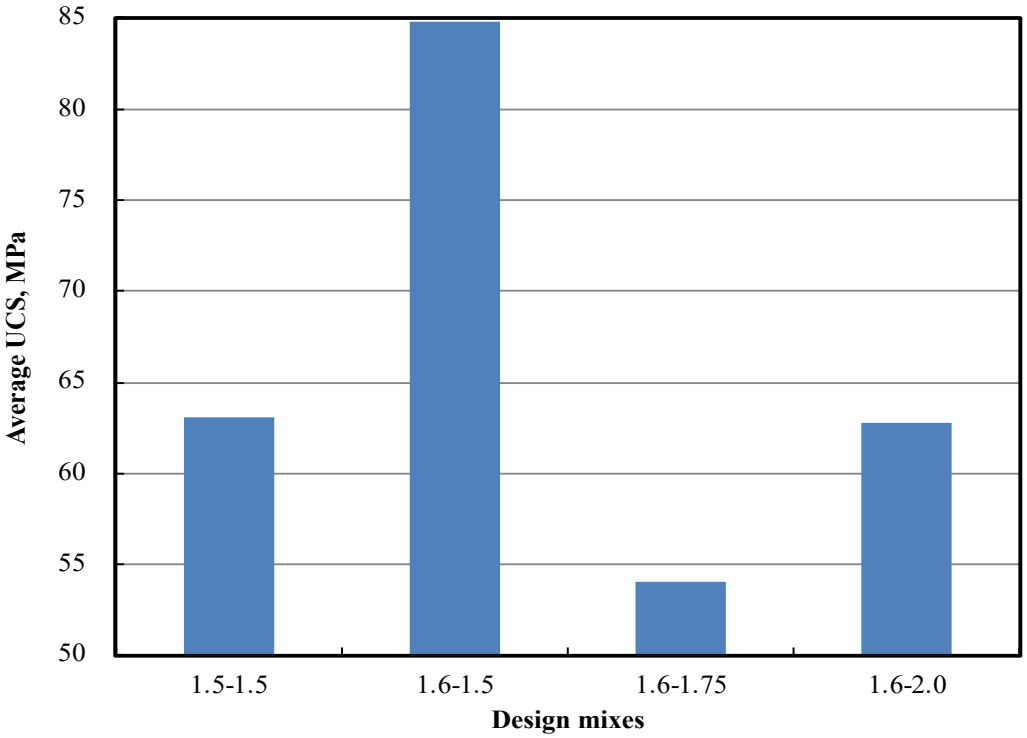

Figure 5.14: Average UCS of geopolymer samples synthesized from YC fly ash.

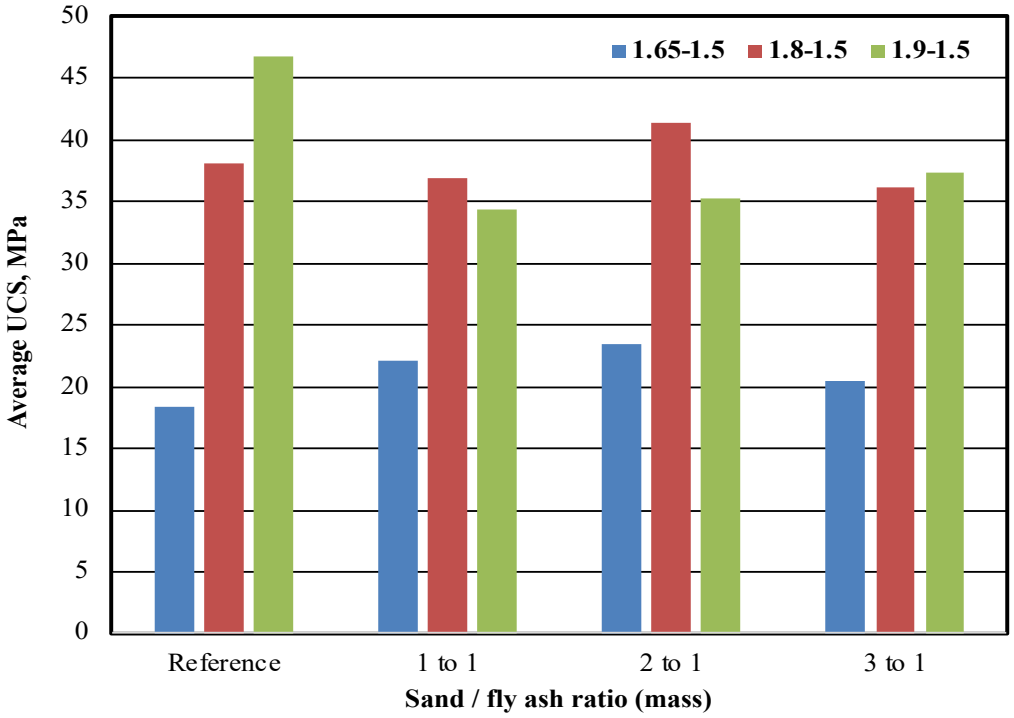

Figure 5.15: Summary of average UCS of geopolymer mortar samples: 1.65-1.5; 1.80-1.5; 1.90-1.5.

Table 5.1: Size fraction (wt.%) and chemical composition (wt.%) of different fly ash.

Composition (%)	Class F Fly ash (JMNY)	Class F Fly ash (YC)
Clay (⩽2 μm)	14.40	16.40
Silt (2-75 μm)	85.60	83.60
Sand (>75 μm)	0.00	0.00
SiO_2	53.40	52.63
Al_2O_3	33.85	33.96
Fe_2O_3	3.41	4.78
MgO	0.82	0.66
CaO	3.24	3.52
SO_3	--	--
K_2O	1.38	1.39
Na_2O	0.77	0.77
P_2O_5	0.49	0.34
TiO_2	1.40	1.27
MnO	0.04	0.05
Moisture	--	--
LOI	0.67	0.61
Total	99.47	99.98

Table 5.2: Details of fly ash-based geopolymer mixture designs.

Mix No.	Molar ratio		Water/Fly ash (mass ratio)	Sand/fly ash (mass ratio)
	Si/Al	Na/Si[a]		
1-1 to 1-9	1.5/1.65 / 1.70 / 1.75 / 1.80 / 1.85 / 1.90 / 1.95 / 2.00	1.25	0.55	---
		1.50		
		2.00		
2-1 to 2-3	1.65 / 1.80 / 1.90	1.50	0.55	---
			0.45	
			0.40	
			0.35	
3-1 to 3-6	1.50 / 1.55 / 1.60 / 1.65 / 1.70 / 1.80	1.50	0.40	---
		1.75		
		2.00		
4-1, 4-2	1.50 / 1.60	1.50	0.20	---
		1.75		
		2.00		
5-1 to 5-3	1.65 / 1.80 / 1.90	1.50	0.55	1:1
				2:1
				3:1

[a] Na/Si molar ratio in activator.

CHAPTER 6

THE POTENTIAL APPLICATION OF FLY ASH-BASED GEOPOLYMER CONCRETE

6.1 Introduction

Concrete is one of the most frequently used man-made materials on earth. It is an important construction material used extensively in buildings, bridges, roads and dams. Its uses range from structural applications, to paviours, kerbs, pipes and drains. It is used more than any other artificial material in the world [132]. Its usage worldwide, ton for ton, is twice that of steel, wood, plastics, and aluminum combined. Concrete is a composite material, consisting mainly of fine and coarse aggregate bonded together with a fluid cement (cement paste) that hardens over time. And OPC is still the prime choice as the binder for concrete prompting massive rise in the production of OPC as much as 3% annually [133]. OPC industry is held responsible for some of the CO_2 emission, which contributes about 64% of global warming as greenhouse gases [2].

Several efforts are in progress to reduce the use of Portland cement in concrete in order to retard the global warming issues. These include the utilization of supplementary cementing materials such as fly ash, silica fume, granulated blast furnace slag, rice-husk ash and metakaolin, and the development of alternative binders to Portland cement.

Davidovits [32–34] proposed that the aluminosilicate materials can react with alkaline solution to generate the production similar to natural zeolite materials, but with amorphous microstructure instead of crystalline. Then it is found that geopolymer binder is potential to replace the use of OPC in concrete [35]. Palomo et al. [41] found that

geopolymer concrete can be easily produced using the current concrete technology and the products are excellent with smaller drying shrinkage.

Fly ash has been proved to be one of the main source materials for synthesizing geopolymer binder [96,97,110,116]. At the same time, the reusing of fly ash will reduce its negative effect on the environmental problem. Tempest et al. [65] investigated the optimization of the mix design and curing regimen for a geopolymer concrete relating strength development to the quality of energy that is consumed to activate the fly ashes and curing the concrete in high temperature. The compression tests revealed that the material strength ranged from 32.5 MPa to 67.5 MPa. And strength development is related to all three variables: activator concentration, aging time, and curing time. Akbarl et al. [134] studied the geopolymer concrete synthesized by two different fly ashes and analyzed several critical factors affecting geopolymer concrete. The range of strength was from 10 to 40 MPa. The results showed the alkali type and concentration, the curing temperature and the H_2O/Na_2O ratio have the most significant effects on the compressive strength. Nath [135] systematically studied the design and development of Class F fly ash-based geopolymer mixture that is suitable for curing in normal ambient condition and investigated the influence of different mixture parameters affecting the setting time, workability and early age compressive strength properties without heat curing. Then the durability properties of geopolymer concrete cured in ambient curing condition was studied and compared with those cured using heat curing. Hardjito and Rangan [136] also did similar work about the mixture of geopolymer concrete and short-term and long-term engineering properties of fresh and hardened fly ash-based geopolymer concrete.

Although so much research has been done, due to the difference of chemical compositions of coal and the processes of combustion, it is still necessary to design the experiments to test the fly ash-based geopolymer concrete. Since the purpose is to apply it in the natural environment, all of samples making in the lab would be cured at room temperature in the whole process of production without any heat curing. Fly ash is still the only source material of aluminosilicate, activated by a mixture of sodium hydroxide and sodium silicate solution (industrial). According to the results of last chapter, the performance of YC fly ash-based geopolymer paste in mechanical properties was better than that of JMNY fly ash, thus YC fly ash was chosen to be used in this research. Fine and coarse aggregates would be added during the blending time. Extra water would be added according to the requirement of design. The compressive strength property of geopolymer concrete samples were mainly studied. This study includes two parts: laboratory test and field test. Laboratory test supplied the optimal proportion and other related information such as mixing time, stirring style, charging sequence, and agitation speed. And then the obtained proportion would be used in the field test.

6.2 Materials and Methods

6.2.1 Materials

Class F fly ash was the main source materials of aluminosilicate for synthesizing the geopolymer concrete specimens, which was supplied by YC power stations on June 2018. The description of fly ash was given in section 5.2.1 of Chapter 5. The chemical composition and size fraction were shown in Table 5.1, while Fig 5.1 showed the particle

size distributions determined by the standard test method ASTM D422 [28]. The mean particle sizes (D_{50}) of fly ashes was 6.5 μm. A combination of sodium hydroxide and sodium silicate solution was used as the activator. Industrial sodium silicate solution was supplied by a chemical industrial company in Tsingtao, China. The chemical composition of sodium silicate solution was 8.39 wt.% Na_2O, 26.94 wt.% SiO_2, and 64.67 wt.% H_2O with specific gravity of about 1.4. And one company in Hebei province, China, offered the analytical grade sodium hydroxide flakes with purity of ≥ 95.0%. Fine and coarse aggregates were purchased and used based on the GB/T14684-2001 and GB/T14685-2011 [62,137]. Tap water was both used in laboratory and field tests.

6.2.2 Sample Preparation

6.2.2.1 Laboratory Test

In the laboratory test, fly ash, sand, and gravel were dried in the oven before experiments in order to accurately control the amount of water in proportion. The geopolymer paste were prepared with same type of Si/Al and Na/Si molar ratio. The slurry was prepared by using water to fly ash mass ratio of 0.25, which was increased, compared to 0.20 in section 5.3.4, to reach enough flow in the consideration of adding aggregates. The NaOH and tap water were firstly mixed by a glass stirring rod and left to cool down to the room temperature. Then the sodium silicate solution was added to the NaOH solution, followed by mixing for at least 5 min and allow them to rest overnight with covering in order to fully blend and non-contact with air. The blended solution was combined with dry fly ash powder, followed by mixing for 5 min in concrete mixer to ensure thorough mixing

among the powder and solution. Then dried and cooled aggregates were added in the concrete mixer (Fig 6.1) followed by mixing up to 10 - 15 min. The detailed mixture designs of concrete are presented in Table 6.1.

Standard cubic mold (Fig 6.2) was used in this part of work, with length of 150 mm. The prepared concrete grout was cast into the mold in two lifts and pounded 25 times per lift with a rod. For consistency, the step of vibrating on shaking table (Fig 6.3) for 1 min after rodding was conducted. Prior to casting, the interior of mold was coated with a thin layer of release agent for easy removal of specimens. The mold with samples were cured in the thermotank (Fig 6.4), with set room temperature. After 7 d in the thermotank, samples were demolded immediately and continue to be left in the thermotank until testing on the 28th day. For each proportion, 3 cubes (Fig 6.5) were tested in compression according to GB/T 50107-2010 [71].

6.2.2.2 Field Test

In the field test, fly ash was supplied directly from YC power station by cement tanker. The field test was carried out at one concrete mixing plant (Fig 6.6), which provided sand and gravel. The proportion was the optimal mix from laboratory tests. Due to large amount of sodium silicate solution and sodium hydroxide used in the field test, they were prepared in advance and stored in plastic buckets, respectively. The NaOH and tap water were firstly mixed by a glass stirring rod and left to cool down to the room temperature. And then NaOH solution were kept in the sealed plastic buckets. Sodium silicate solution was stored in the container. There were some differences in facility between field test and laboratory test, since the charging sequence changed in field test. Fly ash and aggregates

were mixed together thoroughly for 2 min. Then Sodium silicate solution (Fig 6.7) and NaOH solution (Fig 6.8) were added and mixed thoroughly for another 5 min until a consistent mixture was obtained (Fig 6.9). All of concrete grout was poured into one container (Fig 6.10), which was used to transport and cast in prepared mold.

Test specimens include two different parts: cast-in-situ slab and precast slab. Cast-in-situ site was a rectangle area which was divided into four pieces, as shown in Fig 6.11. This site was located on the road of residential community with length of 4 m and width of 5 m. Area as No. 1, 2, and 3 were chosen to be cast-in-place and concrete grout was vibrated by electric vibrating needle (Fig 6.12). Precast slabs were produced at concrete mixer plant and installed at No. 4 area (Fig 6.13).

6.3 Results and Discussion

The proportion of various aggregates in the mixture of geopolymer concrete were designed to study the effect of aggregates on the compressive strength of geopolymer concrete samples cured in ambient environment. The purpose of field test is to investigate the durability of geopolymer concrete samples staying in the natural environment, such as freeze thawing between summer and winter, solar radiation, rain drop erosion, air-slake, friction damage from pedestrian and traveling vehicle, and bearing capacity. The results were summarized below.

6.3.1 Effect of Proportion of Aggregates on Mechanical Performance

The results of compressive strength were presented in Fig 6.14. The No. of design mixes referred to Table 6.1. Compression tests were carried out at curing time of 14 d and

28 d. Most of proportions showed average UCS around 30 MPa at 14 d and 40 MPa at 28 d, with the exception of No. 5 (fly ash : fine aggregate : coarse aggregate = 1 : 0.91 : 0.91). Based on these data, it seems that the ratio of aggregates to fly ash and the ratio of fine to coarse aggregate does not have obvious effect on the mechanical property. But the higher ratio of aggregates to fly ash was, the lower the flow of concrete grout was. As the exception, No. 5 proportion showed the great flow condition at the same time with high performance in mechanical property. Therefore, No. 5 proportion was chosen to be used for field test.

Before field test, in order to guarantee the validity of No. 5 proportion, it is necessary to repeat the same laboratory test by using different batches of fly ash from YC power station (Fig 6.15). It indicated that data fluctuated between 30 and 50 MPa, who's average UCS can reach 40 MPa. The reason causing fluctuation is the difference in the quality of fly ash collected from different time. Even so, this strength still can satisfy the requirement of road-field test.

6.3.2 Durability of Geopolymer Concrete Road

The final construction site was shown in Fig 6.16. In order to monitor the long-term mechanical performance, a lot of cubic specimens were produced at the same time with manufacture of precast slab and placed under natural environment. The compression tests were conducted in 0, 3, 6, 9, and 12 months (Fig 6.17). Strength slowly increased with the increasing month. And trend became gently after 6 months. According to the visual, there are no crack on the surface of road until now. The compression tests will be continued in the future several years to collect more data to verify its durability.

6.4 Conclusions

This chapter showed results of mixture design, mechanical property of fly ash-based geopolymer concrete. The basic mix proportion of geopolymer binder was chosen because of its perfect performance on the mechanical property. 7 different type of composition of fine and coarse aggregates were tested in the laboratory in order to find the optimal recipe for field testing. All of geopolymer concrete binders were cured at ambient environment. The results are summarized below:

According to section 5.3.4, design mix as Si/Al ratio of 1.6, Na/Si ratio of 1.5, and water/ fly ash mass ratio of 0.20 demonstrated the highest strength without any apparent defects. In the view of addition of aggregates and water absorbability of coarse aggregate, water/fly ash ratio was up to 0.25 to guarantee the certain flowability. Compression testing in the lab indicated that the recipe as fly ash/fine aggregate/coarse aggregate = 1:0.91:0.91 generates the best performance in mechanics: high strength up to 50 MPa with great flowability.

In order to verify the effectiveness of the strength, another four sets of fly ash collected in a different time period were used to synthesis geopolymer concrete. Due to the quality fluctuation of fly ash, the strength changed from 30 MPa to 50 MPa. Even so, the lowest strength still can meet the strength standard of road test.

The purpose of field testing is to investigate the short and long-term durability of geopolymer concrete under the effect of natural environment. The strength data has been collected at 0, 3, 6, 9, and 12 months, and results showed that strength increases from 36 MPa to 41 MPa. And that the growth rate gradually fell down after 6 months. Besides,

there are no visible cracks on the surface of road and no obvious sign of efflorescence until now. More data will be gathered in future several years.

Figure 6.1: Concrete mixer, 0.5 m^3.

Figure 6.2: Mold for concrete specimens: 150*150*150 (mm).

Figure 6.3: Shaking table.

Figure 6.4: Thermotank for sample storage.

Figure 6.5: Fly ash-based geopolymer concrete samples.

Figure 6.6: Concrete mixer plant.

Figure 6.7: Sodium silicate solution added from bucket to blender.

Figure 6.8: NaOH solution added into blender.

Figure 6.9: Mixing in blender.

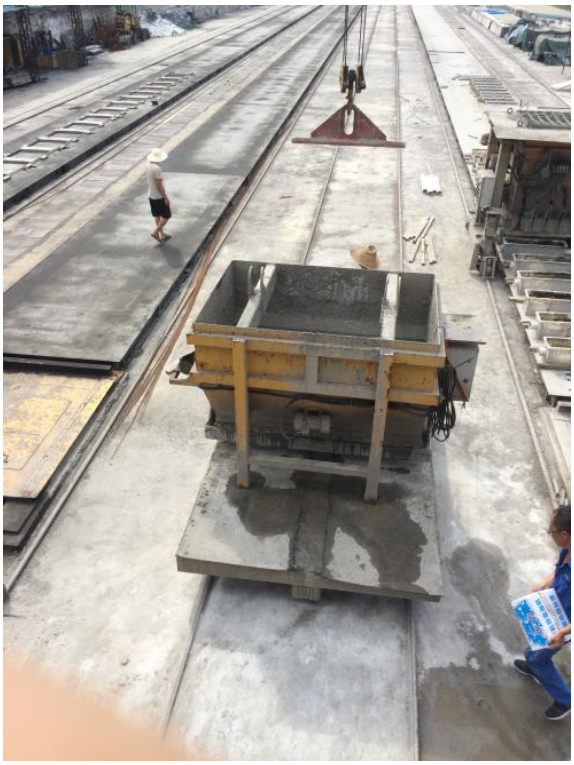

Figure 6.10: Concrete grout container.

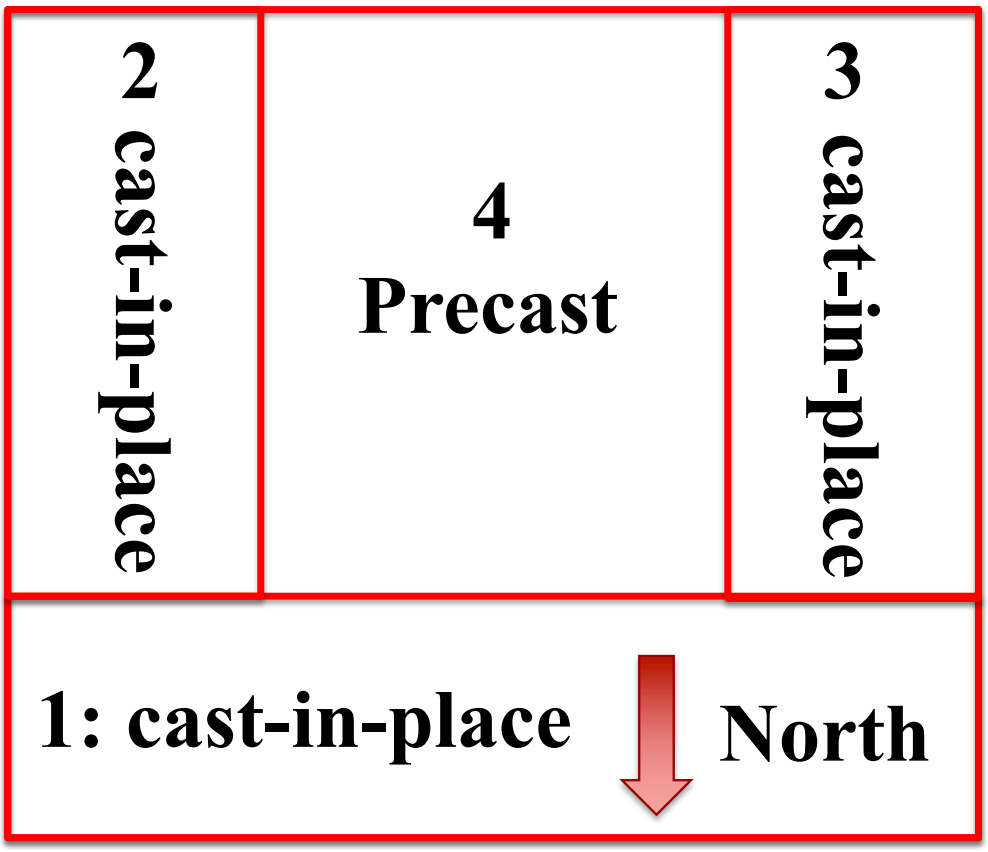

Figure 6.11: Schematic diagram of cast-in-situ site, 4*5 m^2.

Figure 6.12: Construction site of area 1 ,2, 3 (cast-in-place).

Figure 6.13: Precast slabs produced at concrete mixer plant (left graph) and installed at construction site (right graph).

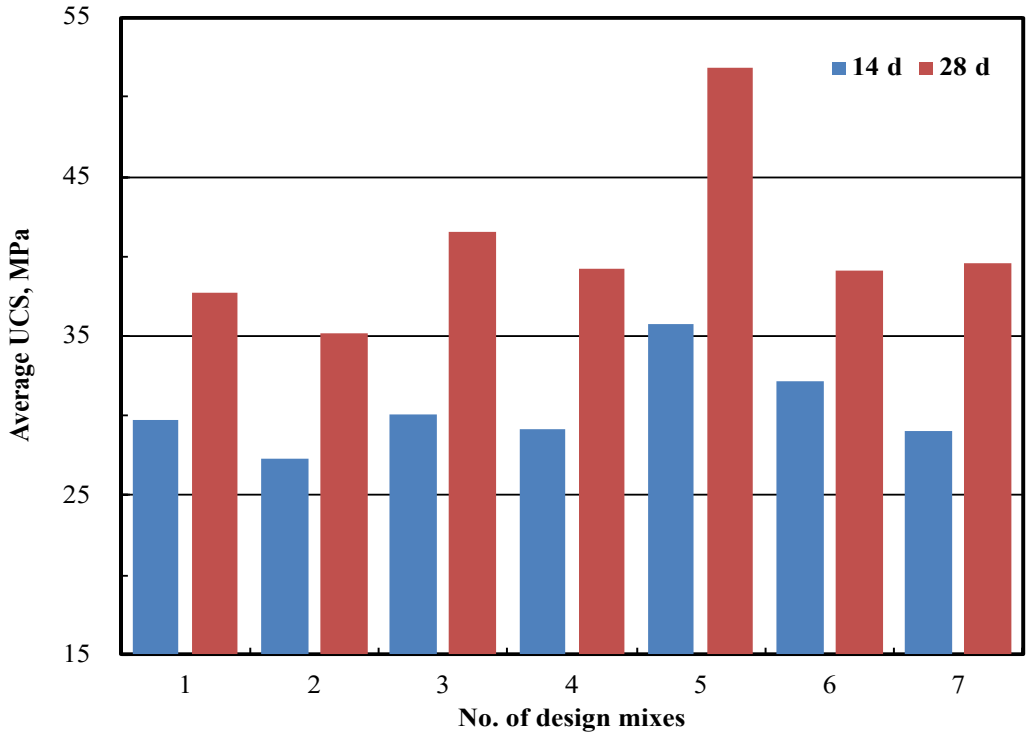

Figure 6.14: Summary of average UCS of geopolymer concrete samples in different proportion of aggregates.

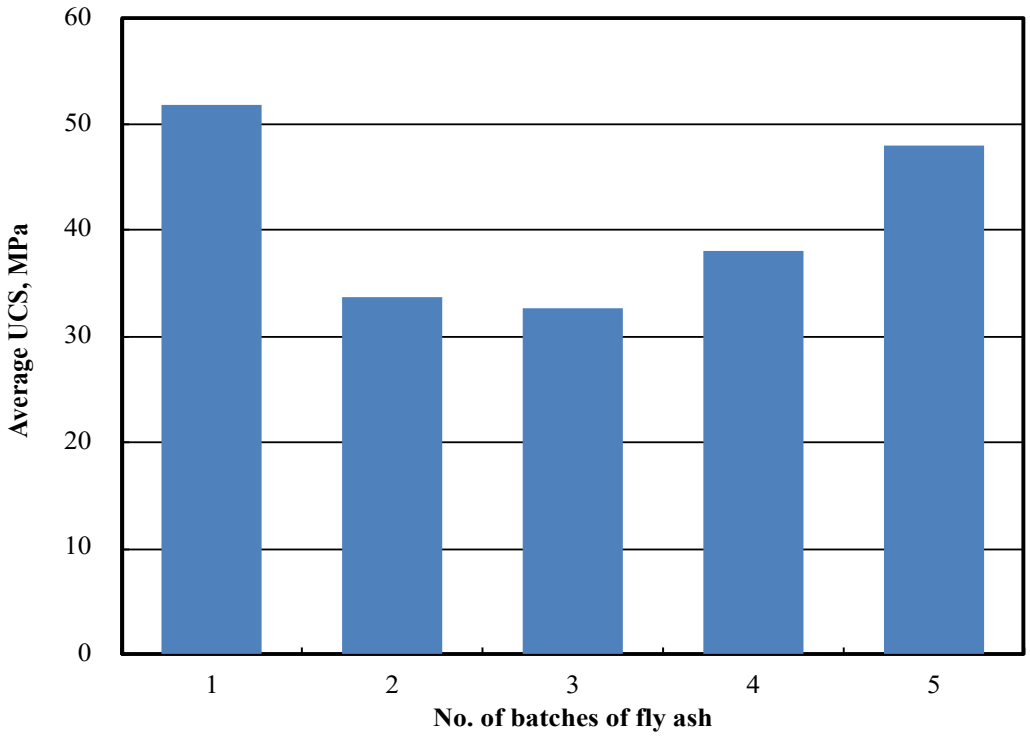

Figure 6.15: Summary of average UCS of geopolymer concrete samples using different batches of fly ash.

Figure 6.16: Construction site.

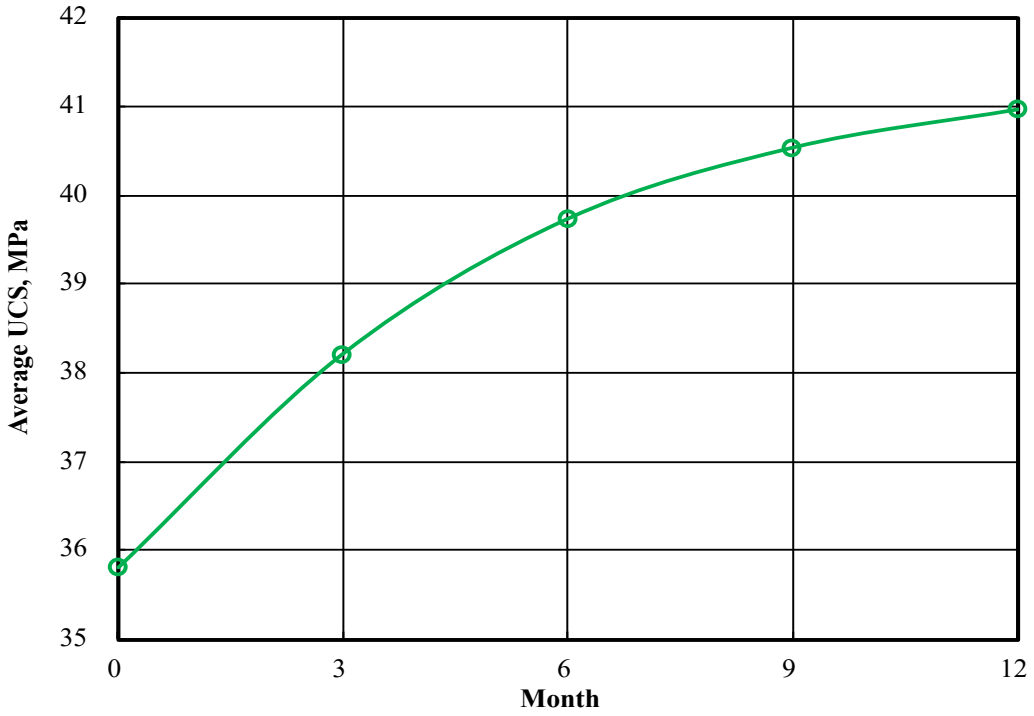

Figure 6.17: Summary of long-term average UCS of geopolymer concrete specimens.

Table 6.1: Details of fly ash-based geopolymer concrete mixture designs.

Mix No.	Molar ratio		Water/Fly ash (mass ratio)	Fine aggregates/fly ash (mass ratio)	Coarse aggregates/fly ash (mass ratio)
	Si/Al	Na/Si[a]			
1	1.6	1.5	0.25	0.91	2.38
2	1.6	1.5	0.25	0.5	1.2
3	1.6	1.5	0.25	0.75	1.8
4	1.6	1.5	0.25	0.5	1.8
5	1.6	1.5	0.25	0.91	0.91
6	1.6	1.5	0.25	0.5	2.38
7	1.6	1.5	0.25	1.3	1.3

[a]Na/Si molar ratio in activator.

CHAPTER 7

CONCLUSIONS

7.1 Overview

This chapter presents the conclusions of the research on the performance of fly ash and metakaolin-based geopolymer cured in saline water and the potential application of fly ash-based geopolymer cement and concrete cured in ambient environment. The study has proved the perfect performance of geopolymer binder on the resistance to sea salt corrosion even under the influence of immediate curing of geopolymer precursor in saline water. And the study also indicated that the fly ash with low activity can also be possibly used to synthesis geopolymer. However, no matter how quality of fly ash it is, results show that the strength has reached up to the general range of application in construction. In the consideration of cost, fly ash with high activity is more suitable for being the raw material to produce the geopolymer cement. Suitable proportion of geopolymer binder have been advised based on the mechanical properties. Such proportion is tested for the mechanical performance and durability of geopolymer concrete. The results present that fly ash-based geopolymer concrete not only satisfies the requirement of strength, but also applies to the ordinary construction technology. Therefore, this study supplies the basic foundation of engineering application of local fly ash (Jincheng, China) as the raw material of synthesizing geopolymer cement and concrete. Some recommendations for future study have been given at the end.

7.2 Conclusions

In the part of research focusing on the effect of Si/Al and Na/Al molar ratios, the geopolymers were synthesized using mixture of Class C fly ash and metakaolin in a mass proportion of 1:1, activated using mixture of sodium hydroxide and sodium silicate solution. The range of Si/Al and Na/Al ratios is 1.78 to 2.0 and 0.67 to 1.0, respectively. 0.5 was chosen as the mass ratio of water/mixture powder. For benchmarking purposes, GOWC was used for strength testing. The specimens cast in porous molds were cured in saline water (0, 15, and 35 ppt) in room temperature for 28 d. And then the curing solutions were tested for pH value and salinity. Demolded samples were tested using UCT, SEM, XRD, and XRF. The following conclusions were extracted from the results of study:

a) In a given salinity, the increase of Si /Al ratio leads to the improvement of strength, but the UCS decreases with increase in the Na/Al molar ratio which means high Na/Al molar ratio is detrimental to the development of UCS of geopolymer cured in salinity environment, possibly due to the existence of excessive OH^- in the alkali-activated medium. In a given Si/Al ratio with low Na/Al ratio, the UCS of geopolymers increases with increased salinity of curing water. However, opposite case happens for High Na/Al ratio.

b) The compositional and microstructural analysis show that all of products are geopolymeric compounds, but not purity, including nonreactive crystalline phases from raw materials and a little part of un-reacted or partially reacted raw materials particles. Therefore, the real Si/Al and Na/Al molar ratios are not totally consistent with the pre-designed. The interior of the sample cured in saline water contains a homogeneous and continuous matrix that will improve the performance of mechanical properties. And the

exterior is weaker than the interior. The characteristic of geopolymers in SEM reflect the change in the mechanical properties, to some extent.

c) The analysis of XRF, pH testing and electrical conductivity proves the existing of ion exchange during the curing both in the exterior and interior. And the major process of exchange will be completed in less than 48 h. Therefore, it is important to consider the influence of salt corrosion from the statement of the sample as the slurry. The content of Na owning obvious alteration is chosen as a typical indicator to trace the situation of ion exchange. To a great extent, the change in the content of Na is consistent with the trend of UCS. It is found that curing water with high salinity not only reduces the leaching but also intrudes the chemical components of curing water into geopolymer specimens. The reduction of leaching is benefit to the improvement of strength. The results of pH and electrical conductivity testing show that ΔpH and Δsalinity of geopolymers and GOWC decrease with an increase in salinity. However, the rate of leaching proves that geopolymers are less affected.

Low-calcium Class F fly ash, as main aluminosilicate source supplied by JMNY and YC power stations (China), was used for the study of the potential application of geopolymer cement, mortar, and concrete. A combination of sodium hydroxide and sodium silicate solution was used as the activator. Fine and coarse aggregates were applied based on the GB/T14684-2001 and GB/T14685-221. Tap water was both used in laboratory and field tests. The geopolymer binder were prepared with different Si/Al (1.5-2.0) and Na/Si (1.25-2.0) ratios. Water/fly ash mass ratio is from 0.55 to 0.2. All of samples were cured in room temperature for 28 d and tested for compressive strength. Influences of Si/Al ratio, Na/Si ratio, water/fly ash mass ratio, sand/fly ash mass ratio, aggregates as well as factor

fly ash from different combustion systems were investigated. Some conclusions are listed from the study as followed:

a) When water/fly ash ratio is 0.55, the Si/Al ratio is confirmed as 1.65-2.0 with Na/Si ratio of 1.0-2.0. The range of compressive strength was from 17 to 55 MPa. When water/fly ash ratio reduced to 0.40, the range of Si/Al ratio amplified to 1.5-2.0. And at the same time, compressive strength changed from 9 to 62 MPa. The workability and setting time increased with the increase in Si/Al and Na/Si ratios. Although the decrease in water/fly ash ratio resulted in the increasing strength, workability dropped quickly. Considering both of mechanical performance and cost, the greatest potential design mixtures were Si/Al ratio of 1.5-1.6, Na/Si ratio of 1.5-2.0, water/fly ash ratio of 0.4.

b) The variation in technology of producing fly ash resulted in the big difference in the quality of fly ash, which would affect the process and degree of geopolymerization. For example, higher temperature combustion results in finer and more activity fly ash particle, which will improve the mechanical properties of geopolymer binder. For same design proportion as Si/Al ratio of 1.5-1.6 and Na/Si ratio of 1.5, water/fly ash ratio drops to 0.2-0.25 with the strength up to 80 MPa. The results of geopolymer mortar showed that the optimal sand/fly ash ratio should be around 2.0 in this study.

c) The proportion used for field testing is based on the mixture of geopolymer cement: Si/Al ratio of 1.6, Na/Si ratio of 1.5, water/fly ash ratio of 0.2, which presents excellent mechanical properties. However, in consideration of additional aggregates and water absorbability of coarse aggregate, water/fly ash ratio of 0.25 is chosen. As a result, the recipe as fly ash/fine aggregate/coarse aggregate = 1:0.91:0.91 leads to the best performance in mechanics: up to 50 MPa with great flowability. Although the strength

fluctuates with the change in the quality of fly ash, the lowest strength is greater than 30 MPa, which can satisfy the requirement of strength for road.

d) The strength data of samples from road has been collected at 0, 3, 6, 9, and 12 months, and results show that strength increases from 36 MPa to 41 MPa. And that the growth rate gradually falls down after 6 months. Besides, there are no visible cracks on the surface of road and no obvious sign of efflorescence until now. More data will be gathered in future several years.

REFERENCES

[1] A. Shafeen, T. Carter, Geological sequestration of greenhouse gases, Environ. Conscious Foss. Energy Prod. (2010) 207–241. https://doi.org/doi:10.1002/9780470432747.ch6.

[2] P. Bertier, R. Swennen, B. Laenen, D. Lagrou, R. Dreesen, Experimental identification of CO_2–water–rock interactions caused by sequestration of CO_2 in Westphalian and Buntsandstein sandstones of the Campine Basin (NE-Belgium), J. Geochemical Explor. 89 (2006) 10–14. https://doi.org/10.1016/J.GEXPLO.2005.11.005.

[3] R.G. Bruant, J. Jr, A.J. Guswa, M.A. Celia, C.A. Peters, Safe storage of CO_2 in deep saline aquifers, 2002.

[4] M.S.A. Perera, P.G. Ranjith, S.K. Choi, D. Airey, Effects of sub-critical and super-critical carbon dioxide adsorption-induced coal matrix swelling on permeability of naturally fractured black coal, 2011. https://doi.org/10.1016/j.energy.2011.09.023.

[5] M.C.M. Nasvi, P.G. Ranjith, J. Sanjayan, A. Haque, Sub- and super-critical carbon dioxide permeability of wellbore materials under geological sequestration conditions: An experimental study, Energy. 54 (2013) 231–239. https://doi.org/10.1016/j.energy.2013.01.049.

[6] R. Kondo, M. Daimon, E. Sakai, H. Ushiyama, Influence of inorganic salts on the hydration of tricalcium silicate, J. Appl. Chem. Biotechnol. 27 (1977) 191–197. https://doi.org/10.1002/jctb.5020270128.

[7] K. Suzuki, T. Nishikawa, H. Ikenaga, S. Ito, Effect of NaCl or NaOH on the formation of CSH, Cem. Concr. Res. 16 (1986) 333–340. https://doi.org/10.1016/0008-8846(86)90108-0.

[8] X. Zhou, X. Lin, M. Huo, Y. Zhang, The hydration of saline oil-well cement, Cem. Concr. Res. 26 (1996) 1753–1759. https://doi.org/10.1016/S0008-8846(96)00176-7.

[9] V. Barlet, G. Rimmelé, B. Goffé, O. Porcherie, Well technologies for CO_2 geological storage: CO_2 -resistant cement, 2007. https://doi.org/10.2516/ogst:2007027.

[10] E. Lécolier, A. Rivereau, G. Le Saoût, A. Audibert-Hayet, Durability of hardened portland cement paste used for oilwell cementing, Oil Gas Sci. Technol. - Rev. IFP. 62 (2007) 335–345. https://doi.org/10.2516/ogst:2007028.

[11] V. Barlet-Gouédard, G. Rimmelé, O. Porcherie, N. Quisel, J. Desroches, A solution against well cement degradation under CO_2 geological storage environment, Int. J. Greenh. Gas Control. 3 (2009) 206–216. https://doi.org/10.1016/J.IJGGC.2008.07.005.

[12] A. Duguid, An estimate of the time to degrade the cement sheath in a well exposed to carbonated brine, Energy Procedia. 1 (2009) 3181–3188. https://doi.org/10.1016/J.EGYPRO.2009.02.101.

[13] A.M. Fernandez-Jimenez, A. Palomo, C. Lopez-Hombrados, Engineering properties of alkali-activated fly ash concrete, ACI Mater. J. 103 (2006) 106–112.

[14] P. Duxson, A. Fernández-Jiménez, J.L. Provis, G.C. Lukey, A. Palomo, J.S.J. van Deventer, Geopolymer technology: the current state of the art, J. Mater. Sci. 42 (2007) 2917–2933. https://doi.org/10.1007/s10853-006-0637-z.

[15] D.L.Y. Kong, J.G. Sanjayan, K. Sagoe-Crentsil, Comparative performance of geopolymers made with metakaolin and fly ash after exposure to elevated temperatures, Cem. Concr. Res. 37 (2007) 1583–1589. https://doi.org/10.1016/j.cemconres.2007.08.021.

[16] C. Bilim, O. Karahan, C.D. Atiş, S. İlkentapar, Influence of admixtures on the properties of alkali-activated slag mortars subjected to different curing conditions, Mater. Des. 44 (2013) 540–547. https://doi.org/10.1016/J.MATDES.2012.08.049.

[17] K.H. Yang, J.K. Song, K.I. Song, Assessment of CO_2 reduction of alkali-activated concrete, J. Clean. Prod. 39 (2013) 265–272. https://doi.org/10.1016/J.JCLEPRO.2012.08.001.

[18] P.K. Sarker, S. Kelly, Z. Yao, Effect of fire exposure on cracking, spalling and residual strength of fly ash geopolymer concrete, Mater. Des. 63 (2014) 584–592. https://doi.org/10.1016/J.MATDES.2014.06.059.

[19] T. Phoo-ngernkham, P. Chindaprasirt, V. Sata, S. Hanjitsuwan, S. Hatanaka, The effect of adding nano-SiO_2 and nano-Al_2O_3 on properties of high calcium fly ash geopolymer cured at ambient temperature, Mater. Des. 55 (2014) 58–65. https://doi.org/10.1016/J.MATDES.2013.09.049.

[20] M. Lassinantti Gualtieri, M. Romagnoli, A.F. Gualtieri, Preparation of phosphoric acid-based geopolymer foams using limestone as pore forming agent – Thermal properties by in situ XRPD and Rietveld refinements, J. Eur. Ceram. Soc. 35 (2015) 3167–3178. https://doi.org/10.1016/J.JEURCERAMSOC.2015.04.030.

[21] M. Shojaei, K. Behfarnia, R. Mohebi, Application of alkali-activated slag concrete in railway sleepers, Mater. Des. 69 (2015) 89–95. https://doi.org/10.1016/J.MATDES.2014.12.051.

[22] J. Davidovits, Geopolymer chemistry and applications, 2nd Ed, 2008.

[23] J. Provis, J. Van Deventer, Geopolymers: structures, processing, properties and industrial applications, 2009.

[24] M. Khalifeh, A. Saasen, T. Vralstad, H. Hodne, Potential utilization of class C fly ash-based geopolymer in oil well cementing operations, Cem. Concr. Compos. 53 (2014) 10–17. https://doi.org/10.1016/J.CEMCONCOMP.2014.06.014.

[25] ASTM D854-14, Standard test methods for specific gravity of soil soilds by water pycnometer, (2014). https://doi.org/http://10.1520/D0854-14.

[26] ASTM D4318-10, Standard test methods for liquid limit, plastic limit, and plasticity index of soils, (2010). https://doi.org/http://10.1520/D4318-10.

[27] ASTM D2216-10, Standard test methods for laboratory determination of water (moisture) content of soil and rock by mass, (2010). https://doi.org/http://10.1520/D2216-10.

[28] ASTM D422, Standard test method for particle-size analysis of soils, (1998). https://doi.org/https://doi.org/10.1520/D0422-63R98.

[29] ASTM D1293-18, Standard test methods for pH of water, (2018). https://doi.org/http://10.1520/D1293-18.

[30] ASTM D5391-14, Standard test method for electrical conductivity and resistivity of a flowing high purity water sample, (2014). https://doi.org/https://doi.org/10.1520/D5391-14.

[31] ASTM C39/39M, Standard test method for compressive strength of cylindrical concrete specimens, (2018). https://doi.org/http://10.1520/C0039_C0039M-18.

[32] J. Davidovits, Geopolymers and geopolymeric materials, J. Therm. Anal. 35 (1989) 429–441. https://doi.org/10.1007/BF01904446.

[33] J. Davidovits, Geopolymers - inorganic polymeric new materials, J. Therm. Anal. 37 (1991) 1633–1656.

[34] J. Davidovits, Chemistry of geopolymeric systems terminology, Proc. 2nd Int. Conf. Geopolymer. (1999) 9–39.

[35] A. Palomo, M.W. Grutzeck, M.T. Blanco, Alkali-activated fly ashes: A cement for the future, Cem. Concr. Res. 29 (1999) 1323–1329. https://doi.org/10.1016/S0008-8846(98)00243-9.

[36] H. Xu, J.S.J. Van Deventer, The geopolymerisation of alumino-silicate minerals, Int. J. Miner. Process. 59 (2000) 247–266. https://doi.org/10.1016/S0301-7516(99)00074-5.

[37] A.O. Purdon, The action of alkalis on blast furnace slag, J. Soc. Chem. Ind. 59 (1940) 191–202.

[38] V.D. Glukhovsky, Soil silicates, Gosstroyizdat, Kiev. 154 (1959).

[39] J.L. Davidovits, J., Sawyer, Early high-strength mineral polymer, 4509985, 1985.

[40] H. Xu, Geopolymerisation of aluminosilicate minerals, 2002. http://hdl.handle.net/11343/38811.

[41] A. Palomo, P. Krivenko, I. Garcia-Lodeiro, E. Kavalerova, O. Maltseva, A. Fernández-Jiménez, A review on alkaline activation: new analytical perspectives, Mater. Construcción. 64 (2014) e022. https://doi.org/10.3989/mc.2014.00314.

[42] J. Davidovits, Properties of geopolymer cements, First Int. Conf. Alkaline Cem. Concr. (1994).

[43] R.A. Fletcher, K.J.D. MacKenzie, C.L. Nicholson, S. Shimada, The composition range of aluminosilicate geopolymers, J. Eur. Ceram. Soc. 25 (2005) 1471–1477. https://doi.org/10.1016/J.JEURCERAMSOC.2004.06.001.

[44] G. Zhang, J. He, R. P. Gambrell, Synthesis, characterization, and mechanical properties of red mud-based geopolymers, 2010. https://doi.org/10.3141/2167-01.

[45] K. Mackenzie, D. Brew, R. Fletcher, C. Nicholson, R. Vagana, M. Schmücker, Advances in understanding the synthesis mechanisms of new geopolymeric materials, in: 2006: pp. 187–200. https://doi.org/10.1002/9781118144114.ch19.

[46] A. Buchwald, M. Hohmann, C. Kaps, H. Bettzieche, J.-T. Kühnert, Stabilised foam clay material with high performance thermal insulation properties, Ceram. Forum Int. 81 (2004) E39–E42.

[47] P. Duxson, J.L. Provis, G.C. Lukey, S.W. Mallicoat, W.M. Kriven, J.S.J. van Deventer, Understanding the relationship between geopolymer composition, microstructure and mechanical properties, Colloids Surfaces A Physicochem. Eng. Asp. 269 (2005) 47–58. https://doi.org/10.1016/J.COLSURFA.2005.06.060.

[48] D. Khale, R. Chaudhary, Mechanism of geopolymerization and factors influencing its development: a review, J. Mater. Sci. 42 (2007) 729–746. https://doi.org/10.1007/s10853-006-0401-4.

[49] L. Verdolotti, S. Iannace, M. Lavorgna, R. Lamanna, Geopolymerization reaction to consolidate incoherent pozzolanic soil, J. Mater. Sci. 43 (2008) 865–873. https://doi.org/10.1007/s10853-007-2201-x.

[50] Z. Yang, N. Ha, M. Jang, K. Hwang, Geopolymer concrete fabricated by waste concrete sludge with silica fume, Mater. Sci. Forum - MATER SCI FORUM. 620 (2009) 791–794. https://doi.org/10.4028/www.scientific.net/MSF.620-622.791.

[51] V. M. and A.A. Ramezanianpour Malhotra, Fly ash in concrete, CANMET Batural Resources Canada, 1994.

[52] ASTM C618, Standard specification for coal fly ash and raw or calcined natural pozzolan for use in concrete, (2017). https://doi.org/https://10.1520/C0618-17A.

[53] R.E. Grim, Applied clay mineralogy, McGraw-Hill, New York, 1962.

[54] W.A. Deer FRS, R.A. Howie, J. Zussman, An Introduction to the rock-forming minerals, (2013). https://doi.org/10.1180/DHZ.

[55] W.L. Pohl (2011) Economic geology: principles and practice. Metals, minerals, coal and hydrocarbons—introduction to formation and sustainable exploitation of mineral deposits, Miner. Depos. 46 (2011) 833. https://doi.org/10.1007/s00126-011-0381-4.

[56] K. Mitchell, J.K. Soga, Fundamentals of soil behavior, 3rd ed., John Wiley & Sons, Ltd, Hoboken, 2005.

[57] S. Salvador, Pozzolanic properties of flash-calcined kaolinite: A comparative study with soak-calcined products, Cem. Concr. Res. 25 (1995) 102–112. https://doi.org/10.1016/0008-8846(94)00118-I.

[58] B. Lothenbach, K. Scrivener, R.D. Hooton, Supplementary cementitious materials, Cem. Concr. Res. 41 (2011) 1244–1256. https://doi.org/10.1016/J.CEMCONRES.2010.12.001.

[59] V.F.F. Barbosa, K.J.D. MacKenzie, C. Thaumaturgo, Synthesis and characterisation of materials based on inorganic polymers of alumina and silica: sodium polysialate polymers, Int. J. Inorg. Mater. 2 (2000) 309–317. https://doi.org/10.1016/S1466-6049(00)00041-6.

[60] J. He, J. Zhang, Y. Yu, G. Zhang, The strength and microstructure of two geopolymers derived from metakaolin and red mud-fly ash admixture: A comparative study, Constr. Build. Mater. 30 (2012) 80–91. https://doi.org/10.1016/J.CONBUILDMAT.2011.12.011.

[61] M. Zhang, H. Guo, T. El-Korchi, G. Zhang, M. Tao, Experimental feasibility study of geopolymer as the next-generation soil stabilizer, Constr. Build. Mater. 47 (2013) 1468–1478. https://doi.org/10.1016/J.CONBUILDMAT.2013.06.017.

[62] GB/T 14685-2011, Standard specification for concrete aggregates, (2011).

[63] M. Olivia, H. Nikraz, Properties of fly ash geopolymer concrete designed by Taguchi method, Mater. Des. 36 (2012) 191–198. https://doi.org/10.1016/J.MATDES.2011.10.036.

[64] D.V. Reddy, J.B. Edouard, K. Sobhan, Durability of fly ash–based geopolymer structural concrete in the marine environment, J. Mater. Civ. Eng. 25 (2013) 781–787. https://doi.org/10.1061/(ASCE)MT.1943-5533.0000632.

[65] B. Tempest, O. Sanusi, J. Gergely, V. Ogunro, D. Weggel, Compressive strength and embodied energy optimization of fly ash based geopolymer concrete, World Coal Ash Conf. 2009 Lexington, KY, USA. (2009).

[66] GB 50010-2002, Standard specification for concrerte design, (2002).

[67] M.J. Atkinson, C. Bingman, Elemental composition of commercial seasalts, 2010.

[68] ASTM C192, Standard practice for making and curing concrete test specimens in the laboratory, (2019). https://doi.org/http://10.1520/C0192_C0192M-19.

[69] ASTM D2166, Standard test method for unconfined compressive strength of cohesive soil, (2016). https://doi.org/http://10.1520/D2166_D2166M-16.

[70] ASTM C109, Standard test method for compressive strength of hydraulic cement mortars (using 2-in. or [50-mm] cube specimens), (2016). https://doi.org/http://10.1520/C0109_C0109M-16A.

[71] GB/T 50107-2010, Standard specification for concrete compressive strength, (2010).

[72] D.J. Stokes, Principles and practice of variable pressure/environmental scanning electron microscopy (VP-ESEM), John Wiley & Sons, Ltd, 2008. https://doi.org/http://10.1002/9780470758731.

[73] W.K.W. Lee, J.S.J. van Deventer, The effects of inorganic salt contamination on the strength and durability of geopolymers, Colloids Surfaces A Physicochem. Eng. Asp. 211 (2002) 115–126. https://doi.org/10.1016/S0927-7757(02)00239-X.

[74] T. Bakharev, Geopolymeric materials prepared using class F fly ash and elevated temperature curing, Cem. Concr. Res. 35 (2005) 1224–1232. https://doi.org/10.1016/J.CEMCONRES.2004.06.031.

[75] Sindhunata, J.L. Provis, G.C. Lukey, H. Xu, J.S.J. van Deventer, Structural evolution of fly ash based geopolymers in alkaline environments, Ind. Eng. Chem. Res. 47 (2008) 2991–2999. https://doi.org/10.1021/ie0707671.

[76] U. Rattanasak, P. Chindaprasirt, P. Suwanvitaya, Development of high volume rice husk ash alumino silicate composites, Int. J. Miner. Metall. Mater. 17 (2010) 654–659. https://doi.org/10.1007/s12613-010-0370-0.

[77] S. Thokchom, P. Ghosh, S. Ghosh, Performance of fly ash based geopolymer mortars in sulphate solution, 2010. https://doi.org/10.25103/jestr.031.07.

[78] H. El-Sayed, S. Abo-El-Enein, H. Khater, S. Hasanein, Resistance of alkali activated water- cooled slag geopolymer to sulphate attack, Ceram. – Silikáty. 55 (2011) 153–160.

[79] K. Kupwade-Patil, E.N. Allouche, Examination of chloride-induced corrosion in reinforced geopolymer concretes, J. Mater. Civ. Eng. 25 (2013) 1465–1476. https://doi.org/10.1061/(ASCE)MT.1943-5533.0000672.

[80] H.M. Giasuddin, J.G. Sanjayan, P.. Ranjith, Strength of geopolymer cured in saline water in ambient conditions, Fuel. 107 (2013) 34–39. https://doi.org/10.1016/J.FUEL.2013.01.035.

[81] M.C.M. Nasvi, P.G. Ranjith, J. Sanjayan, A. Haque, X. Li, Mechanical behaviour of wellbore materials saturated in brine water with different salinity levels, Energy. 66 (2014) 239–249. https://doi.org/10.1016/J.ENERGY.2013.12.003.

[82] Y.Y. Kim, B.-J. Lee, V. Saraswathy, S.-J. Kwon, Strength and durability performance of alkali-activated rice husk ash geopolymer mortar, Sci. World J. 2014 (2014) 209584. https://doi.org/10.1155/2014/209584.

[83] D. Bondar, C.J. Lynsdale, N.B. Milestone, N. Hassani, Sulfate Resistance of alkali activated pozzolans, Int. J. Concr. Struct. Mater. 9 (2015) 145–158. https://doi.org/10.1007/s40069-014-0093-0.

[84] D. Bondar, Alkali activated of Iranian natural pozzolans to produce geopolymer cement and concrete, 2009.

[85] P. Duan, C. Yan, W. Zhou, Influence of partial replacement of fly ash by metakaolin on mechanical properties and microstructure of fly ash geopolymer paste exposed to sulfate attack, Ceram. Int. 42 (2016) 3504–3517. https://doi.org/10.1016/J.CERAMINT.2015.10.154.

[86] F.F. Zainal, S.F.M. Amli, K. Hussin, A. Rahmat, M.M.A.B. Abdullah, Corrosion studies of fly ash and fly ash-slag based geopolymer, IOP Conf. Ser. Mater. Sci. Eng. 209 (2017) 012026. https://doi.org/10.1088/1757-899X/209/1/012026.

[87] S.E. Wallah, D. Hardjito, D.M.J. Sumajouw, B.V. Rangan, Sulfate and acid resistance of fly ash-based geopolymer concrete, (2005).

[88] D.N. Huntzinger, T.D. Eatmon, A life-cycle assessment of Portland cement manufacturing: comparing the traditional process with alternative technologies, J. Clean. Prod. 17 (2009) 668–675. https://doi.org/10.1016/J.JCLEPRO.2008.04.007.

[89] C. Meyer, The greening of the concrete industry, Cem. Concr. Compos. 31 (2009) 601–605. https://doi.org/10.1016/J.CEMCONCOMP.2008.12.010.

[90] K. Suzuki, T. Nishikawa, H. Ikenaga, S. Ito, Effect of NaCl or NaOH on the formation of C-S-H, Cem. Concr. Res. 16 (1986) 333–340. https://doi.org/10.1016/0008-8846(86)90108-0.

[91] S.-J. Lyu, Y.-H. Hsiao, T.-T. Wang, T.-W. Cheng, T.-H. Ueng, Microstructure of geopolymer accounting for associated mechanical characteristics under various

stress states, Cem. Concr. Res. 54 (2013) 199–207. https://doi.org/10.1016/J.CEMCONRES.2013.09.007.

[92] M. Santhanam, M.D. Cohen, J. Olek, Mechanism of sulfate attack: a fresh look: Part 2. Proposed mechanisms, Cem. Concr. Res. 33 (2003) 341–346. https://doi.org/10.1016/S0008-8846(02)00958-4.

[93] J. Davidovits, Environmentally driven geopolymer cement applications, in: Geopolymer 2002 Conf., 2002.

[94] Q. Wan, F. Rao, S. Song, R.E. García, R.M. Estrella, C.L. Patiño, Y. Zhang, Geopolymerization reaction, microstructure and simulation of metakaolin-based geopolymers at extended Si/Al ratios, Cem. Concr. Compos. 79 (2017) 45–52. https://doi.org/10.1016/J.CEMCONCOMP.2017.01.014.

[95] T.W. Cheng, J.P. Chiu, Fire-resistant geopolymer produced by granulated blast furnace slag, Miner. Eng. 16 (2003) 205–210. https://doi.org/10.1016/S0892-6875(03)00008-6.

[96] J.G.S. van Jaarsveld, J.S.J. van Deventer, Effect of the alkali metal activator on the properties of fly ash-based geopolymers, Ind. Eng. Chem. Res. 38 (1999) 3932–3941. https://doi.org/10.1021/ie980804b.

[97] X. Li, X. Ma, S. Zhang, E. Zheng, Mechanical properties and microstructure of class C fly ash-based geopolymer paste and mortar, Materials (Basel). 6 (2013) 1485–1495. https://doi.org/10.3390/ma6041485.

[98] T. Bakharev, Durability of geopolymer materials in sodium and magnesium sulfate solutions, Cem. Concr. Res. 35 (2005) 1233–1246. https://doi.org/10.1016/J.CEMCONRES.2004.09.002.

[99] ASTM C39/39M, Standard test method for compressive strength of cylindrical concrete specimens, (2018). https://doi.org/https://10.1520/C0039_C0039M-18.

[100] Y. Zhang, W. Sun, Q. Chen, L. Chen, Synthesis and heavy metal immobilization behaviors of slag based geopolymer, J. Hazard. Mater. 143 (2007) 206–213. https://doi.org/10.1016/J.JHAZMAT.2006.09.033.

[101] M.-R. Wang, D.-C. Jia, P.-G. He, Y. Zhou, Microstructural and mechanical characterization of fly ash cenosphere/metakaolin-based geopolymeric composites, Ceram. Int. 37 (2011) 1661–1666. https://doi.org/10.1016/J.CERAMINT.2011.02.010.

[102] S. Lee, H.-T. Jou, W. Ickard, C.-M. Chon, N.-H. Kang, Three-dimensional quantification of pore structure in coal ash-based geopolymer using conventional electron tomography, Constr. Build. Mater. 52 (2014) 221–226. https://doi.org/10.1016/j.conbuildmat.2013.10.072.

[103] D.L.Y. Kong, J.G. Sanjayan, Effect of elevated temperatures on geopolymer paste, mortar and concrete, Cem. Concr. Res. 40 (2010) 334–339. https://doi.org/10.1016/J.CEMCONRES.2009.10.017.

[104] T. Bakharev, Resistance of geopolymer materials to acid attack, Cem. Concr. Res. 35 (2005) 658–670. https://doi.org/10.1016/J.CEMCONRES.2004.06.005.

[105] L.K. Turner, F.G. Collins, Carbon dioxide equivalent (CO_2-e) emissions: A comparison between geopolymer and OPC cement concrete, Constr. Build. Mater. 43 (2013) 125–130. https://doi.org/10.1016/J.CONBUILDMAT.2013.01.023.

[106] B. Singh, G. Ishwarya, M. Gupta, S.K. Bhattacharyya, Geopolymer concrete: A review of some recent developments, Constr. Build. Mater. 85 (2015) 78–90. https://doi.org/10.1016/J.CONBUILDMAT.2015.03.036.

[107] J. He, Y. Jie, J. Zhang, Y. Yu, G. Zhang, Synthesis and characterization of red mud and rice husk ash-based geopolymer composites, Cem. Concr. Compos. 37 (2013) 108–118. https://doi.org/10.1016/J.CEMCONCOMP.2012.11.010.

[108] Y. Hou, D. Wang, W. Zhou, H. Lu, L. Wang, Effect of activator and curing mode on fly ash-based geopolymers, J. Wuhan Univ. Technol. Sci. Ed. 24 (2009) 711. https://doi.org/10.1007/s11595-009-5711-3.

[109] K. Gao, K.-L. Lin, D. Wang, C.-L. Hwang, H.-S. Shiu, Y.-M. Chang, T.-W. Cheng, Effects SiO_2/Na_2O molar ratio on mechanical properties and the microstructure of nano-SiO_2 metakaolin-based geopolymers, Constr. Build. Mater. 53 (2014) 503–510. https://doi.org/10.1016/J.CONBUILDMAT.2013.12.003.

[110] U. Rattanasak, P. Chindaprasirt, Influence of NaOH solution on the synthesis of fly ash geopolymer, Miner. Eng. 22 (2009) 1073–1078. https://doi.org/10.1016/J.MINENG.2009.03.022.

[111] L. Szabó, I. Hidalgo, J.C. Ciscar, A. Soria, CO_2 emission trading within the european union and annex b countries: the cement industry case, Energy Policy. 34 (2006) 72–87. https://doi.org/10.1016/J.ENPOL.2004.06.003.

[112] M. Taylor, C. Tam, D. Gielen, Energy efficiency and CO_2 emissions from the global cement industry, 50 (2006).

[113] Z. Usmani, V. Kumar, Characterization, partitioning, and potential ecological risk quantification of trace elements in coal fly ash, Environ. Sci. Pollut. Res. 24 (2017) 15547–15566. https://doi.org/10.1007/s11356-017-9171-6.

[114] T. Magiera, B. Gołuchowska, M. Jabłońska, Technogenic magnetic particles in alkaline dusts from power and cement plants, Water, Air, Soil Pollut. 224 (2012) 1389. https://doi.org/10.1007/s11270-012-1389-9.

[115] D. El-Mogazi, D.J. Lisk, L.H. Weinstein, A review of physical, chemical, and biological properties of fly ash and effects on agricultural ecosystems, Sci. Total Environ. 74 (1988) 1–37. https://doi.org/10.1016/0048-9697(88)90127-1.

[116] M. Steveson, K. Sagoe-Crentsil, Relationships between composition, structure and strength of inorganic polymers, J. Mater. Sci. 40 (2005) 2023–2036. https://doi.org/10.1007/s10853-005-1226-2.

[117] J.C. Swanepoel, C.A. Strydom, Utilisation of fly ash in a geopolymeric material, Appl. Geochemistry. 17 (2002) 1143–1148. https://doi.org/10.1016/S0883-2927(02)00005-7.

[118] A.S. de Vargas, D.C.C. Dal Molin, A.C.F. Vilela, F.J. da Silva, B. Pavão, H. Veit, The effects of Na_2O/SiO_2 molar ratio, curing temperature and age on compressive strength, morphology and microstructure of alkali-activated fly ash-based geopolymers, Cem. Concr. Compos. 33 (2011) 653–660. https://doi.org/10.1016/J.CEMCONCOMP.2011.03.006.

[119] G. Görhan, G. Kürklü, The influence of the NaOH solution on the properties of the fly ash-based geopolymer mortar cured at different temperatures, Compos. Part B Eng. 58 (2014) 371–377. https://doi.org/10.1016/J.COMPOSITESB.2013.10.082.

[120] F. Winnefeld, A. Leemann, M. Lucuk, P. Svoboda, M. Neuroth, Assessment of phase formation in alkali activated low and high calcium fly ashes in building materials, Constr. Build. Mater. 24 (2010) 1086–1093. https://doi.org/10.1016/J.CONBUILDMAT.2009.11.007.

[121] X. Guo, H. Shi, W.A. Dick, Compressive strength and microstructural characteristics of class C fly ash geopolymer, Cem. Concr. Compos. 32 (2010) 142–147. https://doi.org/10.1016/J.CEMCONCOMP.2009.11.003.

[122] E.I. Diaz, E.N. Allouche, S. Eklund, Factors affecting the suitability of fly ash as source material for geopolymers, Fuel. 89 (2010) 992–996. https://doi.org/10.1016/J.FUEL.2009.09.012.

[123] K. Somna, C. Jaturapitakkul, P. Kajitvichyanukul, P. Chindaprasirt, NaOH-activated ground fly ash geopolymer cured at ambient temperature, Fuel. 90 (2011) 2118–2124. https://doi.org/10.1016/J.FUEL.2011.01.018.

[124] F. Puertas, S. Martínez-Ramírez, S. Alonso, T. Vázquez, Alkali-activated fly ash/slag cements: Strength behaviour and hydration products, Cem. Concr. Res. 30 (2000) 1625–1632. https://doi.org/10.1016/S0008-8846(00)00298-2.

[125] P. Chindaprasirt, C. Jaturapitakkul, W. Chalee, U. Rattanasak, Comparative study on the characteristics of fly ash and bottom ash geopolymers, Waste Manag. 29 (2009) 539–543. https://doi.org/10.1016/J.WASMAN.2008.06.023.

[126] S. Patankar, S. Jamkar, Y. Ghugal, Effect of water-to-geopolymer binder ratio on the production of fly ash based geopolymer concrete., Journal. 2 (2013). https://doi.org/10.13140/2.1.4792.1284.

[127] J. Xie, O. Kayali, Effect of initial water content and curing moisture conditions on the development of fly ash-based geopolymers in heat and ambient temperature, Constr. Build. Mater. 67 (2014) 20–28. https://doi.org/10.1016/J.CONBUILDMAT.2013.10.047.

[128] P. Chindaprasirt, T. Chareerat, V. Sirivivatnanon, Workability and strength of coarse high calcium fly ash geopolymer, Cem. Concr. Compos. 29 (2007) 224–229. https://doi.org/10.1016/J.CEMCONCOMP.2006.11.002.

[129] Subaer, Influence of aggregate on the microstructure of geopolymer, Mater. Sci. (2004).

[130] C. Kuenzel, L. Li, L. Vandeperre, A.R. Boccaccini, C.R. Cheeseman, Influence of sand on the mechanical properties of metakaolin geopolymers, Constr. Build. Mater. 66 (2014) 442–446. https://doi.org/10.1016/J.CONBUILDMAT.2014.05.058.

[131] A.R. Kotwal, Y.J. Kim, J. Hu, V. Sriraman, Characterization and early age physical properties of ambient cured geopolymer mortar based on class C fly ash, Int. J. Concr. Struct. Mater. 9 (2015) 35–43. https://doi.org/10.1007/s40069-014-0085-0.

[132] B. Lomborg, The Skeptical environmentalist–measuring the real state of the world, Int. Chem. 25 (2003).

[133] R. McCaffrey, Climate change and the cement industry, GCL Environ. Spec. ISSUE. (2002).

[134] H. Akbari, T. Heller, S. Shin, X. Yang, P. Kolay, S. Kumar, M.. Mohanty, Geopolymer-based concrete to reduce carbon footprint of the construction industry, Min. Enigneering. 65 (2013) 57–62.

[135] P. Nath, Study of fly ash based geopolymer concrete cured in ambient condition., Curtin University, 2014.

[136] D. Hardjito, V. Rangan, Development and properties of low-calcium fly ash-based geopolymer concrete, 2005.

[137] GB/T 14684-2001, Standard specification for standard sand, (2001).